

Medical Faculty of the Martin Luther University Halle-Wittenberg

Regulation of Cellular Function by Mineralocorticoid Receptors

Dissertation

to obtain the academic degree

Doctor rerum medicarum (Dr. rer. medic.)

in the field of molecular medicine

submitted

to the Medical Faculty

of the Martin Luther University Halle-Wittenberg

by Yekaterina Gadasheva

Betreuerin: Prof. Dr. Dr. Claudia Großmann

Gutachter:

Prof. Dr. Rüdiger Horstkorte, Halle (Saale)

Prof. Dr. Regina Heller, Jena

Datum der Verteidigung: 19.03.2025

Summary

The mineralocorticoid receptor (MR) acts as a transcription factor, primarily activated by the adrenal hormone aldosterone (aldo). It is best explored for its physiological role in kidney epithelial cells, where it regulates electrolyte balance and blood pressure via the renin-angiotensin-aldosterone system (RAAS). Clinical and experimental studies show that the MR additionally has an independent role in cardiovascular diseases due to its expression beyond the kidneys. However, its target genes in disease states, cofactors in transcriptional regulation, and downstream effects leading to tissue remodeling remain largely unknown. Consequently, this thesis investigates the impact of activated MRs on cellular function using an inducible MR overexpression HEK cell model. The aim was to understand how MR leads to pathophysiological effects and the molecular mechanisms underlying cellular alterations that cause such effects.

My findings reveal that aldo treatment increases glucose consumption and lactate production in HEK cells, indicating a shift toward glycolytic ATP production without altering total ATP levels. We observed that the aldo/MR interaction triggers a classic cellular stress response pathway, leading to unfolded protein response (UPR), autophagy, and cell death. My experimental findings indicate that activated MR can induce alterations in cellular function by triggering the expression of target genes. For example, NGS data analysis revealed the upregulation of PDK4, a key player in metabolism control.

Interestingly, the response to aldo stimulation was modulated by a peroxynitrite donor SIN-1. We observed changes in MR cellular localization and quantified MR expression under varying concentrations of peroxynitrite. Additionally, we assessed MR functionality within a pathological micromilieu, noting alterations in PDK4 expression and caspase activity.

The observed changes in response to increased aldo/MR activity indicate an adaptive cellular response, particularly relevant in aging where elevated aldo and MR activity have been detected. Our study on MR expression revealed a complex relationship between SIN-1 concentration and MR expression levels, functionality, and receptor distribution, emphasizing the importance of the micromilieu in modulating MR activity and its potential impact on cellular function and disease progression.

Gadasheva, Yekaterina: Regulation of Cellular Function by Mineralocorticoid Receptors, Halle, Univ., Med. Fak., Diss., Pages – 79, Figures – 34, Tables – 16, 2024.

Referat

Mineralokortikoidrezeptoren (MR) wirken als Transkriptionsfaktoren und werden hauptsächlich durch das Nebennierenrindenhormon Aldosteron (Aldo) aktiviert. Am besten ist ihre physiologische Funktion in Nierenepithelzellen erforscht, in denen sie den Elektrolythaushalt und den Blutdruck über das Renin-Angiotensin-Aldosteron-System RAAS regulieren. Unabhängig von ihrer Nierenfunktion spielen MRs eine Rolle bei Herz-Kreislauf-Erkrankungen. Die zugrunde liegenden molekularen Mechanismen, Zielgene, Cofaktoren und zellulären Effekte, die zu Gewebsveränderungen führen, sind jedoch größtenteils unbekannt.

Folglich untersucht diese Arbeit die Auswirkung aktivierter Mineralokortikoidrezeptoren auf die Zellfunktion unter Verwendung eines induzierbaren HEK-Zellmodells mit Überexpression des MRs. Ziel war es, zu verstehen, wie MR zu pathophysiologischen Effekten führt und welche molekularen Mechanismen den zellulären Veränderungen zugrunde liegen.

Meine Ergebnisse zeigen, dass die Aldo-Behandlung den Glukoseverbrauch und die Laktatproduktion erhöhen, was durch eine Verschiebung der ATP-Gewinnung von der oxidativen Phosphorylierung hin zur Glykolyse verursacht wurde, ohne den Gesamt-ATP-Spiegel zu verändern. Wir konnten beobachten, dass die Aldo/MR-Interaktion einen klassischen zellulären Stressreaktionsweg auslöst und zu Unfolded Protein Response (UPR), Autophagie und Zelltod führt. Meine experimentellen Ergebnisse zeigen, dass aktivierter MR Veränderungen der Zellfunktion hervorrufen kann, indem er die Expression von Zielgenen auslöst. So ergab die NGS-Datenanalyse z.B. eine gesteigerte Expression von PDK4, einem wichtigen Regulator des Energiemetabolismus.

Interessanterweise konnte die Wirkung des MRs durch den Peroxynitrit-Donor Sin-1 moduliert werden. Wir beobachteten Veränderungen in der zellulären Lokalisierung und Expression des MRs sowie in der PDK4-Expression und Caspase-Aktivität unter verschiedenen Peroxynitrit-Konzentrationen.

Die Reaktion auf erhöhte Aldo-/MR-Aktivität könnte im Alter relevant sein, wo eine erhöhte Aldo/MR-Aktivität festgestellt wurde. Die komplexe Beziehung zwischen SIN-1-Konzentration, MR-Lokalisation, MR-Expression und –Aktivität betont die Bedeutung des Mikromilieus bei der Modulation der MR-Aktivität und dessen potenzielle Auswirkung auf die Zellfunktion und die Pathogenese von Erkrankungen.

Gadasheva, Yekaterina: Regulation der Zellfunktion durch Mineralocorticoid-Rezeptoren, Halle, Univ., Med. Fak., Diss., Seiten – 79, Abbildungen – 34, Tabellen – 16, 2024.

Table of Contents

1.	Introduction	1
1.1.	Molecular Architecture of the Mineralocorticoid Receptors	1
1.1.1.	N-terminal Domain (NTD).....	2
1.1.2.	The DNA-Binding Domain (DBD)	2
1.1.3.	The Ligand-Binding Domain (LBD).....	3
1.2.	Mechanisms of MR Signaling and Physiological Function	3
1.2.1.	Pathophysiological Function of the MR during Aging and Disease	5
1.3.	Evolution of MRs Antagonists (MRAs).....	8
1.4.	Alternative Mechanisms and Micromilieu Influences on MR	9
2.	Aims of the Study	10
3.	Material and Methods.....	11
3.1.	Cell Culture	11
3.2.	Quantification of Cell Number	11
3.3.	Protein Isolation and Western Blot	11
3.4.	RNA Isolation	13
3.5.	RNA integrity measurement for NGS.....	14
3.6.	cDNA Synthesis for qPCR.....	14
3.7.	Real-Time quantitative reverse transcription PCR (RT-qPCR)	15
3.8.	Glucose Measurement Assay.....	16
3.9.	Lactate Measurement	16
3.10.	Caspase-3 Activity Assay	17
3.11.	LDH measurement	17
3.12.	Oxygen Consumption Rate and Extracellular Acidification Rate.....	18
3.13.	Assay Parameters for Mitochondrial Function	20
3.14.	Glycolytic Rate Assay Parameters	20

3.15.	Autophagic Flux	21
3.16.	Measurement of ATP Content in Cells	22
3.17.	Immunofluorescence	22
3.18.	NGS Data Analysis	23
3.19.	Statistical Analysis	23
3.20.	Buffers	24
3.21.	Software/Programs	24
3.22.	Devices	25
4.	Results	26
4.1.	Metabolic Shifts in HEK Cells Under Aldo/MR stimulation	26
4.1.1.	Mitochondrial Function Assessment, Experimental Parameters	27
4.1.2.	Proton Efflux Rate in MR-Overexpressing HEK Cells	28
4.1.3.	Distinguishing Between ATP Production Pathways	29
4.2.	Aldo/MR Target Genes	30
4.3.	PDK4 Protein Upregulation by aldo/MR	33
4.4.	Additional Analyses of NGS Data	34
4.5.	Aldo/MR Interaction Initiates ER-stress Signaling Pathway	35
4.6.	Activated MR by Aldo Triggered Autophagic Flux Increase	37
4.7.	Increased Cell Death Marker Expression via aldo-Induced MR Signaling	39
4.8.	Influence of Micromilieu on MR	40
4.8.1.	Translocation Ability of MR Without Aldo Activation in HEK TO MR Cells	40
4.8.2.	Genes regulation by SIN-1/MR	41
4.8.3.	Effect of Nitrosative Stress on MR/PDK4 Interaction	43
4.8.4.	Protein Expression of PDK4	45
4.8.5.	Influence of the Nitrosative Stress on Aldo/MR Function (Cell Death)	45
4.8.6.	MR Expression Under Nitrosative Stress	47

4.8.7.	Effect of SIN-1 on Protein Expression of Glucocorticoid Receptor.....	48
5.	Discussion.....	49
5.1.1.	Energy Metabolism Involves MR Regulation in HEK Cells	49
5.1.2.	MR Serves as an Upstream Regulator of Genes of Energy Metabolism.....	52
5.1.3.	ER Stress Signaling Pathways Regulated by MR.....	55
5.1.4.	Autophagy as a Result of Possibly Failed UPR Response	56
5.1.5.	Cell Death as a Consequence of Altered Cellular Behavior	58
5.2.	Activation of MR under Nitrosative Stress	59
5.2.1.	MR Translocates and Activates Genes Under the Nitrosative Stress	59
5.2.2.	MR Effects and Expression under Nitrosative Stress	62
5.3.	Conclusion and Suggestions.....	63
5.4.	Limitations.....	65
6.	Reference	67
7.	Theses	79
8.	Supplement material	lxxx
	List of manufacturers and distributors.....	lxxx
	Declarations	lxxxvii
	Acknowledgements	lxxxviii

List of Abbreviations

2-DG	2-deoxyglucose
AA	antimycin A
ACE	angiotensin-converting enzyme
AF-1	activation function-1
AFC	7-amino-4-trifluoromethyl coumarin
AGT	angiotensinogen
APS	ammonium persulfate
AR	androgen receptor
ARTS-HF	Mineralocorticoid receptors Antagonist Tolerability Study-Heart Failure
AT II	angiotensin II
ATG	autophagy-related gene
ATF6	activating transcription factor-6
ATP	adenosine triphosphate
BCA	bicinchoninic acid
BCL2	B-Cell lymphoma 2 apoptosis regulator
BF	buffer factor
BH4	tetrahydrobiopterin
BLAST	Basic Local Alignment Search Tool
BMP4	bone morphogenetic protein-4
NT-proBNP	N-terminal prohormone of brain natriuretic peptide
BSA	Bovine serum albumin
BSO	L -Buthionine-sulfoximine
CFTR	cystic fibrosis transmembrane conductance regulator
CHAPS	(3-((3-cholamidopropyl) dimethylammonium)-1-propane sulfonate)
CHIP	carboxyl-terminal hsp70 interacting protein
COS	fibroblast-like cell lines derived from monkey kidney tissue
CTGF	connective tissue growth factor
CTP	cytidine triphosphate
CVD	cardiovascular disease
DAPI	4',6-diamidino-2-phenylindole
DBD	DNA-binding domain
DEVD-AFC	acetyl-Asp-Glu-Val-Asp-7-amino-4-trifluoromethyl coumarin
DMEM	Dulbecco's Modified Eagle Medium

DNA	deoxyribonucleic acid
DOC	deoxycorticosterone
DTT	dithiothreitol
DUB	deubiquitinating enzymes
ECAR	extracellular acidification rate
ECL	enhanced chemiluminescence
EDTA	ethylenediaminetetraacetic acid
EGFR	epidermal growth factor receptor
EPHESUS	Eplerenone Post-Acute Myocardial Infarction Heart Failure Efficacy and Survival Study
ER	endoplasmic reticulum stress
ERAD	ER-associated degradation
ERK	extracellular signal-regulated kinase
FCCP	carbonyl cyanide-p-trifluoromethoxyphenyl-hydrazone
FCS	fetal bovine serum
FKBP	FK506 binding proteins
FOSL2	FOS like 2, AP-1 Transcription Factor Subunit
FPM	Fragments per Million mapped
G6PD	Glucose-6-phosphate dehydrogenase
GCs	glucocorticoids
GLUT	glucose transporters
GR	glucocorticoid receptor
GRE	glucocorticoid response element
GRP75	glucose-regulated protein 75
GTP	guanosine-5'-triphosphate
H ₂ O ₂	hydrogen peroxide
HEK	human embryonic kidney
HEPES	4-(2-hydroxyethyl)-1-piperazineethanesulfonic acid
HF	heart failure
HK2	immortalized proximal tubule epithelial cell line
HRE	hormone response element
HRP	horseradish peroxidase
11 β -HSD1	11 β -Hydroxysteroid dehydrogenase type 1
11 β -HSD2	11 β -Hydroxysteroid dehydrogenase type 2

HSP70	heat shock protein 70
HSP90	heat shock protein 90
HUVEC	human umbilical endothelial cells
ICAM	Intercellular Adhesion Molecule 1
eIF2 α	eukaryotic initiation factor 2
IP3R	inositol trisphosphate receptor
IRE1	inositol-requiring enzyme type 1
JNK	c-Jun N-terminal kinases
LBD	ligand binding domain
LC-MS-MS	liquid chromatography with tandem mass spectrometry
LC3B	tubule-associated protein 1 light chain 3 beta
LDH	lactate dehydrogenase
LTCC	L-type calcium channel
MAM	mitochondria-associated membrane
MAP3K6	mitogen-activated protein kinase kinase kinase 6
MCP	monocyte chemotactic protein-1
Post-MI	Post-myocardial Infarction
MMP15	matrix metalloproteinases
MOPS	3-(N-morpholino)propane sulfonic acid
MR	mineralocorticoid receptors
MRA	mineralocorticoid receptors antagonists
NAD	nicotinamide adenine dinucleotide
NADH	nicotinamide adenine dinucleotide hydrogen
NADP	nicotinamide adenine dinucleotide phosphate
NCBI	National Center for Biotechnology Information
NEDD8	neural-precursor-cell-expressed developmentally down-regulated 8
NGS	Next-Generation Sequencing
NHE1	sodium-hydrogen antiporter 1
NLS	nuclear localization signal
NO	nitric oxide
NOS	nitric oxide synthase
NOX	NADPH oxidase
NR	nuclear receptor
NBR1	autophagy cargo receptor

NTD	N-terminal domain
NTP	nucleoside triphosphate
NYHA	New York Heart Association
OCR	oxygen consumption rate
OMM	outer mitochondrial membrane
ONOO	peroxynitrite
OXPPOS	oxidative phosphorylation
PACS	phosphofurin acidic cluster sorting protein-2
PBS	phosphate-buffered saline
PCR	polymerase chain reaction
PDHA	pyruvate dehydrogenase E1 component subunit alpha
PDK	pyruvate dehydrogenase kinase
PDP1	pyruvate dehydrogenase phosphatase 1
PERK	protein kinase RNA-like ER kinase
PGC	peroxisome proliferator-activated receptor γ coactivator
PIPES	1,4-Piperazinediethanesulfonic acid
PP2A	activation of protein phosphatase 2A
PPAR	peroxisome proliferator-activated receptors
PRKAB2	AMP-Activated Protein Kinase Beta 2 Non-Catalytic Subunit
PTM	posttranslational modification
PTPIP51	protein tyrosine phosphatase interacting protein-51
RAAS	renin-angiotensin-aldosterone system
RALES	Randomized Aldactone Evaluation Study
RIPA	radioimmunoprecipitation assay buffer
RNA	ribonucleic acid
RNS	reactive nitrogen species
ROS	reactive oxygen species
ROX	6-carboxyl-X-Rhodamine
SDS page	sodium dodecyl-sulfate polyacrylamide gel electrophoresis
SGK1	serum glucocorticoid-regulated kinase 1
SHR	spontaneously hypertensive rat
SIN	3-morpholinopyridone hydrochloride
SIRT1	sirtuin
SKIDA1	SKI/DACH Domain-Containing 1

SLC2A3	solute carrier family 2 member 3
SMC	smooth muscle cells
SNAP	S-nitroso-N-acetylpenicillamine
SUMO	sumoylation
SYBR	green fluorescent DNA stain
TBS	tris-buffered saline
TBST	tris-buffered saline tween
TCA	tricarboxylic acid
TEMED	tetramethylethylenediamine
TGF- β	transforming growth factor-beta
TRIS	tris(hydroxymethyl)aminomethane
TTP	thymidine triphosphate
UPR	unfolded protein response
ULK1	Unc-51 like autophagy activating kinase 1
UVRAG	UV radiation resistance associated
VAPB	vesicle-associated membrane protein-associated protein B
VCAM1	vascular cell adhesion protein 1
VDAC1	voltage-dependent anion-selective channel 1
VSMC	vascular smooth muscle cells
XPB	X-box binding protein 1

1. Introduction

1.1. Molecular Architecture of the Mineralocorticoid Receptors

The MR, a ligand-activated transcription factor, stands out among steroid receptors as a crucial receptor for two hormone classes: mineralocorticoids, including aldosterone and deoxycorticosterone (DOC), and glucocorticoids, such as cortisol, in humans. The MR is part of the nuclear receptor subfamily 3 (NR3), alongside the glucocorticoid receptor (GR), progesterone receptor (PR), estrogen receptor (ER), and androgen receptor (AR). The MR was cloned as the last of this subfamily 37 years ago (Arriza et al., 1987). The human MR gene on chromosome 4 in the q31.1–q31.2 region spans approximately 450 kilobases and consists of 10 exons (Morrison et al., 1990). Eight exons encode the 984 amino acid MR protein. Exon 1 α and exon 1 β form alternative promoters and allow the generation of two distinct MR transcripts, hMR α and hMR β , with the same translation product (Zennaro, 1997).

The MR follows a protein structure akin to other nuclear receptor superfamily members, comprising three key domains (Figure 1): the amino-terminal domain (NTD), the central DNA-binding domain (DBD), the hinge region, and the C-terminal ligand-binding domain (LBD) (Green and Chambon, 1987). Exon 2 encodes the NTD, housing activation function-1 (AF-1) (Fuller et al., 2017). Exons 3 and 4 encode the DBD, containing zinc fingers interacting with hormone response elements. The last five exons encode the LBD, which includes a ligand binding pocket and activation function-2 (AF-2) (Viengchareun et al., 2007).

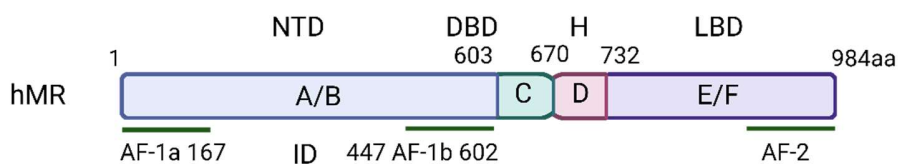


Figure 1. Domain structure of the human MR (hMR). hMR consists of 984 amino acids. The N-terminal domain (NTD) is comprised of two activatory domains (AF1a and AF1b) and the inhibitory domain (ID). Subsequently, there is the DNA binding domain (DBD) and the ligand binding domain (LBD) featuring activation function 2 (AF-2). Created in BioRender. Gadasheva, Y. (2024) <https://BioRender.com/t26w626>.

1.1.1. N-terminal Domain (NTD)

The NTD of the MR is the least conserved domain among nuclear receptors (NRs) (Fischer et al., 2010). Despite its distinctiveness compared to other steroid receptors, the MR NTD exhibits significant conservation across mammalian species, demonstrating approximately 85 % amino acid homology (Agarwal and Mirshahi, 1999). The NTD comprises two distinct domains, AF1 (a and b) and an inhibitory domain. The MR recruits co-activator or co-repressor complexes through its functional domains (AFs or ID) (Vlassi et al., 2013). The ID, when fused to either of the trans-activating domains, is sufficient to limit the activity of the NTD, further highlighting the intricacy of the MR's function. The AF-1 is responsible for modulating the selectivity of the MR for ligand and cofactor interactions, as well as intramolecular interactions with the ligand-binding domain (LBD). AF-1 is constitutively active but is suppressed by the C-terminal E/F domain (LBD domain) without a ligand (Jausonslofreda et al., 1994). The MR-NTD can undergo posttranslational modification, including phosphorylation and sumoylation (SUMO).

1.1.2. The DNA-Binding Domain (DBD)

The MR binds to hormone response elements (HRE) as a transcription factor through its DBD (Lombès et al., 1994). The DBD features two zinc ions, each tetrahedrally coordinating four cysteine residues, forming stable 'two zinc fingers' crucial for DNA recognition, binding, and receptor homo- and hetero-dimerization (Fuller et al., 2017; Luisi et al., 1991). Specifically, the zinc finger in proximity to the N-terminal domain is pivotal in mediating the interaction between the MR and DNA. This zinc finger contains a P-box, facilitating its engagement with half-sites of a glucocorticoid response element (GRE) through intercalation into the major groove of the DNA. A specific selective HRE for MR among family receptor members has not yet been described, and it is known that the MR interacts with diverse glucocorticoid response elements, given that the MR DBD shares ~94 % identity with the GR (Arriza et al., 1987; Funder, 1993; Lombès et al., 1992).

The hinge region is a segment that connects the DBD and the LBD. It features a proline stretch facilitating a twist in the DNA-binding domain. This twist is instrumental in appropriately orienting the receptor for contact with the general transcription machinery (Pascual-Le Tallec and Lombès, 2005). In the case of MR, the hinge region likely contributes to the flexibility and adaptability of the receptor. This flexibility is crucial for the receptor to

undergo structural changes in response to ligand binding, allowing it to effectively regulate gene transcription (Tsai and O'Malley, 1994).

1.1.3. The Ligand-Binding Domain (LBD)

The LBD of the MR is a multifunctional domain sharing approximately 55 % homology with the androgen receptor, progesterone receptor, and glucocorticoid receptor and around 85 % homology across different species (Sturm et al., 2005). The LBD's structure comprises 12 α -helices and one β -sheet, forming three antiparallel layers (Pascual-Le Tallec and Lombès, 2005). Without a ligand, the LBD establishes multiple contact sites with chaperone proteins, such as HSP90, 70, and various immunophilins (Rogerson et al., 2004). The LBD can bind both agonist and antagonist ligands. Upon aldo binding, the MR undergoes a conformational change, stabilizing helix 12 (Fuller et al., 2021). The LBD also contains sites for phosphorylation and sumoylation, playing a crucial role in regulating the interaction of the MR with co-regulators in a context- and promoter-dependent manner.

1.2. Mechanisms of MR Signaling and Physiological Function

The preferential occupation of MR by aldo in classical kidney epithelial target tissues is maintained by the enzymatic process facilitated by the expression of 11 β -hydroxysteroid dehydrogenase type 2 (11 β HSD2). This enzyme metabolizes cortisol or corticosterone into inactive forms that cannot bind to MR in MR-containing epithelia (Edwards et al., 1988).

MRs have been identified in diverse cell types, including classically in epithelial tissues like kidney, colon, and salivary glands but also in non-epithelial cells like immune cells, cardiomyocytes, vascular cells, and adipocytes (Funder, 2005a; Lombès et al., 1992; Prager et al., 2010). Within living cells, the unstimulated MR is predominantly situated in the cytoplasm in the kidney epithelium and many other cells, and hormone activation results in its accumulation in the nucleus (Figure 2) (Fejes-Tóth et al., 1998; Tanaka et al., 2005; Hernández-Díaz et al., 2010).

The MR associates with chaperones in the cytoplasmic compartment, including HSP90, HSP70, p23, and various immunophilins like FKBP51, rendering it transcriptionally inactive (Galigniana et al., 2010). Engaging with its chaperones, the MR maintains a conformation suitable for aldo binding and is shielded from rapid degradation (Binart et al., 1995; Caamano et al., 1993).

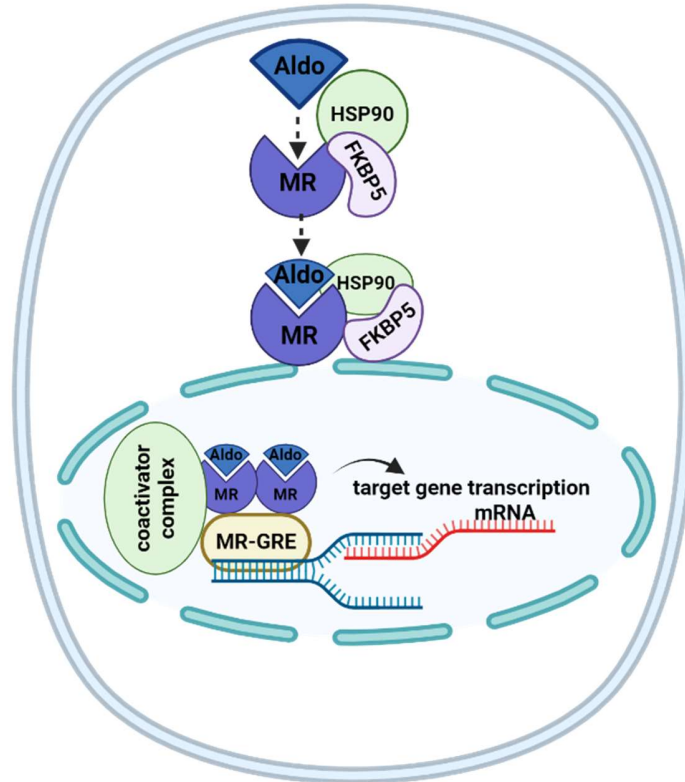


Figure 2 depicts a schematic representation of MR signaling. MR is associated with its chaperones in the cytosol, which aid in the receptor's translocation from the cytosol to the nucleus and facilitate its binding to the hormone response element of target genes. Upon binding to the physiological ligand aldo, MR undergoes conformational changes, and a repositioning of chaperones is initiated. To initiate the transcription of target genes, MR must assemble the transcriptional machinery along with cofactors. Created in BioRender. Gadasheva, Y. (2024) <https://BioRender.com/c95c522>.

Recent research challenges previous assumptions, suggesting that ligand binding doesn't lead to immediate dissociation of MR from HSP90. Instead, there is a shift in associated proteins from FKBP51 to FKBP52 (Grossmann et al., 2012). Moreover, HSP90 supports DNA binding of the MR, affects transactivation activity, and may influence the degradation of receptors (Galigniana et al., 2010; Grossmann et al., 2012; Hernández-Díaz et al., 2010; Stavreva et al., 2004).

Traditionally, NRs homodimerize and bind to DNA to initiate gene expression, but higher oligomeric structures like tetramers have been reported (Hudson et al., 2014; Watson et al., 2013). HSP90 is crucial for MR dimerization, with its dissociation necessary for homodimerization (Savory et al., 2001). Furthermore, the formation of MR-GR heterodimers has been confirmed through co-immunoprecipitation assays, occurring in both ligand and

non-ligand states and influenced by the cellular environment, chaperones, and post-translational modifications (Kiilerich et al., 2015; Trapp et al., 1994).

In classical epithelial cells like renal principal cells of the collecting duct, MR is known for increasing sodium and water reabsorption as well as potassium and proton secretion by inducing the expression of different channels and transporters like ENaC, ROMK, and Na⁺K⁺ATPase (Grossmann et al., 2012). Upon activation, the MR regulates the ENaC through multiple mechanisms, primarily by modulating the Ser/Thr kinase SGK1 and the ubiquitin ligase NEDD4-2. One of MR's essential functions is to ensure the stability of ENaC at the plasma membrane. Additionally, Aldo-induced proteins such as Glucocorticoid-induced leucine-zipper protein 1 (GILZ1) and the connector enhancer of kinase suppressor of Ras isoform 3 (CNKSR3), which are MR target genes, form a multiprotein complex that also regulates ENaC stability (Shibata, 2017).

Sodium reabsorbed via ENaC is transported to the extracellular fluid by Na⁺/K⁺-ATPase, which comprises α , β , and γ subunits. Aldo increases Na⁺/K⁺-ATPase activity in principal cells through direct and indirect effects (Taylor et al., 2003).

Inhibition of renal salt reabsorption is counterbalanced by increased salt appetite and vice versa, highlighting the advantage of targeting both pathways. Current pharmacological interventions to manage salt retention and appetite include MR antagonists (Barrera-Chimal et al., 2019).

1.2.1. Pathophysiological Function of the MR during Aging and Disease

The MR plays a crucial role in the RAAS, particularly in the context of physiological water-electrolyte homeostasis, but also independent of the effects on blood pressure in cardiovascular disease (CVD) (Hirono et al., 2007). The RAAS signaling system constitutes a well-established hormonal cascade, where, physiologically, the activation of MR by Aldo represents the final step of this cascade (Figure 3) (Ibrahim et al., 1997). The MR is involved in numerous diseases beyond its traditional role in kidney function. It significantly influences cardiovascular, renal, immune, metabolic, and neurological disorders (Table 1).

MR activation in nontraditional tissues, including endothelial and smooth muscle cells, inflammatory cells, podocytes, and fibroblasts, can harm kidney structure and function, contributing to the development and progression of chronic kidney disease. The MR also

assumes a central role in tissue remodeling processes, which is evident, for example, in the context of CVDs, but likewise evident during aging (Figure 3) (Fiebeler and Haller, 2003).

Table 1. MR implication in various diseases.

Health disorders	Diseases with MR involvement	References
Cardiovascular and renal pathology	Valve disease	(Zendaoui et al., 2012)
	Heart failure	(Cezar et al., 2015)
	Myocardial infarction	(Wang et al., 2004)
	Atherosclerosis	(Sakurabayashi-Kitade et al., 2009)
	Hypertension	
	Chronic kidney disease	(Barrera-Chimal et al., 2019)
Metabolic disorders	Obesity	(Parasiliti-Caprino et al., 2022)
	Diabetes	(Igbekele et al., 2022)
	Metabolic syndrome	(Feraco et al., 2020)
Immune system disorders	Autoimmune	(Alvarez Quintero et al., 2024)
	Encephalomyelitis	
Neurological and psychiatric	Hypertension	(Kellner and Wiedemann, 2008)

The mechanisms behind these pathophysiological changes have yet to be well understood. The effects of MR in cardiovascular tissue are highly versatile and context-dependent, suggesting additional regulatory mechanisms beyond direct gene expression.

Several molecular mechanisms explain aldosterone/MR's contribution to aging and disease: telomere attrition, inflammation, fibrosis, cardiovascular dysfunction and oxidative stress, and mitochondrial dysfunction.

Telomere shortening, associated with oxidative stress and inflammation, is shorter in CVD patients, linking aldosterone to these conditions (Benetos et al., 2005).

MR's reaction to aldosterone-activated ERK1/2 in older arteries is linked to increased EGFR production, angiotensin II levels, and inflammation-associated gene activation (Krug et al., 2010). In endothelial cells, MR activation promotes cardiac inflammation and remodeling via VCAM1 (Lothar et al., 2016) and regulates leukocyte adhesion to coronary artery endothelial cells through ICAM-1 overexpression (Marzolla et al., 2017).

RNA-seq data from aging VSMCs show a pro-fibrotic gene profile induced by MR, including CTGF, MMPs, BMP4, and TGF- β , contributing to vascular stiffness (Kim et al., 2018). Many MR target genes remain unidentified, though some are induced through MR-responsive elements in gene promoters and interactions with transcription factors like NF κ B and AP-1 (Fiebeler et al., 2001).

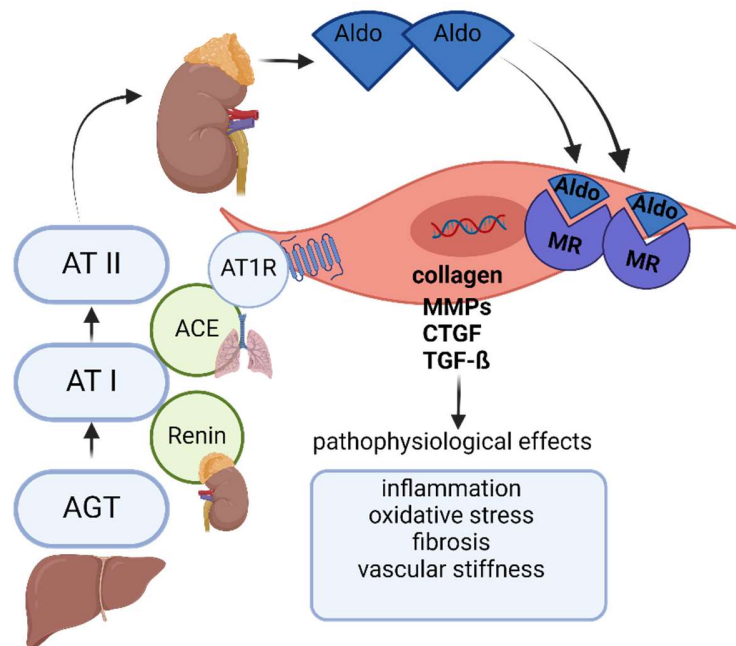


Figure 3. The physiological and pathophysiological roles of the RAAS system, with a focus on the MR. The RAAS cascade begins with stimuli like low blood pressure, reduced sodium levels, or sympathetic nervous system activation, triggering renin release from kidney juxtaglomerular cells. Renin cleaves liver-produced angiotensinogen (AGT) into angiotensin I (AT I). Angiotensin-converting enzyme (ACE), primarily in the lungs, converts AT I to angiotensin II (AT II). This potent vasoconstrictor raises blood pressure and stimulates aldo release from the adrenal glands. Aldo activates MR in the kidneys, promoting sodium and water reabsorption and increasing blood volume and pressure. However, aldo also enhances AT II secretion, overactivating the RAAS system. MR activation in vascular smooth muscle cells triggers profibrotic gene transcription (MMP, collagen, CTGF, TGF β), leading to inflammation, oxidative stress, stiffness, and fibrosis, contributing to age-related vascular changes. Created in BioRender. Gadasheva, Y. (2024) <https://BioRender.com/y01j756>.

MR overexpression mediates T-type calcium channel remodeling, contributing to myocardial electrical dysfunction and cardiac arrhythmias (Tsai et al., 2010). MR expression in the vascular wall increases with age, affecting blood pressure regulation and myocardial function (DuPont et al., 2016; Krug et al., 2013). In aged humans, serum miR-155 governs SMC contractile function, with MR-antagonist therapy affecting its expression (Armstrong and Editor, n.d.). Increased MR expression suppresses miR-155, targeting LTCC (DuPont et al., 2016). By acting through the MR, aldo has been shown to reduce the expression and activity of G6PD. This reduction leads to increased oxidative stress and decreased NO levels, a pattern similar to what is observed in G6PD-deficient endothelial cells. The compromised vascular function fails to protect against reactive radicals and maintain bioavailable NO (Leopold et al., 2007).

Aldo also contributes to mitochondrial dysfunction, impacting mitochondrial dynamics and adipocyte regeneration, leading to accelerated aging in visceral fat tissue (Lefranc et al., 2021). MR-dependent suppression of UCP1 expression in brown adipocytes has been observed (Kuhn et al., 2019).

Additionally, aldo/MR induction mediates cellular senescence in the kidney, influencing the ROS/SIRT1/p53/p21 pathway, with increased p53 expression and reduced mitochondrial renewal observed in aging rat hearts (Hu et al., 2020).

Combined, these mechanisms profoundly impact aging and age-related diseases, highlighting the importance of understanding aldo/MR's role in cellular function and aging.

1.3. Evolution of MRs Antagonists (MRAs)

Evidence supports the role of aldo/MR interplay in cardiac remodeling, highlighted by the effectiveness of MR antagonists (MRAs) in treating heart failure with reduced ejection fraction, particularly in older adults (Pitt, 2012; Pitt et al., 2014; Zannad et al., 2011). The RALES trial showed that adding spironolactone to standard therapy significantly improved mortality and morbidity in patients with advanced heart failure (NYHA class III-IV) (Pitt et al., 1999). The EPHESUS trial found that when added to optimal therapy, eplerenone reduced mortality and heart failure hospitalizations in post-MI patients (Pitt et al., 2003). The EMPHASIS-HF trial further demonstrated that eplerenone reduced mortality and hospitalizations in patients with NYHA class II heart failure (Zannad et al., 2011).

Despite its benefits, eplerenone has a lower affinity for MRs than spironolactone, increasing the risk of hyperkalemia (Parfianowicz et al., 2022; Zannad et al., 2012). To address this, finerenone, a non-steroidal selective MRA, has shown comparable efficacy with improved safety, reducing hyperkalemia risk (Filippatos et al., 2016). The ARTS-HF trial confirmed finerenone's tolerability and ability to lower NT-proBNP levels similarly to eplerenone in heart failure patients with reduced ejection fraction, diabetes, and chronic kidney disease (Filippatos et al., 2016). Finerenone inhibits MR signaling and the recruitment of transcription cofactors linked to hypertrophy, inflammation, and fibrosis (Xue et al., 2023).

MRAs also counter oxidative stress, reducing myocardial oxidative stress, fibrosis, and inflammation. Eplerenone has shown efficacy in preventing heart failure progression in a pressure-overload mice model and reversing BH4 oxidation, thereby preventing eNOS uncoupling induced by MR activation (Chen et al., 2016; Johar et al., 2006; Virdis et al., 2002).

1.4. Alternative Mechanisms and Micromilieu Influences on MR

In RALES and EPHEBUS, it was noted that participants' aldosterone plasma levels were not elevated, suggesting an alternative molecular mechanism for pathologic MR activity in CVDs (Funder, 2005b). Eplerenone effectively reduced left ventricular mass in patients with left ventricular hypertrophy and hypertension, even with normal aldosterone levels (Bakris et al., 2020; Pitt et al., 2003).

Since aldosterone is not the only MR agonist in humans, there is a hypothesis that glucocorticoid overstimulation of MR causes excessive MR activity without elevated aldosterone levels (Chapman et al., 2013), especially since 11 β -HSD2 expression is low in non-epithelial tissues. Thus, MR should be constantly bound by GCs in cardiomyocytes (Yang et al., 2022).

Genes induced by MR with cortisol activation in cardiomyocytes differ from those with aldosterone activation, with CTGF and TGF- β being "aldosterone-specific genes" (Messaoudi et al., 2013). MR does not significantly contribute to cortisol-induced cardiac remodeling (Rossier et al., 2010). Despite normal aldosterone levels, glucocorticoid activation of MR does not fully explain pathologic MR activity. Evidence shows that aldosterone's susceptibility in spontaneously hypertensive rats is partially mediated by higher MR expression in vascular cells (Rossier et al., 2010). Cardiac MR expression increases with age in rats (Hu et al., 2020), promoting ion channel remodeling and potentially cardiac arrhythmias associated with heart failure (Tsai et al., 2010).

Preclinical and clinical studies indicate micromilieu changes are relevant in MR-induced pathologies (Griesler et al., 2022). The cellular redox status significantly influences MR signaling pathways, with ROS acting as modulators. Aged endothelial cells, a source of ROS, contribute to changes in endothelial eNOS activity. eNOS synthesizes NO, a vasodilator, and BH4 influences its activity. BH4 depletion in aged endothelial cells uncouples eNOS, increases ROS/RNS production, and lowers NO generation (Förstermann and Münzel, 2006). Aldosterone and MR interaction inhibits eNOS function by oxidizing BH4 and activating protein phosphatase 2A (PP2A), dephosphorylating p-eNOS Ser 1177 (Nagata et al., 2006). In HUVEC cells, aldosterone reduced eNOS phosphorylation and NO production in response to vascular endothelial growth factor. In patients with primary aldosteronism, BH4 depletion and oxidative stress impair endothelial healing after injury (Chen et al., 2016).

2. Aims of the Study

The MR, primarily acknowledged for its critical role in maintaining sodium balance within renal epithelial cells, remains incompletely elucidated regarding its pathophysiological functions in non-epithelial cells (Buonafine et al., 2018). Upon activation in endothelial and smooth muscle cells, MR can mediate vascular diseases by inducing oxidative stress, inflammation, and acceleration of vascular remodeling and calcification (Artunc and Lang, 2014). Aldo and MR are significantly upregulated and activated with advancing age (Bauersachs et al., 2015). Consequently, there is a need to investigate the influence of MR on fundamental cellular processes to better understand its unique physiological and pathophysiological contributions. Therefore, we aimed to explore metabolic changes, cell death, ER stress, and mitochondrial function in cells treated with aldo and MR. Because of the instability and low expression of the MR, an inducible MR-overexpression HEK cell clone was utilized. Previous research has indicated that the micromilieu significantly influences the transition of MR action from physiological to pathophysiological states. Consequently, we evaluated the impact of the micromilieu factor peroxynitrite on MR localization, expression, and function.

3. Material and Methods

3.1. Cell Culture

T-Rex™ 293 cells (Life Technologie #R71007) were stably transfected with the MR expression plasmid pcDNA4-TO-hMR to create the tetracycline-inducible MR overexpressing clone HEK-TO-MR.

EA.hy926 cells are a cell line established by fusing primary human umbilical vein cells with a thioguanine-resistant A549 clone using polyethylene glycol (PEG). This line expresses endogenous MR. The cell culture was conducted under a sterile workbench (Herasafe, Thermo Fisher Scientific). The cells were split once weekly at 90 % confluency at a 1:20 ratio. The protocol involved several steps: aspirating the old medium, washing with EDTA buffer (Table 13), applying 0.1 % trypsin (Sigma-Aldrich) to detach cells, neutralizing with DMEM+FCS medium (Sigma-Aldrich), and reseeding. HEK-TO-MR cells were cultured in DMEM/Ham's F-12 medium with 25 mM glucose, 10 % fetal bovine serum FCS (Sigma-Aldrich), 5 µg/mL blasticidin S (Life Technologies), 200 µg/mL zeocin (Invitrogen), and 2 g/L NaHCO₃ at 37°C, 5 % CO₂ and 95 % humidity. For experiments, HEK-TO-MR cells were starved in serum-free media with 5.5 mM glucose for at least 4 hours, then treated with 0.25 µg/ml tetracycline (tet) (Invitrogen) for 24 hours to induce MR expression. Concurrent treatments included DMSO (vehicle control), 10 nM aldo (Sigma-Aldrich), 10 µM eplerenone (Sigma-Aldrich), Sin-1 hydrochloride (200-800 µM, Merck), 40 µM ebselen, and 10 mg/ml lysosomal inhibitors pepstatin A and aloxistatin. EA.hy926 cells were cultured at 37°C, 5 % CO₂, and 95 % humidity in DMEM with 5.5 mM glucose and underwent the same starvation conditions as HEK-TO-MR cells.

3.2. Quantification of Cell Number

Cell counting was performed using the CASY cell counter (OMNI Life Science GmbH). The viable cells per mL were calculated to determine the number of cells for experiments.

3.3. Protein Isolation and Western Blot

Cells were scraped and collected into ice-cold PBS buffer (Table 14) with proteinase inhibitor cocktail 1 and 3 (Sigma-Aldrich) and centrifuged. The pellet was dissolved in RIPA buffer (Table 14) with benzonase (Merck) to prepare cell lysates. The ultrasound sonication (UP100H; Hielscher) was the next step for the lysates. After centrifugation, protein concentrations were determined using bicinchoninic acid (BCA assay, Thermo Fisher Scientific). As protein standards, concentrations of 100 mg/l, 300 mg/l, 500 mg/l, 700 mg/l,

and 1000 mg/l of BSA were used. A complex is formed between Cu⁺ and two molecules of bicinchoninic acid, resulting in the distinctive purple coloration that can be measured spectrophotometrically at 562 nm (Smith et al., 1985).

Fresh cell lysates were incubated at 37°C for 30 minutes with 6× Red-Mix. Equivalent protein amounts (30 or 50 µg) were loaded on 12 % or 15 % SDS-PAGE minigels. The separation protocol was 0.36 hours at 22 mA/gel and 1.10 hours at 44 mA/gel. The nitrocellulose membrane and filter papers were immersed in a Petri dish containing 1× transfer buffer before initiating protein transfer onto the membrane in the blotting chamber of the Trans-Blot Turbo Transfer System (Bio-Rad).

The membrane was incubated overnight at 4°C with a 1:2000 primary antibody dilution (Table 2) in 1× TBS + 0.1 % Tween-20 + 5 % BSA (Capricorn Scientific). The next day, it was washed three times (5 minutes each) with 1× TBS-Tween, then incubated with secondary antibodies (Table 3) in 5 % non-fat dry milk in TBS-Tween for 2 hours. All buffers for the western blot are represented in Table 4.

Table 2. Primary antibody.

Antibodies name	Species	Distributor
rMR 1-18 1D5	anti-mouse	Developmental Studies Hybridoma Bank
LC3B	anti-rabbit	Cell Signaling 2775
PDK4	anti-rabbit	Boster PB9773
PDHA total (9H9AF5)	anti-mouse	Abcam ab110330
PDHA1 (phospho S293)	anti-rabbit	Abcam ab 92696
HSP90	anti-rabbit	Cell Signalling 4874
IRE1α (14C10)	anti-rabbit	Cell Signaling 3294
IRE1α [p SER724]	anti-rabbit	Novus-bio NB100-2323
eIF2α	anti-rabbit	Cell Signaling 9722
eIF2α (Ser51), Phospho-	anti-mouse	Cell Signaling 53085

Table 3. Secondary antibody. LI-COR antibodies were diluted at a ratio of 1:20.000, while HRP was employed at a dilution of 1:3.000.

Antibodies name	Species	Distributor
HRP-linked Antibody	anti-mouse IgG	Cell Signalling 7076S
HRP-linked Antibody	anti-rabbit IgG	Cell Signalling 7074S
IRDye 680RD	anti-mouse	LI-COR 926-68070
IRDye 800CW	anti-mouse	LI-COR 926-32210
IRDye 680RD	anti-rabbit	LI-COR 926-68071
IRDye 800CW	anti-rabbit	LI-COR 926-32211

Table 4. Western blot buffers.

Buffers name	Buffers content
1× TBS-Tween pH 7.4	20 mM Tris base, 150 mM NaCl, 0.05 % Tween-20
0.5 M Tris-HCl pH 6.8	0.5 M Tris base, pH 6.8 (30 % HCl, ca. 30 ml)
1.5 M Tris-HCl pH 8.8	1.5 M Tris base, pH 8.8 (30 % HCl, ca. 16 ml)
1× Trans-Blot Turbo Transfer Buffer	20 % 5× Trans-Blot Turbo Buffer, 20 % Ethanol (96 %), 60 % water
10× Running buffer	250 mM Tris base, 1 % SDS, 1.92 M Glycine
Redmix	0.5 M TRIS pH 6.8, 10 % SDS, 10 % Glycerol Bromophenol Blue 4.8 mg / 40 ml, Mercaptoethanol 2.4 ml / 40 ml

Protein bands were detected and quantified using the LI-COR Odyssey Imaging System (LI-COR Biosciences) and ImageQuant System (GE Healthcare). For horseradish peroxidase-coupled secondary antibodies, chemiluminescence was detected with ECL reagent (BioRad) using the ChemiDoc XRS (BioRad). Densitometric measurements were performed with Image Studio Lite (BioRad).

3.4. RNA Isolation

After the cell incubation period, the culture medium was aspirated from 6 cm Petri dishes, and cells were washed once with 1× PBS at 4°C. Next, 1 ml BlueZol reagent (Serva) was added to the Petri dishes. Cells were detached with a cell scraper, collected, and transferred to a 2.0 ml Eppendorf tube. The mixture was left for 5 minutes at room temperature. Then, 200 µl chloroform (Sigma-Aldrich) per 1 ml BlueZol was added, shaken for 15 seconds, and incubated for 3 minutes at room temperature. Samples were centrifuged at 12,000 g and 4°C for 15 minutes, resulting in three phases. The colorless aqueous phase containing RNA was transferred to a new tube.

500 µl isopropanol per 1 ml BlueZol was added and mixed. Tubes were incubated overnight at -20°C for RNA precipitation. The next day, samples were centrifuged for 10 minutes at 12,000 g and 4°C, and the supernatant was removed. The RNA pellet was washed three times with 1 ml 75 % ethanol, vortexed, and centrifuged each time for 10 minutes at 12,000 g and 4°C, discarding the supernatant after each wash. The RNA pellet was dried at 55°C for 10 minutes.

Finally, the RNA was dissolved in 50 μ l RNase-free water, incubated at 55°C for 5 minutes, and placed on ice for 30 minutes. RNA was quantified using NanoVue (GE Healthcare) and stored at -80°C.

3.5. RNA integrity measurement for NGS

For DNase digestion of RNA, we used the Turbo DNA-free Kit (Thermo Fisher Scientific). RNA was diluted to 8 μ g in steril RNase-free water. Next, diluted RNA was mixed with 6.5 μ l of a master mix, consisting of 5 μ l 10 \times buffer and 1.5 μ l Turbo-DNase, to make a 50 μ l solution, which was incubated for 30 minutes at 37°C. Next, 1.5 μ l of 2 U/ μ l Turbo-DNase was added, mixed thoroughly, and incubated for 30 minutes at 37°C. The reaction was stopped with 5 μ l of 10 \times DNase inactivation buffer, incubated for 5 minutes at room temperature with intermittent vortexing, and centrifuged at 10,000 g for 1.5 minutes. The DNA-free RNA supernatant was transferred to a new tube and adjusted to 180 μ l with RNase-free water.

To this, 18 μ l of 3 M sodium acetate and 0.5 μ g/ μ l glycogen were added. After vortexing, 600 μ l ice-cold 100 % ethanol was added, and the RNA was precipitated overnight at -20°C. The mixture was centrifuged at 10,000 g for 30 minutes at 4°C. The pellet was washed twice with 900 μ l 70 % ethanol, centrifuging at 13,000 g for 5 minutes at 4°C. The pellet was dried at room temperature and dissolved in 50 μ l RNase-free water.

RNA integrity and concentration were evaluated using the Agilent 2100 Bioanalyzer with the RNA 6000 Nano Kit (Agilent Technologies). For NGS analysis, RNA requirements were a minimum of 2 μ g, a concentration of at least 50 ng/ μ l, and an RNA Integrity Number (RIN) of 6.8 or higher.

3.6. cDNA Synthesis for qPCR

First, genomic DNA contaminations were removed by DNase digestion. 1 μ g of RNA was used for digestion with 2 DNase (NEB) units in 1 \times reaction buffer. The digestion was performed in a thermocycler (Biometra), incubating for 10 minutes at 37°C, followed by 10 minutes at 75°C for DNase inactivation. Next, the RNA was reverse transcribed in a thermocycler using the master mix described in Table 5 with an initial step at 25°C for 5 minutes, followed by 42°C for 30 minutes, and 95°C for 5 minutes.

Table 5. Master mix components for reverse transcription.

Reaction mix	Initial concentration	(+) RT for 1× μl	(-) RT for 1× μl
H ₂ O		15.47	7.33
First-strand buffer Thermo Fisher	5×	5.71	2.29
DTT Thermo Fisher	100 mM	0.36	0.14
dNTPs Peqlab	10 mM	1.43	0.57
RnaseOut Thermo Fisher	40 U/μl	0.71	0.29
RandomPrimer Thermo Fisher	0.3 μg/μl	0.96	0.38
Reverse Transcriptase Thermo Fisher	200 U/μl	0.36	-
Template (digested 1 μg RNA)		10	4
Total volume in the reaction tube		35	15

3.7. Real-Time quantitative reverse transcription PCR (RT-qPCR)

The master mix was prepared following table 6. Quantitative PCR was conducted with primers listed in Table 8 utilizing the SsoAdvanced Universal SYBR Green Supermix from BioRad and the Applied Biosystems 7900HT Fast Real-Time PCR System, according to the protocol in Table 7. Quantification was performed using the $\Delta\Delta Ct$ method, with 18S RNA as the reference molecule.

Table 6. Master mix for RT-qPCR.

Reagents	Volume (μl)
2× Supermix	6.25
Wasser	3.225
ROX	0.025
Primer sense 10 pmol/μl	0.5
Primer antisense 10 pmol/μl	0.5
cDNA sample	2
Total volume in the tube	12.5

Table 7. RT-qPCR amplification protocol. XPBs primer annealing temperature is 64°C.

	Temperature	Time
40× cycles	95°C	15 minutes
	95°C	30 seconds
	60°C	15 seconds
	72°C	30 seconds
dissociation curve	95°C	1 minute
	60°C	15 seconds
	95°C	30 seconds

Table 8. Designed primers. Below is a list of the RT-qPCR primers.

Gene (human)	Forward sequence	Reverse sequence
18S	CTCAACACGGGAAACCTCAC	CGGACATCTAAGGGCATCAC
MR	TCTGGGCAGAGCTGGCAGAGGTT	AGCATTGCGGGGAAGCTTACCTT
PDK4	TCAAGGAGATCTGAATCTCTACTC	GCTCATCTGATAATGTTTGAAGGC
PRKAB2	GTTTGTATCATGGCAGCAGGAT	GAACTTGTATTGGTGCTCTCCC
MAP3K6	GTGAGAGCTTCAGCATGACCA	GAATGGTCTCCCGGAAATAGCC
SGK1	GAGCGGAATGTTCTGTTGAAGA	CTGGAGAGGCTTGTTGAGAAT
XBPs	CTGAGTCCGAATCAGGTGCAG	ATCCATGGGGAGATGTTCTGG
FOSL2	AACTTTGACACCTCGTCCCG	GATGAATGCACTGCCTGAGC
MMP15	GCGGGGAGATGTTCTGTT	CGAAAGAGCCAGTAGCGGT
SKIDA1	CTTGTACCATCTGGCCTCCG	TCTCAGCGAAACAAGCTCCC

3.8. Glucose Measurement Assay

Glucose concentrations in cell culture media were determined using a photometric assay based on the hexokinase method (Dickson et al., 2019). Media samples were collected and centrifuged at 200 g and 4°C for 5 minutes. Glucose standards (0, 1, 3, 5, 6, 12, 25 mM) were prepared (Sigma-Aldrich). The reaction buffer consisted of TEA buffer (Table 14) supplemented with 2.5 mM MgSO₄, 250 mM triethanolamine hydrochloride, 1.81 mM ATP, 0.65 mM NADP sodium salt hydrate, and 33.04 mU/ml hexokinase + glucose-6-phosphate dehydrogenase (Sigma-Aldrich). Each 5 µl sample or standard was mixed with 100 µl reaction buffer and incubated for 15 minutes at room temperature. Absorbance was measured at 340 nm, and the glucose concentration was proportional to the generated NADPH.

3.9. Lactate Measurement

Lactate measurement follows an enzymatic reaction where lactate dehydrogenase (LDH) oxidizes L-lactate to pyruvate, generating NADH (Smutok et al., 2013). Pyruvate reacts with hydrazine in the buffer, forming pyruvate hydrazine (Bergmeyer, 2012), which reduces free pyruvate concentrations, promoting lactate oxidation. The reaction mix included hydrazine-glycine buffer (pH 9.0, hydrazine hydrate 0.4 M), glycine (0.5 M), LDH (68.5 µg/ml, Roche), and NAD⁺ (4.384 mM, Roche). Standards (0, 1, 2, 4, 10 mM) were prepared using the sodium salt of lactic acid (Sigma-Aldrich). A 200 µl reaction mix was combined with 10 µl of samples or standards and incubated at 37°C for 30 minutes. NADH absorption was measured at 340 nm.

3.10. Caspase-3 Activity Assay

Caspase-3 activity was measured using the following protocol (Schwerdt et al., 2007). Cells were lysed with MOPS buffer (Table 14) for 15 minutes, then centrifuged at 10,000 g for 10 minutes at 4°C. Activated caspase-3 cleaves the fluorogenic substrate DEVD-AFC, with fluorescence directly proportional to caspase-3 activity. The reaction buffer (Table 14) was prepared by mixing 400 µl of 5× reaction buffer, 10 µl of 1M DTT, and 590 µl distilled water. In a 96-well plate, 60 µl of cell lysate, 60 µl of 1× reaction buffer, and 5 µl of 40 µM DEVD-AFC (Biomol ABD) in DMSO were added per well. As blank, 60 µl lysis buffer, 60 µl 1× reaction buffer, and 5 µl DEVD-AFC were used. A calibration curve was established (Table 9), and 125 µl of each calibration probe was pipetted into corresponding wells. Fluorescence (400 nm excitation, 505 nm emission) was measured using a Tecan™, and caspase-3 activity was calculated from the calibration curve using known AFC concentrations.

Table 9. Calibration probes pipetting scheme for caspase-3 activity.

Concentration AFC (µM)	Calibration probes dilutions				
	0	1	2	4	8
80µM AFC (µl)	0	2.5	5	10	20
1× Reaction buffer + Lysis buffer (µl)	200	197.5	195	190	180

3.11. LDH measurement

Plasma membrane permeabilization is a crucial indicator of necrotic cells. Necrosis in tissue culture can be quantified by measuring and comparing lactate dehydrogenase (LDH) activity in cell media and lysates by determining the declining NADH concentrations (Decker and Lohmann-Matthes, 1988). For LDH activity measurement in media, 40 µl of fresh media was pipetted into a 96-well plate, followed by 160 µl of warm LDH buffer (15 ml HEPES-Ringer (Table 14), 0.2 mM NAD hydrate, 1 mM pyruvate). For cell lysate measurements, cells were lysed with MOPS/Triton (pH 7.4), scraped, and centrifuged at 10,000 g for 5 minutes at 4°C. A multi-channel pipette was used for quicker pipetting speed, and 195 µl of preheated (37°C) LDH buffer was fast added to 5 µl of lysate. Measurements were taken on a Tecan Infinite at 37°C, with readings at 334 nm for 30 minutes. LDH activity was calculated using the Beer-Lambert law:

$$E = cde$$

Where (d) is the path length, (c) is the concentration of LDH activity, and (ϵ) is the molar extinction coefficient for NADH (6.11 cm²/μmol). (E) was obtained from the slope of absorbance vs. time for media and lysate samples.

LDH activity was calculated using:

$$LDH \text{ activity} = \frac{(E * V_{well})}{\epsilon * d * V_{probe}}$$

The activity was reported as nmol/min/mL (milliunits/mL).

3.12. Oxygen Consumption Rate and Extracellular Acidification Rate

Measurements were performed using the Agilent Seahorse XFe96 Analyzer (Seahorse Bioscience). HEK-TO-MR cells (8,000–10,000 cells/well) were plated overnight in 96-well Seahorse analyzer plates under specified growth conditions. The next day, cells were stimulated with 10 nM aldo for 24 hours, including tet for MR expression. On the measurement day, cells were washed and incubated for 1 hour with stimulants (aldo, tet) in Seahorse XF DMEM medium (pH 7.4, 1 mM pyruvate, 2 mM glutamine, 10 mM glucose, and 5 mM HEPES) without CO₂.

The sensor cartridge was incubated with XF Calibrant overnight in a 37°C non-CO₂ incubator. The next day, it was extracted, set up with 200 μL sterile water per well, and incubated at 37°C non-CO₂ for 1 hour. Assay parameters for mitochondrial function, ATP production rate, and glycolytic rate were derived by injecting specific inhibitors (Table 10, Figure 4) and using mathematical algorithms for calculation, according to the manufacturer's suggestions. Reagents were added to the corresponding ports, and the utility plate with the sensor cartridge was placed into the Seahorse machine. Each well had three rate measurements. The injection of inhibitors order is shown in Figures 5 and 6. Data was collected from three readings after compound injection and represented as pMoles/min/well or mpH/min/well (y-axis) versus time (x-axis).

Table 10. Stock concentration of inhibitors.

Reagent name	Media	Stock concentration
Oligomycin	630 μM	100 μM
Rot/AA	540 μM	50 μM
FCCP	720 μM	100 μM
2-DG	3000 μM	500 mM

We determined the concentration of inhibitors in optimization experiments and pipetted them according to the scheme in Tables 11 and 12.

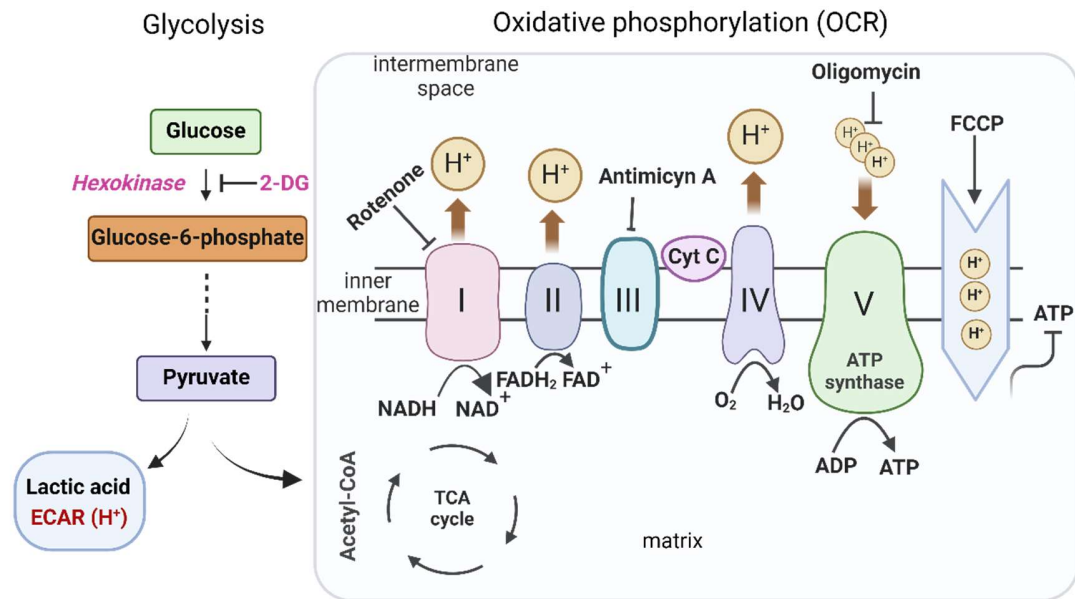


Figure 4. Explanation of Seahorse inhibitors function. Cells generate ATP via glycolysis and oxidative phosphorylation. Seahorse inhibitors disrupt these processes to measure metabolic activity. 2-DG inhibits glycolysis by blocking glucose-6-phosphate formation. Rotenone and antimycin A inhibit mitochondrial complexes I and III, respectively, while oligomycin blocks complex V. FCCP uncouples oxidative phosphorylation by permeabilizing the mitochondrial membrane to protons. The Seahorse assay measures oxygen consumption rate (OCR) and extracellular acidification rate (ECAR) to assess cellular respiration and glycolysis. Created in BioRender. Gadasheva, Y. (2024) <https://BioRender.com/x09e346>.

Table 11. Final concentrations for each port in the sensor cartridge. Each reagent was added to its designated port for a final volume of 200 μL , with Hoechst added to the same port as Rot/AA.

Reagents	Final (μM)	Stock solution μL	Media μL	10 \times Port (μM)	Port volume (μL)
Port A Oligomycin	2	600	2400	20	20
Port B FCCP	1	300	2700	10	22
Port D Rot/AA	0,5	300	2700	5	25
Hoechst (cells dye)	4	6	3000	40	25

Table 12. Reagents preparation for Glycolytic Rate Assay.

Reagents	Final (μM)	Stock solution μL	Media μL	10 \times Port (μM)	Port volume (μL)
Port A Rot/AA	0,5	300	2700	5	25
Port B 2-DG	50	3000	0	500	20
Hoechst	4	6	3000	40	25

3.13. Assay Parameters for Mitochondrial Function

Mathematical calculations were applied to derive the measurements (Figure 5). Basal respiration represents the oxygen consumption rate without inhibitors. The rate of ATP production is assessed by introducing oligomycin, which inhibits ATP synthase and ATP-linked respiration. Proton leak, indicating the remaining basal respiration is not coupled to ATP production, is also measured. Maximal respiration represents the maximum oxygen consumption rate achieved by adding the uncoupler FCCP. Spare respiratory capacity indicates the cell's potential to increase energy demand and is calculated as a percentage of maximal respiration relative to basal respiration (Figure 5). Non-mitochondrial respiration refers to oxygen consumption that persists due to specific cellular enzymes continuing to utilize oxygen even after the introduction of rotenone and antimycin A. This aspect is crucial for obtaining precise mitochondrial respiration measurements and is calculated by taking the minimum rate measurement observed after introducing Rot/AA.

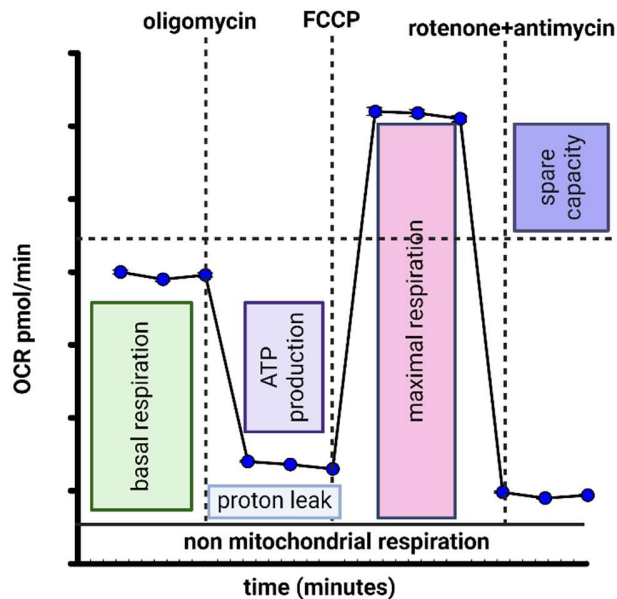


Figure 5. The Agilent Seahorse XF Cell Mito Stress Measurement. Baseline OCR was measured without pharmacological agents. Injection 1 (Oligomycin, 2 μ M) inhibited ATP synthase to measure ATP production and proton leak. Injection 2 (FCCP, 1 μ M) uncoupled oxidative phosphorylation to assess maximum mitochondrial respiratory capacity. Injection 3 (Rot/AA, 0.5 μ M) blocked mitochondrial electron transport. Created in BioRender. Gadasheva, Y. (2024) <https://BioRender.com/i90f527>.

3.14. Glycolytic Rate Assay Parameters

Agilent Technology derived the total Proton Efflux Rate (PER in pmol of H^+ /min) from the ECAR measurement (in mpH/min) based on pH range, buffer capacity (BF), chamber

volume (Vol), and a volume scaling factor (Kvol) from lactate production measurements. Glycolysis-based Proton Efflux Rate (glycoPER) was calculated by subtracting mitochondrial PER (mitoPER) from the total PER (basal PER, last total PER measurement before Rot/AA injection). Mito PER was calculated by determining mitoOCR multiplied by a CO₂ contribution factor (CCF). Where mitoOCR is basal OCR subtracted OCR after introducing Rot/AA to suppress mitochondrial acidification. Agilent's calculations provided the following parameters. Compensatory PER is a maximum glycoPER measurement after Rot/AA injection. Post-2-DG PER is a minimum glycoPER measurement after 2-DG injection (Figure 6). Since one glucose molecule yields two molecules of lactate and ATP, glycoPER equals glycoATP production rate. Mitochondrial ATP (mitoATP) was calculated using OCR_{ATP}, and post-oligomycin injection was determined. It requires additional parameters: multiplied by two and the P/O ratio (derived by Agilent using various substrates), corresponding to the reduced number of ATP molecules per oxygen atom.

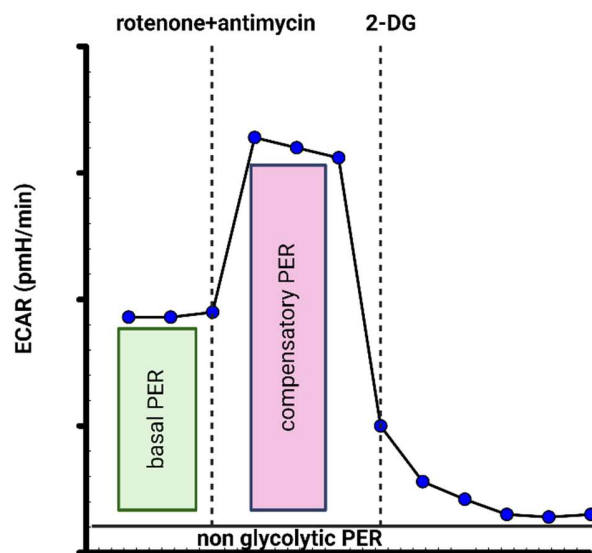


Figure 6. Glycolytic Rate assay. Rot/AA at a concentration of 0.5 μ M was introduced to inhibit the mitochondrial source of acidification, thereby triggering compensatory glycolysis. 2-DG at 50 μ M, a hexokinase inhibitor, was used to halt glycolysis. This enabled the assessment of non-mitochondrial and non-glycolytic origins of acidification or proton production. Created in BioRender. Gadasheva, Y. (2024) <https://BioRender.com/a88y153>.

3.15. Autophagic Flux

For autophagosome formation evaluation, cells were treated with lysosomal degradation inhibitors, aloxistatin (10 mg/ml, Selleckchem), and pepstatin A (10 mg/ml, Sigma) for 24 hours during the stimulation phase. These inhibitors prevent autophagosome-lysosome

fusion, allowing the measurement of LC3B-II protein levels. The difference in LC3-II levels between treated and untreated cells indicates autophagic flux. An elevated flux shows increased LC3-II in the presence of inhibitors (Klionsky, 2020). Quantification of LC3-II was performed using Western blotting with dilution 1:2000 anti-rabbit LC3B-II antibodies (Table 2), incubated overnight at 4°C. The appropriate secondary antibody was used following the standard Western blot protocol.

3.16. Measurement of ATP Content in Cells

The ATP Bioluminescence Assay Kit HS II (Roche) was used according to the manufacturer's instructions. For measurements, cells were lysed with 50 µL MOPS buffer. MOPS buffer without samples served as control. A dilution buffer from the kit (50 µL) was used as a blank. For analysis, diluted samples (50 µL) or ATP standards were added to a white 96-well plate. Luciferase activity was measured with the Berthold Tristar LB 941 illuminometer and Mikrowin 2000 software, with a 1-second delay and 5-second integration period.

3.17. Immunofluorescence

Multitest slides (6 mm diameter, Dunn Labortechnik GmbH) were coated with preheated poly-L-lysine (0.1 mg/ml). After 5-10 minutes, excess poly-L-lysine (Sigma-Aldrich) was aspirated, and the slides were washed with media. Cells were incubated for 5 hours at 37°C, and 10 nM aldosterone and 200 µM SIN-1 were added for 1 hour at 37°C after MR expression activation. Cells were fixed with 40 µl of 4 % formaldehyde (Fischer Scientific) for 15 minutes at room temperature (Table 13).

Table 13. Prepared reagent solutions for immunofluorescence.

Solutions	Composition
4 % paraformaldehyde	10 g paraformaldehyde in 250 ml 1× PBS, pH 7.4, heated to 65°C, and added NaOH until fully dissolved
Glycine solution 100 mM	in 1× PBS, pH 7.4
Blocking solution	10 % goat serum, 10 % donkey serum, 1 % BSA in 1× PBS
DAPI 1 µg/ml	diluted 1 µl DAPI (10 mg/ml) stock solution in 10 ml PBS

Cells were washed three times for 5 minutes each with 1× PBS, permeabilized with 1 % TritonX-100/PBS for 30 minutes, and washed again with PBS/1 % SDS/100 mM glycine followed by PBS/100 mM glycine (Serva). Blocking was done with PBS/10 % goat serum/1 % BSA for 30 minutes. The primary antibody, anti-Myc-Tag (monoclonal mouse 2276,

1:1000, Cell Signaling) in PBS/1 % goat serum/1 % BSA, was applied (40 μ l per well) and incubated overnight at 4°C. The next day, three 5-minute washes with 1 \times PBS were performed. The secondary antibody, Oregon Green 488 BAPTA-2 (O6809, Molecular Probes), was applied at 1:1000 dilution for 45 minutes at room temperature in the dark. Washing steps were repeated. Cells were stained with DAPI (3 μ g/ml, Sigma-Aldrich) and washed with 1 \times PBS. Dako fluorescence mounting medium (Agilent) and coverslips were applied. Background fluorescence was assessed using samples treated only with secondary antibodies. Immunofluorescence analysis was conducted using the BioZero BZ-8100 fluorescence microscope (Keyence).

3.18. NGS Data Analysis

After DNA digestion and RNA integrity confirmation via Bioanalyzer, our samples were sequenced at Novogen. Our NGS data analysis team used EdgeR and DESeq2 for differential expression analysis. We continued selecting genes with more than 5 FPM (Fragments per Million mapped). EdgeR and DESeq2 calculated Log₂ fold change and FDR (false discovery rate). Differential expression (DE) categories were defined as -1 (down-regulation), 0 (no regulation), and 1 (up-regulation), with an FDR cut-off of lower than 0.05. We used an overlapping column (applies both EdgeR and DESeq2) indicating whether a gene was found in DESeq2 and EdgeR results (1) or not (0).

3.19. Statistical Analysis

Data are presented as mean \pm standard error of the mean. Students' t-test, One Way ANOVA, or signed rank test were used as applicable according to pre-test data analysis by SigmaPlot 14. T-tests were unpaired and two-tailed unless stated otherwise in the text. Grubbs tests were performed to identify outliers. A p-value < 0.05 was considered statistically significant.

3.20. Buffers

All buffers used in the experiments above are represented in Table 14.

Table 14. Buffer's content.

Buffers name	Buffers content
MOPS-Triton pH 7.4	20 mM MOPS, 0.01 % Triton X-100
RIPA	150 mM NaCl, 10 mM Tris base (pH 7.4), 1 % NP-40, 0.1 % SDS, 1 % Na-deoxycholate, 0.1 % Triton X-100, 1 mM EDTA, 1 mM Na-Orthovanadate, 1:500 Protease-Inhibitor-Cocktail
HEPES buffer pH 7.4	24 mM NaHCO ₃ , 0.8 mM Na ₂ HPO ₄ × 2H ₂ O, 0.2 mM Na ₂ HPO ₄ × 2H ₂ O, 86.5 mM NaCl, 5.4 mM KCl, 1.2 mM CaCl ₂ × 2H ₂ O, 0.8 mM MgCl ₂ , 20 mM Hepes, 11 mM Glucose
TEA pH 7.5	2.5 mM MgSO ₄ × 7H ₂ O, 250 mM triethanolamine
10× PBS pH 7.4	137 mM NaCl, 2.7 mM KCl, 8.1 mM Na ₂ HPO ₄ × 2H ₂ O, 1.5 mM KH ₂ PO ₄
5× Caspase reaction buffer pH 7.4	50 mM PIPES, 10 mM EDTA, 0.5 % CHAPS
EDTA pH 7.1-7.3	0.4 g EDTA-Titriplex III, 16 g NaCl, 0.4 KCl g, 2.3 g Na ₂ HPO ₄ × 2H ₂ O, 0.4 g KH ₂ PO ₄

3.21. Software/Programs

The study employed the following software tools for result analysis. Additionally, internet information platforms and programs were utilized in the research (Table 15).

Table 15. Software/Web Tools

Software name	Distributor
BioRad ImageLab Software 6.1	BioRad
Casy software 2021	OMNI life science
Win Image Studio Lite 5.2.5	LI-COR Biosciences
Mikrowin 2000	Berthold Technologies
SigmaPlot 14	Systat Software
Seahorse Wave Desktop V2.6	Agilent Technologies
Agilent 2100 Expert BioAnalyser	Agilent Technologies
7900 SDS v2.4.1 software	Applied Biosystems
Primer-Blast	Primer Blast
NCBI	database
Nucleotide- Blast	Nucleotide-Blast
BioRender	Created in https://BioRender.com

3.22. Devices

Table 16 lists all the machines and devices used in the laboratory.

Table 16. Device/Equipment.

Device name	Distributor
Safety cabinet Herasafe 2025	Thermo Fischer Scientific
Thermoshaker TS-100C	Biosan
Incubator Heracell	Thermo Fischer Scientific
CASYworX 1.2 TT-2BA-1000	OMNI Life Science GmbH
NanoVue spectrophotometer	GE Healthcare
Tecan Sunrise Microplate reader	Tecan
Tecan Infinite Microplate reader	Tecan
Ultrasound sonicator	UP100H Hielscher
Gel electrophoresis chambers	Biometra
Trans-Blot-Turbo-Transfersystem	BioRad
ChemiDoc XRS	BioRad
ChemiDoc Imaging System	BioRad
Vortex Mixer (GENIE2)	Scientific Industries
Thermocycler PCR Module 96 070-911	Biometra
7900HT RT PCR System 384-Well Block	Applied Biosystems
Bioanalyzer 2100	Agilent
Biofluorescence Bertold Tristar LB 941	Berthold Technologies
UV-Transilluminator M-26V	UVP BioDoc-It
Multipipette	Integra Bioscience
Fluorescence microscope BioZero 8100	Keyence
Centrifuge Heraeus Fresco 21	Thermo Fischer Scientific
AirflowControl MC6	Waldner
Optical microscope	Ernst Leitz Wetzlar
Vacuum pump	KNF Laborport
Water bath Alpha	Lauda

4. Results

4.1. Metabolic Shifts in HEK Cells Under Aldo/MR stimulation

New studies have shed light on the potential influence of MR in regulating glucose and energy metabolism (Jia et al., 2021; Wei et al., 2020). In our pursuit of unraveling fundamental metabolic parameters, a series of experiments focused on measuring glucose consumption was conducted (Figure 7).

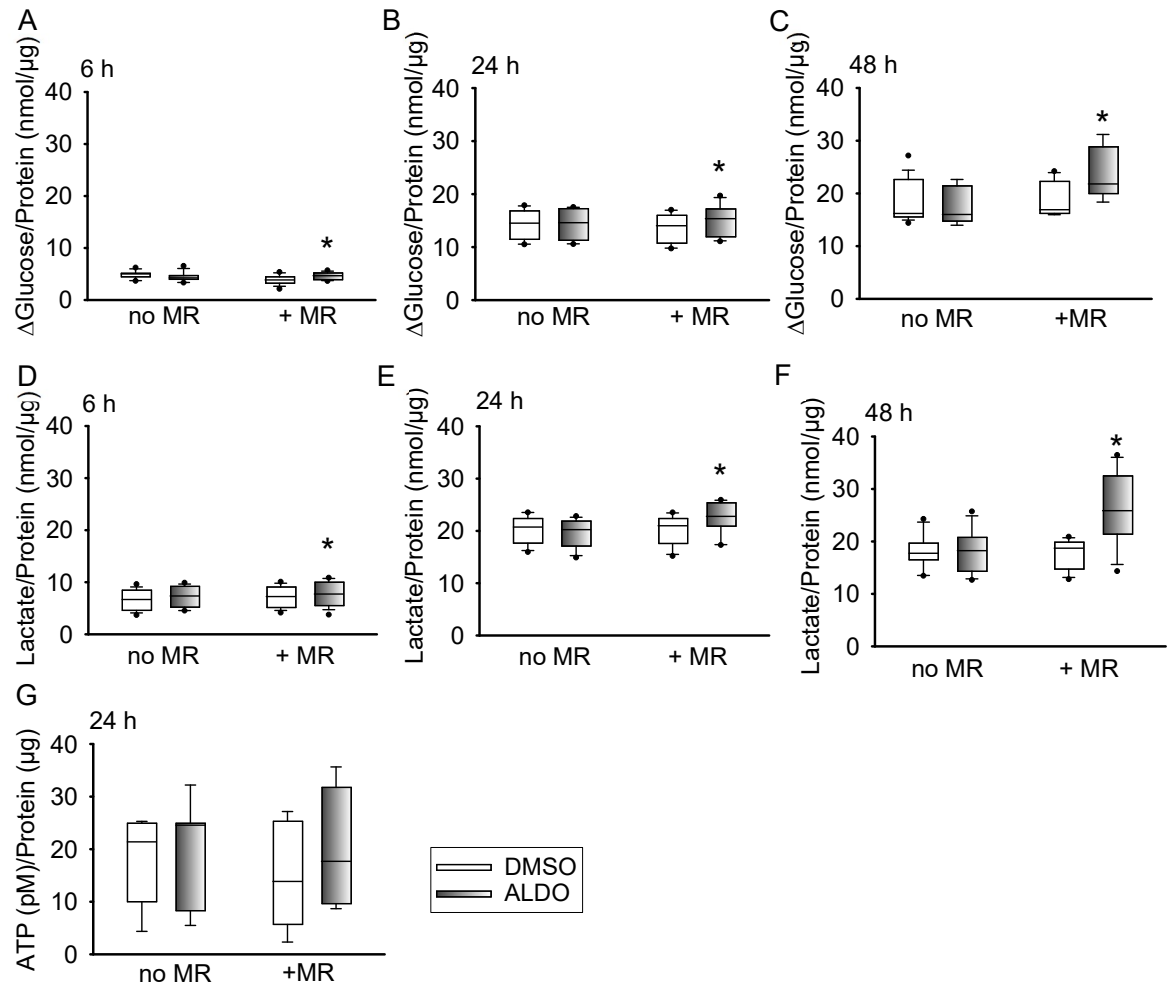


Figure 7. Metabolic profiling of HEK cells overexpressing MR. The manipulation of MR presence in these cells involved a 10 nM aldo stimulus, and their metabolic responses were contrasted with those of a control group (0.1 % dimethyl sulfoxide (DMSO-vehicle)). The cells were cultured in Dulbecco's Modified Eagle Medium (DMEM) containing 5.5 mM glucose. Glucose measurement followed with time points (6 h (A), 24 h (B), and 48 h (C)). Additionally, the same time points for lactate measurement were used (6 h (D), 24 h (E), and 48 h (F)). Additionally, ATP was measured (G) after 24 h; N=4, n=12, *p<0.05 indicates a comparison between the control group (DMSO) vs. treatment group (10 nM aldo).

The hexokinase assay disclosed increased glucose consumption (Δ glucose) of MR-overexpressing HEK cells when exposed to 10 nM aldo, compared to the control group treated with DMSO. This effect was consistently observed at various time points, precisely at 6 hours (Figure 7 A), 24 hours (Figure 7 B), and 48 hours (Figure 7 C) post-stimulation.

Moreover, we continued with quantifying lactate production. An elevation in lactate production was observed in MR-overexpressing HEK cells following 10 nM aldo stimulation at the time points mentioned above (Figure 7 D, 7 E, and 7 F).

Importantly, cells lacking MR expression displayed no significant differences in glucose consumption and lactate production between the control group and the aldo-stimulated cells.

In addition to these results, luciferase activity assays were employed to assess total ATP production in MR-overexpressing HEK cells. These measurements indicated no biologically significant increase or decrease in ATP production in cells stimulated with 10 nM aldo (Figure 7 G) compared to control HEK cells subjected to DMSO stimulation and MR overexpression. Notably, ATP levels remained consistent with cells lacking MR expression in the aldo-stimulated and DMSO-stimulated groups.

4.1.1. Mitochondrial Function Assessment, Experimental Parameters

In cells subjected to 10 nM aldo stimulation for 24 h in the presence of MR, a lower baseline oxygen consumption rate was observed compared to control cells treated with vehicle only (Figure 8 A, B). The baseline of oxygen consumption was adjusted by subtracting the oxygen consumed by processes not involving mitochondria (non-mito O₂, Figure 8 A). The level of non-mito O₂ was slightly decreased, indicating a shift in overall oxygen consumption in the cells under the aldo treatment. Notably, cells lacking MR but exposed to aldo and DMSO-treated control cells showed no significant alterations in mitochondrial measured parameters (Figure 8 B, D), except non-mitochondrial O₂ consumption, where aldo had an influence per se without MR. Aligning with baseline oxygen consumption rate findings, cells treated with 10 nM aldo exhibited increased spare respiratory capacity. At the same time, maximum respiration (max) remained unchanged when comparing aldo-stimulated cells without MR and control cells (Figure 8 A, B). Additionally, the spare capacity of cells without aldo and MR remained unchanged (Figure 8 B). The measurement of ATP production, specifically the ATP produced by mitochondria, decreased in aldo-stimulated cells, suggesting a shift between metabolic pathways. However, the proton leak, representing

protons migrating into the mitochondrial matrix without contributing to ATP production, did not increase in any treated groups (Figure 8 C, D).

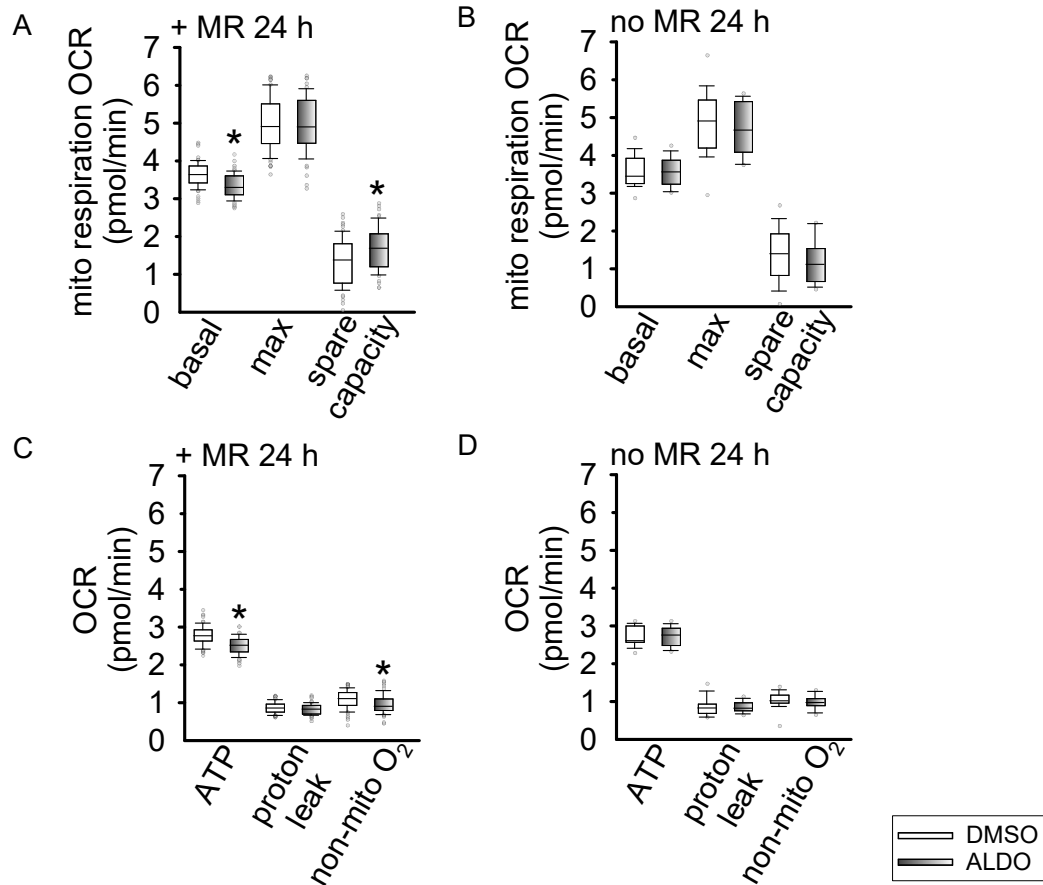


Figure 8. Mitochondria functionality in MR. 10 nM aldo stimulation for 24 hours decreased basal respiration and mitochondrial ATP production (A, C) while increasing spare respiratory capacity (A), indicating a shift in oxygen consumption in MR-expressing cells. Maximal respiration and proton leak remained unchanged (A, C). In MR-lacking cells (B, D) and MR-expressing cells stimulated with DMSO as the control (A, C), there were no changes except for a decrease in non-mitochondrial oxygen consumption (non-mito O₂) (C, D). N=5, n=57-63, *p < 0.05.

4.1.2. Proton Efflux Rate in MR-Overexpressing HEK Cells

Our focus shifted to evaluating the extracellular acidification rate (ECAR), a metric reflecting changes in the glycolytic pathway (Figure 9). Notably, before the detection phase, the cells underwent a one-hour incubation in Seahorse XF DMEM medium to stabilize measurements and minimize pH fluctuations. In MR-expressing cells, the basal Proton Efflux Rate (PER) increased in the presence of aldo, indicating heightened acidification (Figure 9 A). This was due to an increase in the glycolytic rate. Conversely, cells treated

with DMSO exhibited lower glycolytic rates and total PER. This method enabled us to evaluate the specific contributions of glycolysis and mitochondria to the overall PER. The results indicated that in aldo-treated samples, glycolytic PER (glycoPER) increased, while mitochondrial PER (mitoPER) decreased. Upon halting mitochondrial function, a compensatory glycolysis (compen. gly) process led to a more significant proton efflux in aldo-stimulated cells (Figure 9 B). Following the introduction of 2-DG and Rot/AA, post-acidification resulting from other cellular sources was measured (Figure 9 A, 2-DG). No noticeable difference was observed between aldo and DMSO-treated cells after employing 2-DG. This analysis indicated an increased production of protons stemming from the glycolytic pathway in aldo/MR-expressing cells.

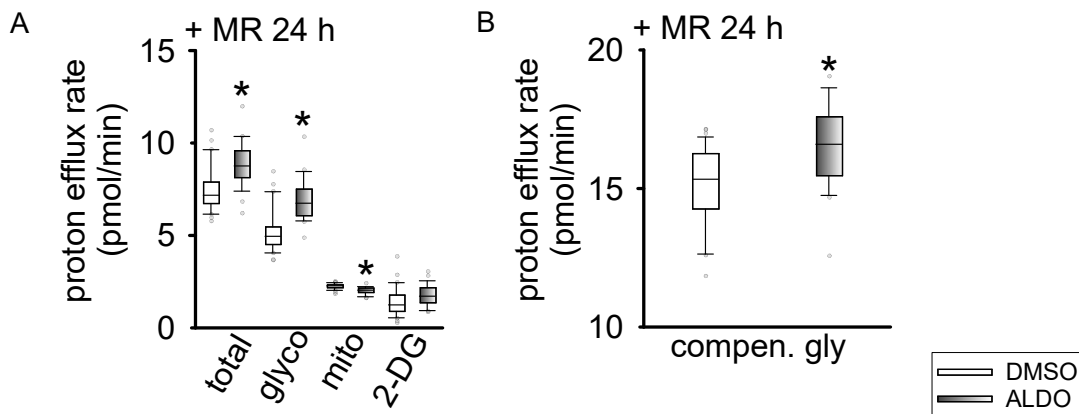


Figure 9. The proton efflux rate from the glycolytic pathway. Applying 10 nM aldo had notable effects on overexpressed MR HEK cells, increasing total (basal) PER, glycoPER, and compensatory glycolysis (A). Rot/AA was used to quantify PER from glycolysis, revealing heightened acidification due to increased proton generation in the glycolytic pathway (B). By inhibiting both mitochondrial and glycolytic acidification sources, the contribution of other potential sources was evaluated using 2-DG. No significant differences were observed between aldo-treated and DMSO-treated cells in post-2-DG (A); N=3, n=25-23, *p < 0.05.

4.1.3. Distinguishing Between ATP Production Pathways

Our goal was to evaluate the shift in ATP production between two fundamental pathways, oxidative phosphorylation (OXPHOS) and glycolysis. To this end, we sequentially introduced two inhibitors (oligomycin and Rot/AA) during real-time Seahorse measurements (Figure 5). This step allowed us to account for acidification associated with mitochondria and, when combined with the PER data, facilitated the calculation of the glycoATP Production Rate. While the total ATP production remained unchanged, a shift towards the glycolytic pathway was observed, indicated by the lowered mito ATP production (Figure 10 A). At the same time, glycolysis also increased ATP production (Figure 10 A). These

observed changes were explicitly associated with cells stimulated with 10 nM aldo in the presence of MR. No such alterations were observed in the control groups, including DMSO-stimulated cells with MR (Figure 10 B) and cells without MR exposed to DMSO and 10 nM aldo. Importantly, it was emphasized that the effect was not mediated by aldo alone but rather was facilitated by MR.

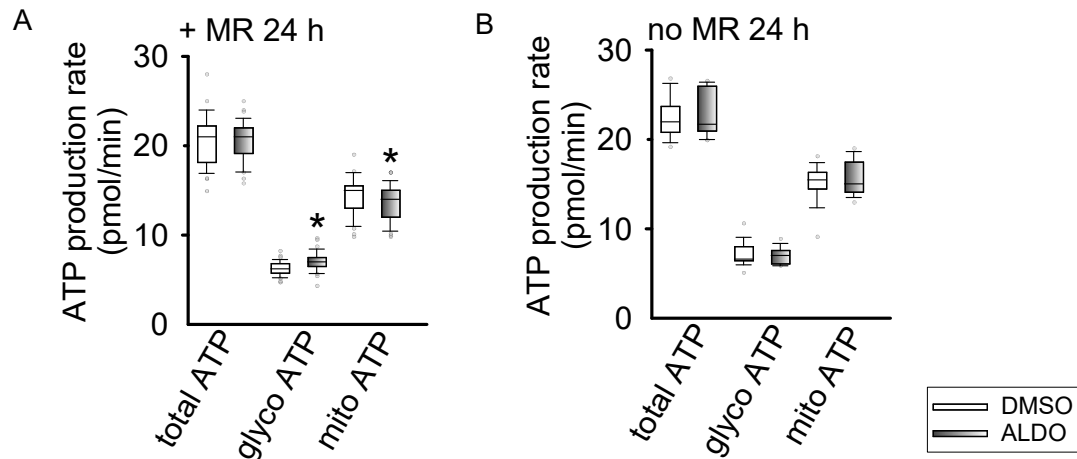


Figure 10. Measurement of pathways contributing to ATP production. Notably, there were no significant changes in overall ATP production (A). However, there was a shift towards the glycolytic pathway, reducing mitoATP production (A). These observed changes are linked explicitly to cells stimulated with 10 nM aldo in the presence of the MR. In contrast, control groups, including DMSO-stimulated cells with MR (A) and those lacking MR for both DMSO and 10 nM aldo (B), showed no alterations; N=4, n=38-39; *p < 0.05.

4.2. Aldo/MR Target Genes

We conducted an NGS analysis followed by qPCR experiments to identify MR target genes in our tetracycline-inducible MR-overexpressing HEK cells. MR induction was confirmed by comparing two control groups: one with 0.25 μ g/ml tetracycline, where MR expression increased approximately tenfold after tetracycline incubation, and the other without tetracycline, where no expression was detected (Figure 11 A, B). Subsequently, MR protein expression was validated. A clear band was observed in samples treated with DMSO and 0.25 μ g/ml tetracycline, indicating MR protein expression. Conversely, distinct bands of MR protein were visible in the sample groups treated with DMSO and subjected to tetracycline incubation. MR expression confirmation also extended to aldo-stimulated samples, where the band appeared as a smear, suggesting the characteristic posttranslational modifications associated with MR protein under aldo stimulation (Figure 11 C).

Furthermore, NGS data analysis using EdgeR and DESeq2 to compare 10 nM aldo/MR-regulated samples against DMSO-treated samples revealed differential expression of 1440 protein-coding genes, as well as the genes of non-coding RNA and pseudogenes with FDR analysis for the significance (Figure 12). Notably, several kinases were highly regulated among these genes, including PDK4 (Pyruvate Dehydrogenase Kinase 4), a critical regulator of cellular energy metabolism. Its expression significantly increased following stimulation with 10 nM aldo compared to the control condition.

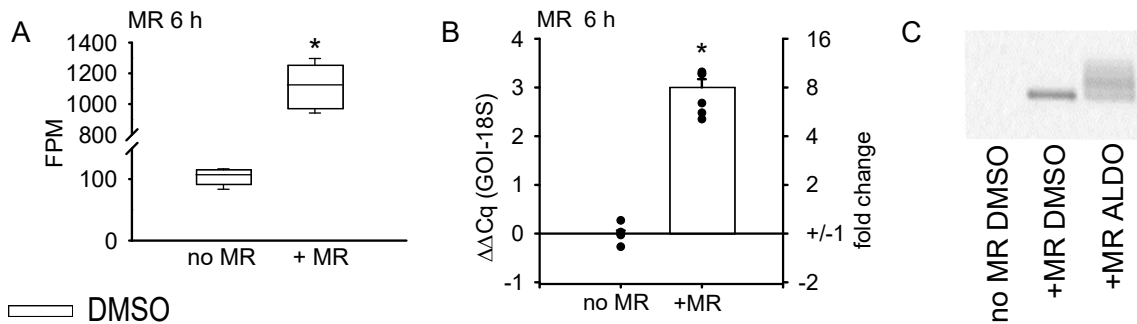


Figure 11. Validation of the T-Rex system efficiency. We compared DMSO samples with and without tetracycline to induce MR expression. In our 0.25 $\mu\text{g/ml}$ tetracycline-inducible MR HEK cells, MR gene expression increased ~ 10 -fold (A), confirmed by qPCR (B); N=6, n=12, * $p < 0.05$. Western blot showed no band in cells not stimulated with tetracycline (no MR DMSO), while tetracycline-treated DMSO samples displayed a distinct band. A smear band appeared after 10 nM aldo stimulation (C); N=3, n=6, * $p < 0.05$.

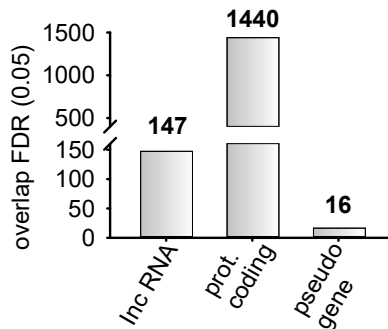


Figure 12. False discovery analysis of genes from NGS data. We utilized EdgeR and DESeq2 statistical tools to assess the significance of protein-coding genes in samples DMSO vs. aldo (FDR < 0.05), N=6, n=12.

Additionally, MAP3K6 (Mitogen-Activated Protein Kinase Kinase Kinase 6), PRKAB2 (AMP-Activated Protein Kinase Beta 2 Non-Catalytic Subunit), and SGK1 (Serum/Glucocorticoid Regulated Kinase 1) were among the highly regulated genes related to metabolism regulation in HEK cells. The induction of metabolic kinases by aldo/MR was further

confirmed through qPCR. Additionally, we validated the regulation of the known MR target gene, TSC22D3 (Figure 13 A-E). A more in-depth analysis of the RNA-seq data revealed that the isoforms PDK1, PDK2, and PDK3 were not regulated by 10 nM aldo (Figure 14).

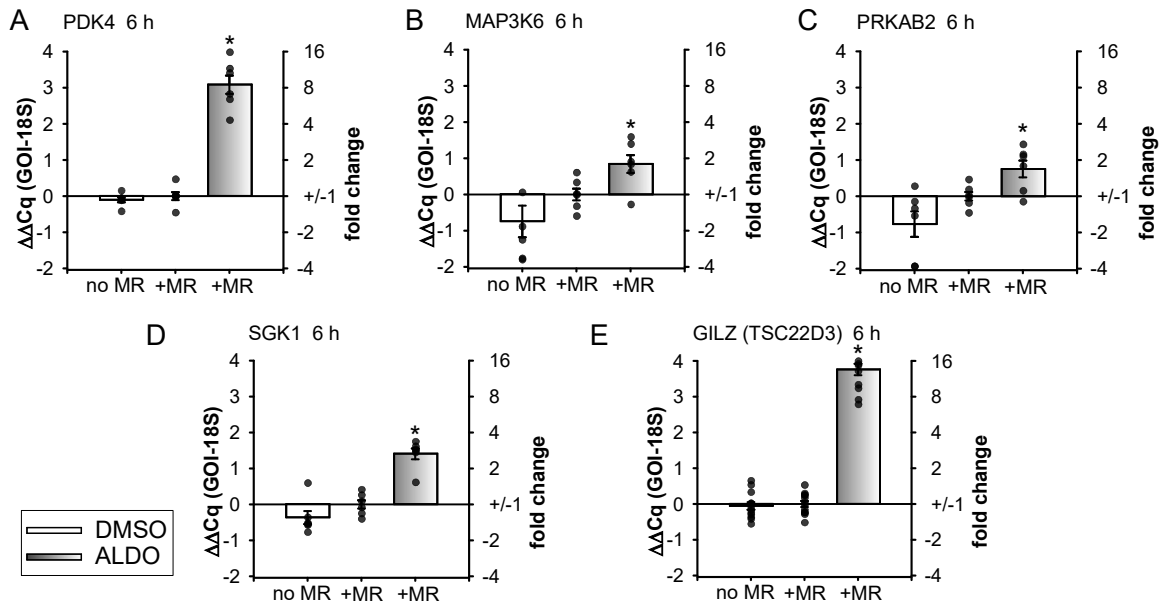


Figure 13. Detection of metabolic genes expression in MR-overexpressing HEK cells. Notably, genes such as MAP3K6, PRKAB2, SGK1, and PDK4 emerged as candidates influenced by the induction of the MR during 24 h tetracycline incubation and 6 h incubation period with 10 nM aldo. The target gene GILZ (TSC22D3) expression was used as an internal control for the MR-overexpressing system; N=6, n=12, * $p < 0.05$.

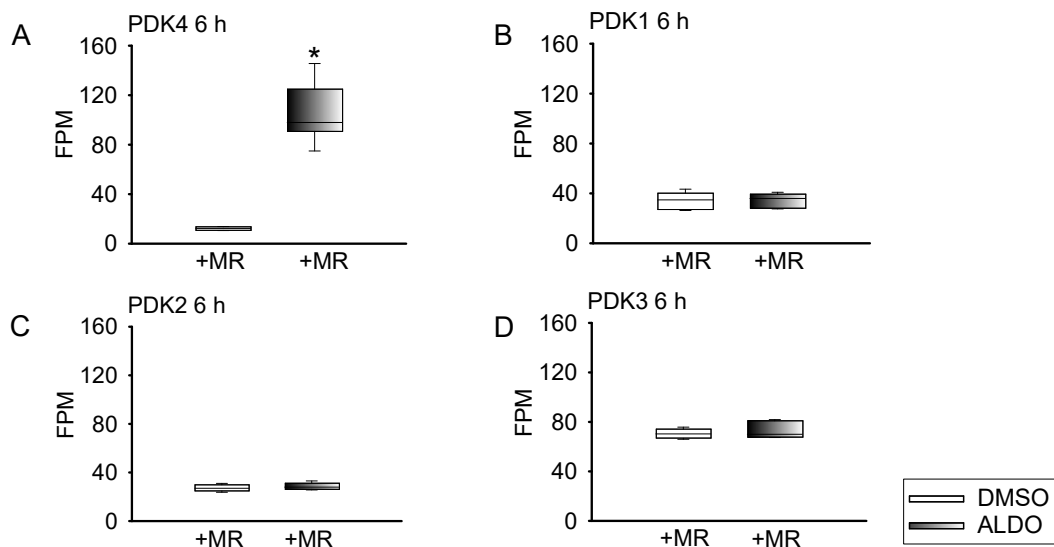


Figure 14. Regulation PDK isoforms. Expanding the inquiry into glucose metabolism regulation, an in-depth analysis of RNA-seq data excluded the regulation of PDK1, PDK2, and PDK3 isoforms by 10 nM aldo in HEK cells after a 6 h incubation, thus emphasizing the regulation of PDK4 under aldo/MR (A-D); N=6, n=12, * $p < 0.05$.

Only PDK4 expression was upregulated in Aldo-treated samples in the presence of MR activation, confirming its regulation by the Aldo/MR signaling pathway.

4.3. PDK4 Protein Upregulation by Aldo/MR

We observed an increase in the protein expression of PDK4 in HEK cells under 10 nM Aldo/MR stimulation after 24 hours, where PDK4 protein expression responded to Aldo stimulation (Figure 15 A, D). In samples without MR activation, the levels of PDK4 protein expression corresponded to control levels (DMSO), indicating the absence of any regulation (Figure 15 A, D).

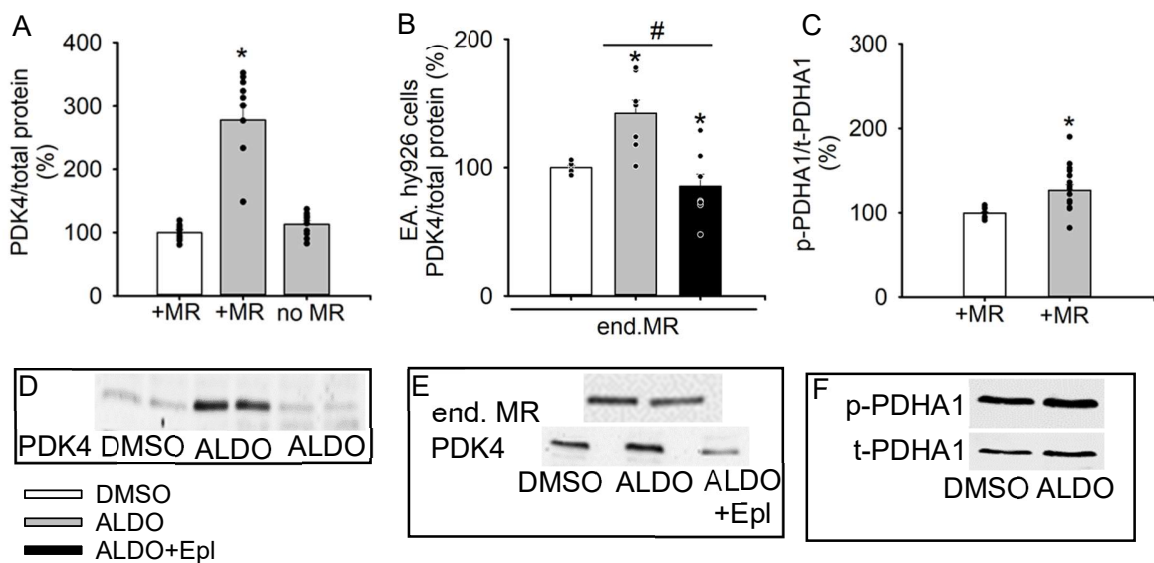


Figure 15. PDK4 upregulation confirmation. PDK4 protein expression increased after 24 hours of incubation with 10 nM Aldo in the presence of MR in HEK cells but not in cells lacking MR (A, D; N=3, n=8-12, *p<0.05). In EA.hy926 cells with endogenous MR (E), 10 nM Aldo altered PDK4 expression (B, F; N=3, n=4-7, *p<0.05). Administering 2 μ M Eplerenone (Epl) one hour before Aldo reduced PDK4 expression, confirming its dependence on MR activity (B, F; Aldo vs. Aldo+Epl #p<0.05). Additionally, p(S293)-PDHA1 expression increased in Aldo-stimulated cells, indicating a metabolic shift from the TCA cycle to anaerobic glycolysis (C, G); N=9, n=18, *p<0.05.

Furthermore, we examined the expression of PDK4 protein levels in endothelial-like cells (Ea.hy926). We evaluated the endogenous expression of MR in these cells without adding any stimulants (as illustrated in Figure 15 E), revealing a robust presence of MR protein. Western blot analysis demonstrated elevated protein levels of PDK4 in Ea.hy926 cells (Figure 15 B, E). To emphasize the specificity of MR regulation on PDK4 protein levels in EA.hy926 cells, we introduced an MR antagonist, 2 μ M eplerenone. Upon comparing two sample groups—10 nM Aldo-stimulated cells and 10 nM Aldo-stimulated cells with a 1-hour

pre-treatment of 2 μ M eplerenone, we observed a reduction in the Aldo/MR effect in the presence of eplerenone stimulation (Figure 15 B, E).

To assess PDK4 activity, we analyzed the phosphorylation of the downstream PDK4 target, PDHA1 (Pyruvate dehydrogenase E1 component subunit alpha), which leads to a metabolic shift of glucose metabolism from the tricarboxylic acid (TCA) cycle to anaerobic glycolysis. The p-(S293)-PDHA1 expression was increased in Aldo-stimulated cells (Figure 15 C, F). These findings collectively suggested that the activated MR acts as an upstream regulator of PDK4 and may modulate energy metabolism.

4.4. Additional Analyses of NGS Data

Furthermore, our Next-Generation Sequencing (NGS) data examined genes implicated in glucose metabolism. In Aldo/MR stimulated cells, we observed the presence of genes associated with heightened glucose uptake. Specifically, we detected increased expression of GLUT 3 (Solute Carrier Family 2, Facilitated Glucose Transporter, SLC2A3) and SWEET1 (Solute Carrier Family 50, Member 1, SLC50A1) (Figure 16 A, B). Additionally, the interaction between Aldo and MR suppressed the expression of PDP1, a gene responsible for the dephosphorylation of the PDHA1 complex (Figure 16 C). We also examined gene regulation associated with autophagy and apoptosis (Figure 17) in relation to the MR.

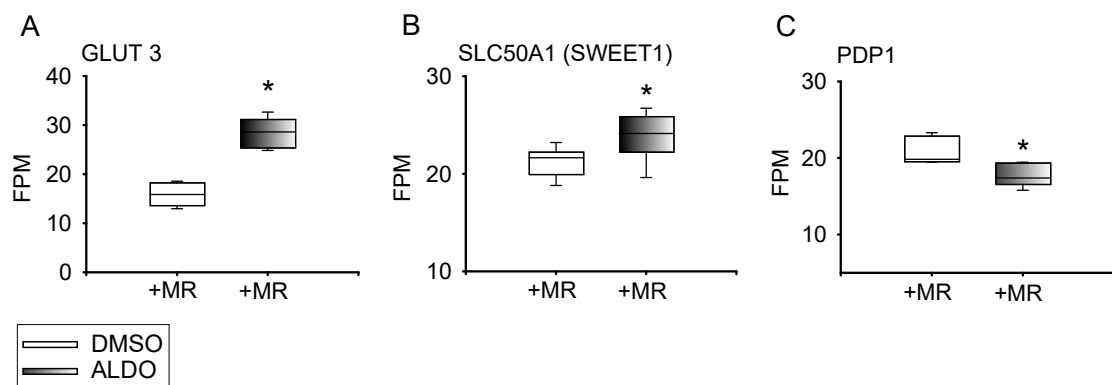


Figure 16. Genes involved in glucose metabolism. Samples stimulated with 10 nM Aldo/MR for 6 hours exhibited elevated levels of GLUT 3 and SWEET1 (A, B), alongside downregulation of PDP1(C) compared to control samples treated with DMSO; N=6, n=12, *p < 0.05.

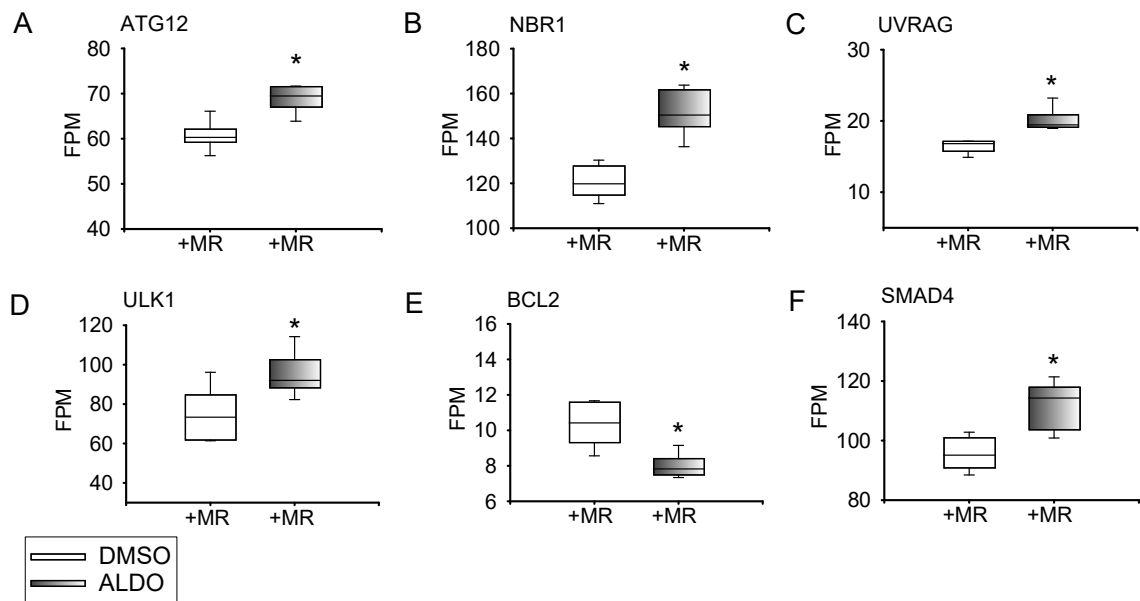


Figure 17. Genes involved in autophagy and apoptosis. The genes ATG12 (autophagy-related 12), NBR1 (autophagy cargo receptor), UVRAG (UV radiation resistance-associated gene protein), ULK1 (Unc-51-like kinase 1) BCL2 (from B-cell lymphoma 2, anti-apoptotic), and SMAD 4 (SMAD family members) were upregulated following a 6-hour incubation with 10 nM aldo; N=6, n=12, *p < 0.05.

4.5. Aldo/MR Interaction Initiates ER-stress Signaling Pathway

The investigation broadened its scope to examine the possible induction of the Unfolded Protein Response (UPR) due to Endoplasmic Reticulum (ER) stress, subsequently leading to the activation of apoptosis and autophagy. This process could be attributed to the upregulation of PDK4 expression. The examination conducted in HEK-TO-MR cells aimed to assess the expression of ER stress markers. The UPR, consisting of three primary pathways regulated by upstream effectors, encompasses Inositol-Requiring Enzyme α (IRE α), Protein Kinase R-like ER Kinase (PERK), and Activating Transcription Factor 6 (ATF6). NGS data analysis unveiled the upregulation of ATF6 in response to the interaction with 10 nM aldo/MR after a 6-hour treatment, indicating the activation of a pathway associated with ER stress response (Figure 18 A). Another conservatively regulated pathway in response to 10 nM aldo within 6 hours was the gene ERN1, which encodes the protein IRE α (Figure 18 B). Similarly, our NGS data revealed that aldo/MR regulates IP3R1, which is localized in the membrane of the endoplasmic reticulum (Figure 18 C). Given the association of ER stress with an enhanced translational response, protein expression was further evaluated through Western blot in HEK cells expressing MR. The results indicated

that the presence of 10 nM aldo/MR within 24 hours increased the expression of the IRE α protein. In contrast, samples lacking MR induction did not show alterations in the expression of the target protein (Figure 19 A, C).

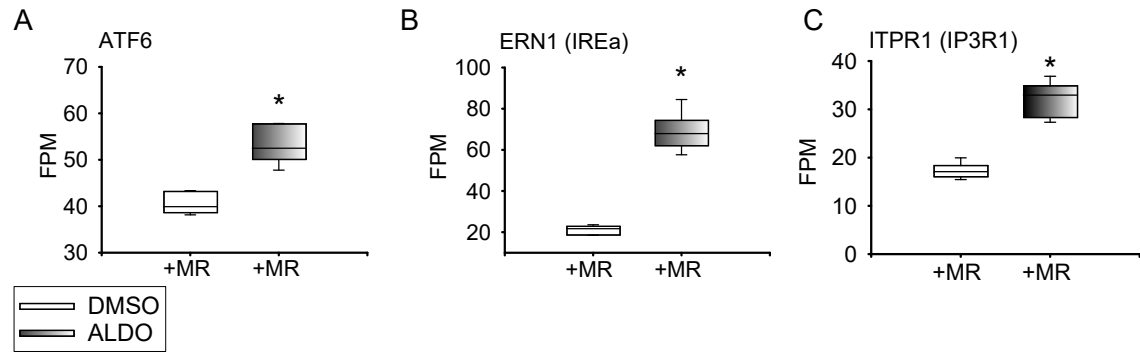


Figure 18. Contribution of MR/Aldo interplay to ER-stress. In NGS data, we observed an elevation in the ER-stress markers after 10 nM aldo-stimulated HEK cells 6 h, such as ATF6 and ERN1 (IRE α) (A, B). The IP3R1, an endoplasmic reticulum protein responsible for calcium regulation, exhibited upregulation compared to cells stimulated with DMSO (C); N=6, n=12, * $p < 0.05$.

Subsequently, within the IRE α pathway, the next step involves auto-phosphorylation of the IRE α protein itself. Measurements demonstrated that in cells stimulated with 10 nM aldo, there was an increase in the auto-phosphorylated form of the IRE α protein after 24 hours of incubation (Figure 19 B, D).

Additionally, the investigation into the downstream target of the IRE α pathway, XBP1, revealed an elevation in spliced XBP1 (XBPs) mRNA levels in 24 hours of exposure to 10 nM aldo, while the control samples exhibited no significant changes (Figure 20).

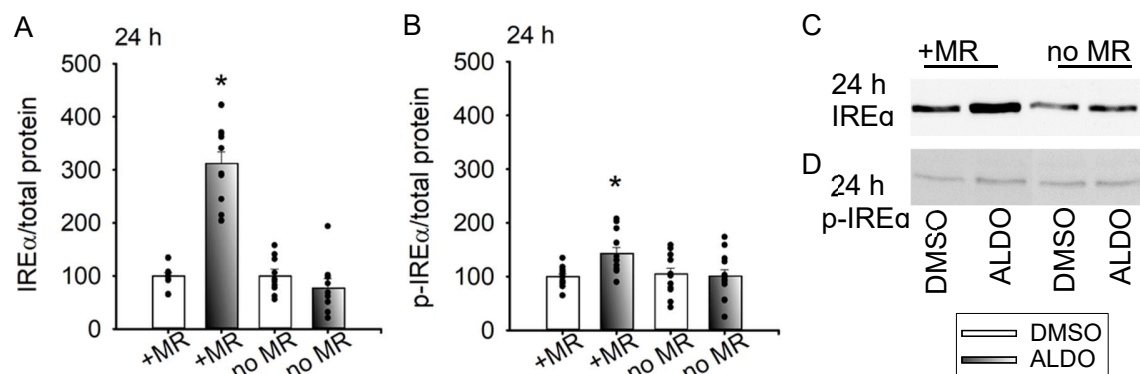


Figure 19. Aldo/MR interplay activates the IRE α pathway. Western blot confirmed increased IRE α expression (A, C) and moderate autophosphorylation (B, D) in HEK-TO-MR cells after 10 nM aldo vs. DMSO. No changes in MR-lacking samples; N=3, n=12, * $p < 0.05$.

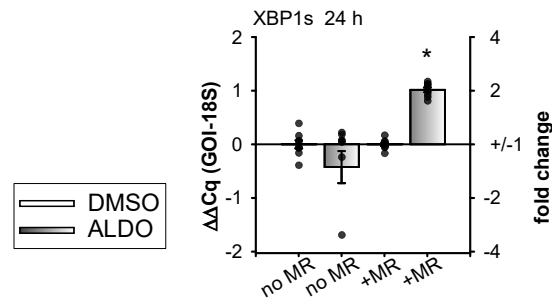


Figure 20. The downstream target of the IRE α . Activation of the IRE α pathway after 24 h was observed by identifying the downstream target, the spliced form of the XBP1. In cells stimulated with 10 nM aldo, where active IRE α was detected, an elevation in the spliced form of XBP1 was also observed. Conversely, in HEK cells with no MR and MR-expressing cells with DMSO, there was no discernible increase in the spliced form of XBP1s; N=4, n=8; *p < 0.05.

No changes were detected when the PERK pathway was assessed by measuring the downstream target eIF2 α after 1 hour and 24 hours of treatment (Figure 21). This observation suggests that the aldo/MR relationship specifically regulates specific ER-stress pathways, emphasizing the selectivity of the cellular response to aldo-induced ER stress (Figure 21 A-D).

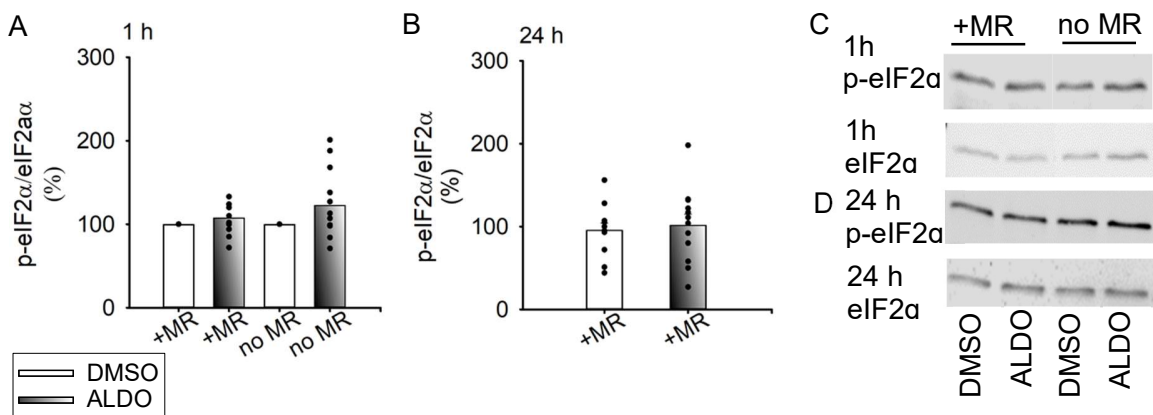


Figure 21. The downstream target of the PERK. PERK downstream target eIF2 α did not display an increase in expression that could be attributed to aldo/MR within the 24-hour (B, D) time frame and during a shorter incubation period like 1h (A, C); N=3, n=12; *p < 0.05.

4.6. Activated MR by Aldo Triggered Autophagic Flux Increase

To assess the potential induction of autophagy stemming from the interaction between aldo and the MR, autophagic flux was examined using lysosomal inhibitors, precisely 10 μ g/ml each of pepstatin and aloxistatin. These inhibitors were utilized to monitor LC3B II turnover from LC3B I, preserving autophagosomes labeled with the LC3B II marker by preventing

lysosomal degradation. It quantifies accumulated autophagosomes and autophagic flux by subtracting samples without inhibitors from samples with inhibitors and estimating autophagosome formation following 10 nM aldo stimulation over 24 hours. Upon 24 hours of 10 nM aldo/MR stimulation, a noticeable increase in autophagy flux was observed, while samples lacking MR did not exhibit enhanced autophagy (Figure 22 A).

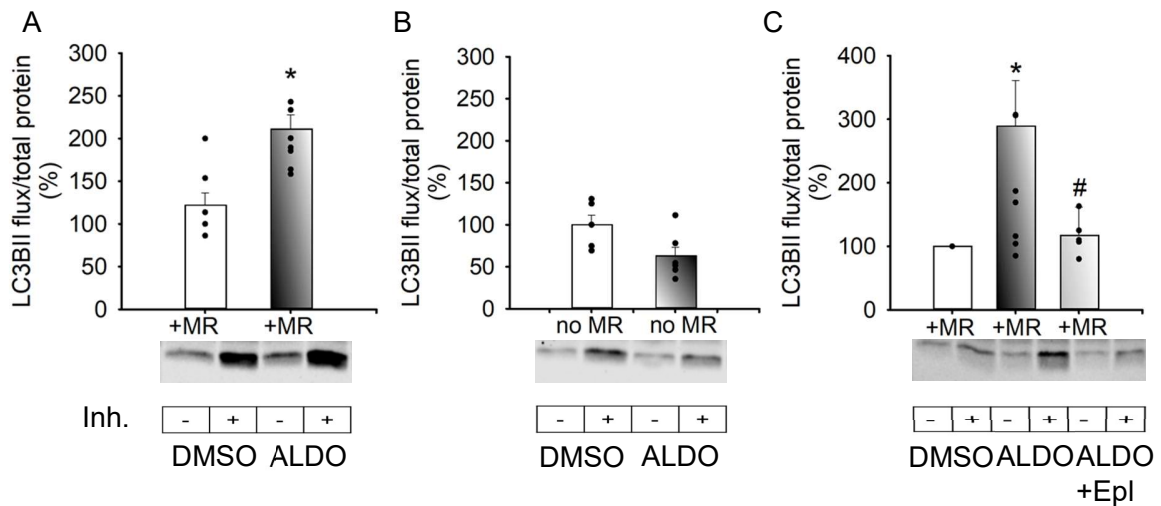


Figure 22. Autophagy triggered by aldo/MR. This experiment illustrates the investigation of autophagy by 10 nM aldo and MR. Upon 24 hours of 10 nM aldo/MR stimulation (A), a noticeable increase in autophagy flux was observed, while samples lacking MR did not exhibit enhanced autophagy (B); N=3, n=7-8, *p < 0.05. As an alternative method to evaluate the impact of MR, MR antagonist, 10 μ M eplerenone (Epl) was employed with a 1-hour incubation period before aldo addition (C); N=3 n=5-9, *p < 0.05. The bands from samples treated with DMSO and inhibitors (DMSO+Inh) were compared to those treated with aldo and inhibitors (aldo+Inh) to compare autophagic flux visually. For visual estimation of bands with the MR antagonist, eplerenone (Epl), the band of cells treated with aldo+Inh was compared with the band of cells treated with aldo, eplerenone, and inhibitor (aldo+Epl+Inh).

To verify the specificity of the rise in autophagy attributed to the aldo/MR interaction, samples from HEK-TO-MR without MR induction were examined. In this scenario, 10 nM aldo failed to induce autophagy (Figure 22 B). Additionally, the MR antagonist eplerenone attenuated MR activation, resulting in a decrease in autophagic flux. Eplerenone demonstrated its ability to inhibit autophagic flux, displaying observable effects in cells lacking MR induction (Figure 22 C). These investigations suggest that the heightened autophagic flux results from altered cellular behavior induced by the aldo/MR interaction, where aldo/MR might serve as an upstream regulator in modulating autophagy dynamics.

4.7. Increased Cell Death Marker Expression via Aldo-Induced MR Signaling

Cell death markers were evaluated to explore the implications of aldo/MR stimulation, focusing primarily on apoptosis and necrosis. The investigation unveiled a significant rise in the apoptosis marker, particularly an elevation in caspase-3 activity, in HEK cells overexpressing MR and exposed to aldo. After 24 hours of exposure to 10 nM aldo, a noticeable increase in caspase-3 activity was observed (Figure 23 A). This effect was even more evident during the subsequent 48-hour treatment (Figure 23 B), indicating a time-dependent escalation in the apoptotic response to aldo/MR stimulation. In contrast, control conditions involving HEK cells treated with DMSO/MR and HEK cells lacking MR did not show any elevation in caspase-3 levels, highlighting the specificity of the observed apoptotic response to aldo/MR (Figure 23 A, B). Significantly, the assessment of necrosis markers, particularly lactate dehydrogenase (LDH), did not reveal changes similar to caspase activity in aldo/MR-stimulated cells after 24 and 48 hours (Figure 24 A, B). The measurement covered fresh samples, where LDH activity was measured in the media of HEK cells (media LDH activity) from the respective cell groups and normalized to the total LDH activity in both media and lysates. Aldo treatment without MR expression did not induce LDH activity after 24 or 48 hours. These results highlight the specificity of the aldo/MR response in HEK-TO-MR cells, leading to increased apoptosis without inducing necrosis.

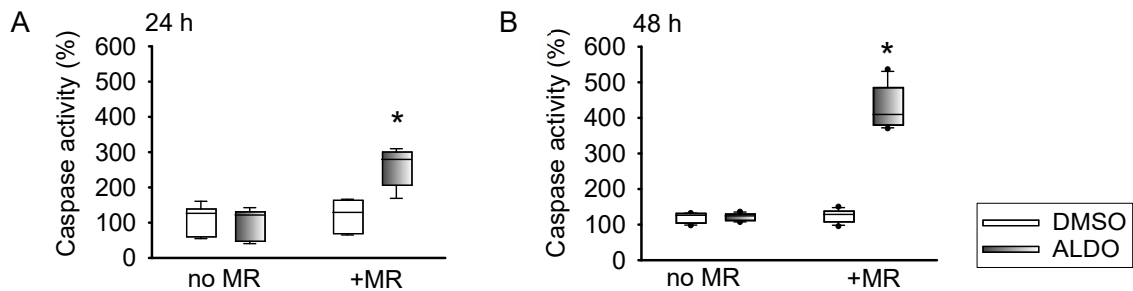


Figure 23. Caspase activity under aldo/MR stimulation. We measured fluorescence increase in MR-overexpressing HEK cells, specifically detecting caspase-3 activity, a recognized marker of apoptosis, within 24 h (A), with a more pronounced effect seen at 48 h (B). Cells stimulated with DMSO in the presence of MR showed no caspase-3 activity, similar to the control group of HEK cells without MR expression (A, B); N=4, n=6-8, *p < 0.05.

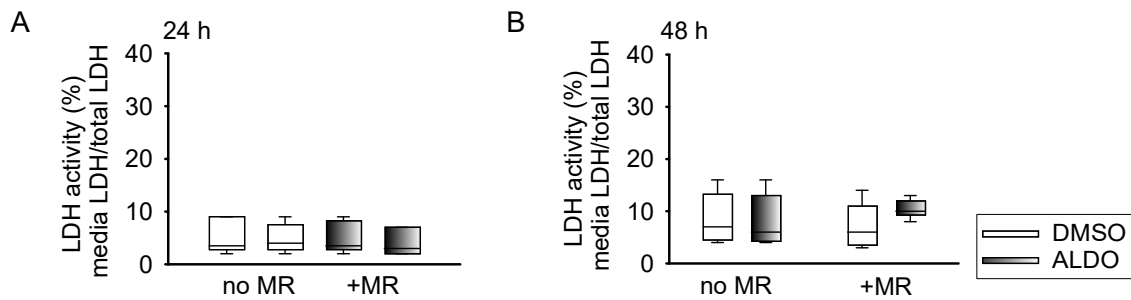


Figure 24. LDH activity under aldo/MR stimulation. Necrosis marker, LDH, after 24 and 48-hour incubation, showed no discernible rise in LDH activity in HEK overexpressing MR cells treated with 10 nM aldo. The control cell groups, including those treated with DMSO in the presence of MR and cells without MR induction, did not exhibit any elevation in LDH activity; N=4, n=6-8, *p < 0.05.

4.8. Influence of Micromilieu on MR

As previously discussed, numerous preclinical and clinical studies indicate that alterations in the micromilieu are crucial in the development of MR-induced pathologies. Furthermore, these changes are associated with aging, as elevated oxidative stress (nitrosative stress) levels and increased MR expression and activity are observed in the vascular walls of older individuals. The objective was to elucidate MR signaling and function and MR expression under nitrosative stress conditions induced by the peroxynitrite donor SIN-1.

4.8.1. Translocation Ability of MR Without Aldo Activation in HEK TO MR Cells

We conducted immunofluorescence analysis to investigate whether MR can undergo translocation independent of classic ligands. Our cells were treated with a final concentration of 200 μ M SIN-1 for one hour, omitting the addition of aldo while ensuring well-expressed MR in the cell model. The control group consisted of cells treated with DMSO, and the classic ligand activation involved treatment with 10 nM aldo for one hour (Figure 25 A, B, E). In cells treated with SIN-1, MR was located in the cytosol and the nucleus (Figure 25 C, E). In contrast, MR was observed mainly in the cytoplasm of cells in the negative control group. In cells treated with 10 nM aldo, MR was concentrated in the nucleus following classic ligand activation (Figure 25 B, D, E). Simultaneous stimulation with aldo and SIN-1 also initiated the translocation of MR from the cytosol to the nucleus.

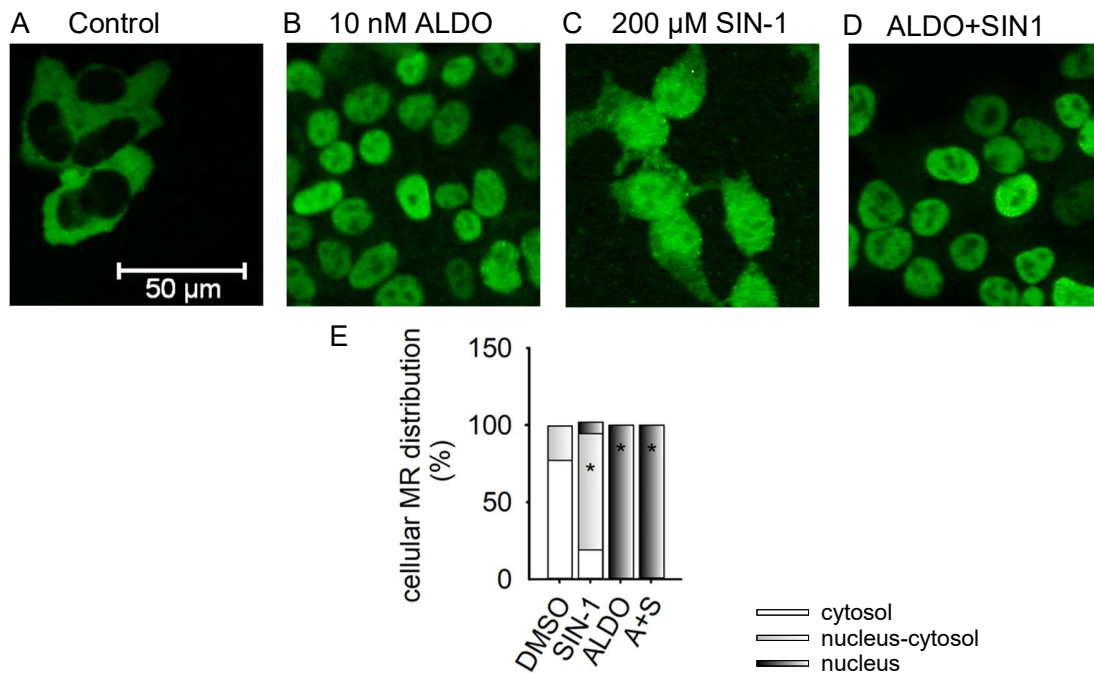


Figure 25. MR translocation under nitrosative stress. The influence of nitrosative stress on MR translocation was studied by exposing cells to 10 nM aldo (B), 200 μM SIN-1 (C), and aldo+SIN-1 (A+S) (D) for 1 hour. In the control group (A, DMSO), MR was mainly in the cytosol. Aldo treatment caused MR to move entirely to the nucleus. SIN-1 induced partial nuclear translocation, but complete translocation was not achieved after 1 hour in A+S samples. Thus, more MR was transitioning from cytoplasm to nucleus (E), with a reduced cytoplasmic MR fraction in the presence of SIN-1. N=4; n=150 per condition, *p < 0.05 vs cytosol DMSO.

4.8.2. Genes regulation by SIN-1/MR

NGS data analysis of 200 μM SIN-1/MR-treated samples identified only 35 differentially regulated protein-coding genes (Figure 26). Interestingly, in cells stimulated with 200 μM SIN for 6 h, we observed the regulation of genes associated with the onset of CVDs. The gene SKIDA1 (SKI/DACH Domain-Containing 1) was found to be downregulated by both aldo and SIN-1, acting through the MR, compared to control conditions. However, the combined effect of aldo and SIN-1 did not surpass the individual effects of either compound alone (Figure 27 A).

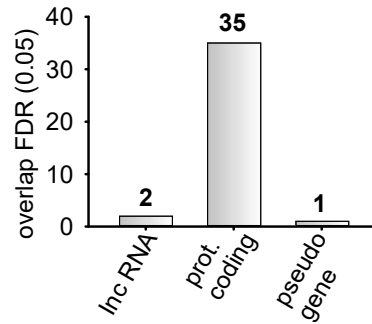


Figure 26. NGS data analysis with 200 μ M SIN-1. We utilized EdgeR and DESeq2, identifying genes regulated by 200 μ M SIN-1 to the vehicle DMSO. (FDR < 0.05), N=6, n=12.

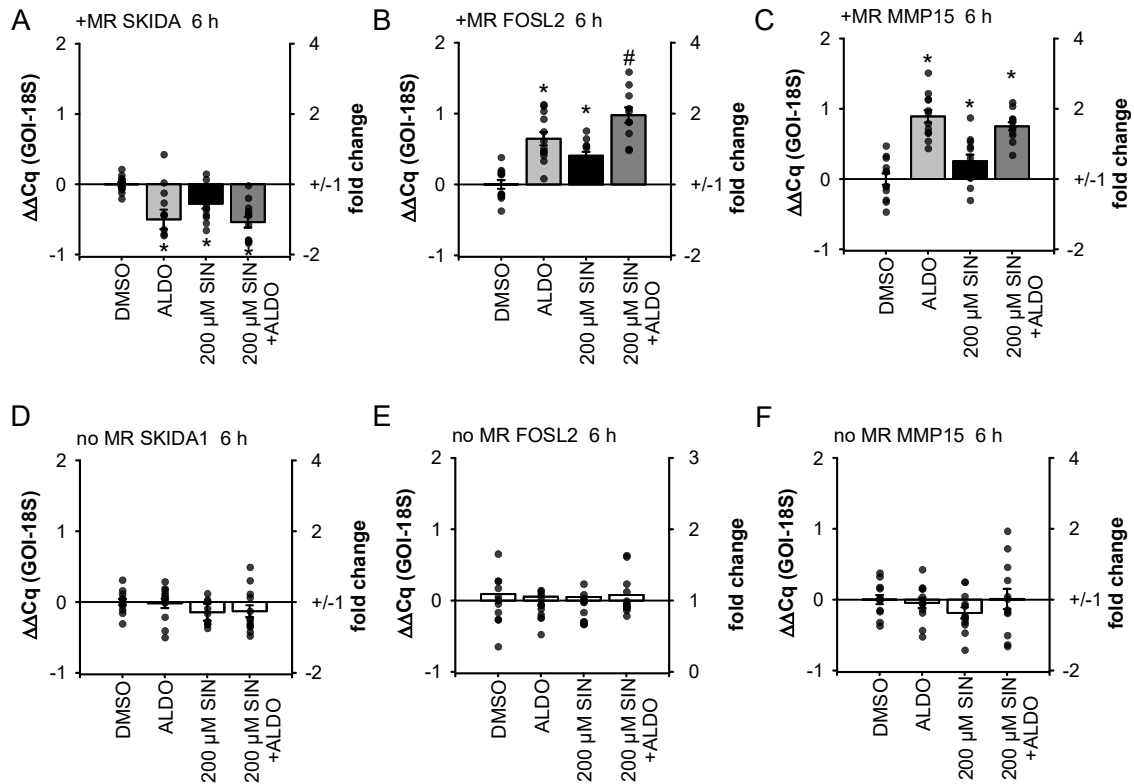


Figure 27. The activation of genes by SIN-1 acts through the mineralocorticoid receptors. SKIDA1 shows regulation by 10 nM aldo/MR and 200 μ M SIN-1/MR following 6 hours of treatment with the stimulants, preceded by 18 hours of MR expression (A, D). FOSL2 demonstrates an additive effect when treated with a combination of aldo and SIN-1 compared to cells treated with aldo or SIN-1 alone. MMP15 exhibits robust regulation by aldo and a slightly lesser effect by SIN-1. Control experiments without MR expression reveal no regulation of these genes; N=6, n=12, *p < 0.05 vs. control; #p < 0.05 vs. aldo.

For the gene FOSL2 (FOS like 2, AP-1 Transcription Factor Subunit), both aldo/MR and SIN-1/MR stimulation enhanced expression, although SIN-1 alone showed slightly lower

activity. Notably, when aldo and SIN-1 were combined, there was an increase in FOSL2 expression compared to either compound alone (Figure 27 B).

Regarding MMP15 (Matrix Metalloproteinase 15), aldo demonstrated significant regulation, confirming its status as an MR-regulated gene. However, the expression activation induced by SIN-1/MR was slightly less pronounced compared to aldo/MR. Additionally, the combination of aldo and peroxyntirite did not elicit greater regulation than aldo alone (Figure 27 C).

Furthermore, when MR expression was absent, no effect was observed on these three genes despite the same stimulating agents (Figure 27 D-F).

These findings indicate that 200 μ M SIN may activate MR-driven transcriptional activity. Aldo's regulation of these genes further supports their status as MR-regulated genes, as evidenced by the absence of aldo regulation in negative control experiments.

4.8.3. Effect of Nitrosative Stress on MR/PDK4 Interaction

To assess the expression of the MR target gene PDK4, we first examined its regulation under 200 μ M SIN treatment. After 6 hours, no additional modulation of PDK4 expression was observed in the samples treated with aldo and 200 μ M SIN compared to the aldo control. In the control samples lacking the MR, we detected a slightly higher PDK4 expression than the control without MR (Figure 28).

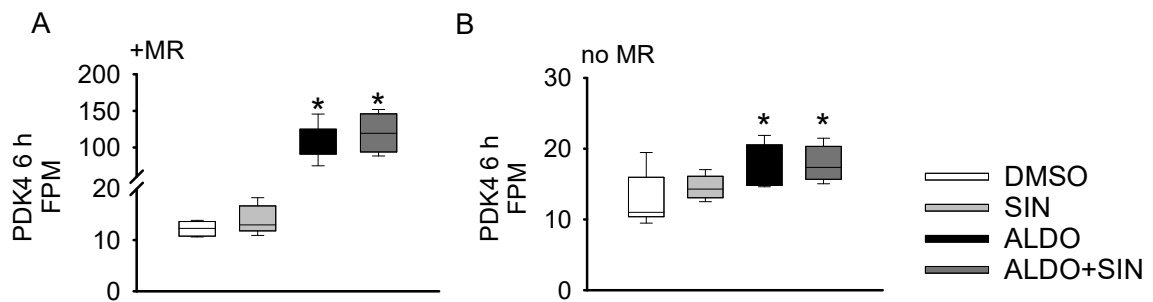


Figure 28. Under 200 μ M SIN treatment, PDK4 expression in NGS was assessed. In the context of nitrosative stress, the sample treated with aldo and 200 μ M SIN-1 showed no significant changes in PDK4 expression compared aldo alone, indicating that the effect of aldo is maintained in the aldo/200 μ M SIN-1 condition. In the sample treated with 200 μ M SIN-1 alone, no PDK4 gene expression was observed after 6 hours. In samples lacking MR, aldo, and aldo combined with SIN-1 induced a slight upregulation of PDK4. However, in the presence of MR, this upregulation was significantly enhanced. N=6, n=12, with *p < 0.05 vs. control.

The next step involved evaluating the effects of higher concentrations of SIN-1 on PDK4 expression. HEK-TO-MR cells were exposed to higher concentrations of SIN-1, namely 600

μM and $800 \mu\text{M}$, for 24 hours (Figure 29). Additionally, cells were stimulated with 10 nM aldo. The control included DMSO-treated cells with MR overexpression but no activation and HEK cells lacking MR overexpression but subjected to other stimulants, such as 10 nM aldo, $600 \mu\text{M}$, and $800 \mu\text{M}$ SIN-1, to examine the effect of MR.

Our findings demonstrated a notable reduction in PDK4 MR-dependent mRNA expression under aldo+SIN-1 stimulation compared to aldo (Figure 29 A, B).

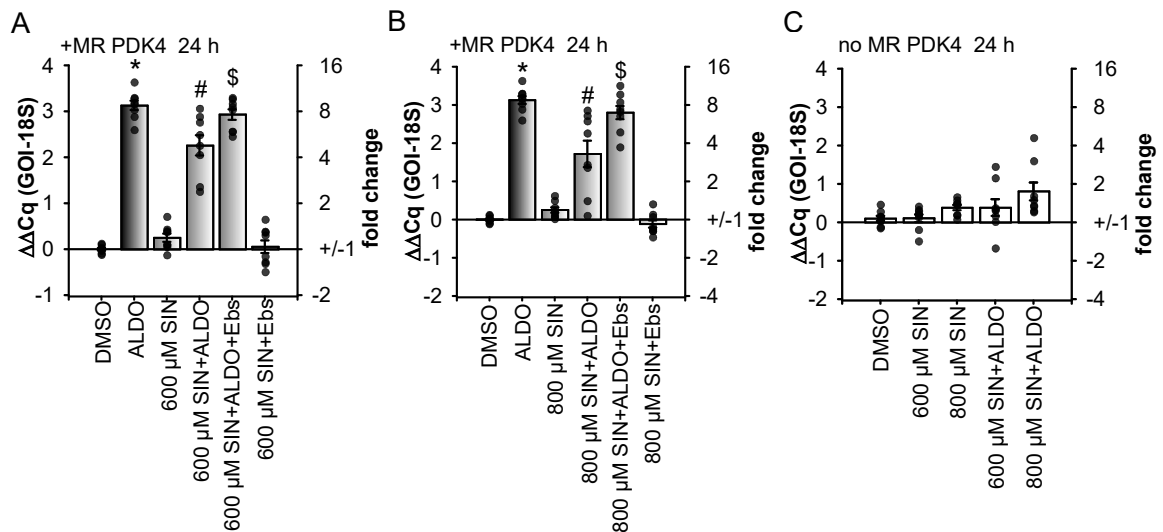


Figure 29. mRNA expression of PDK4 under SIN-1/MR regulation. In the presence of nitrosative stress, aldo/MR induced less increase in PDK4-mRNA after 24 hours, particularly evident with high concentrations of SIN-1 such as $600 \mu\text{M}$ and $800 \mu\text{M}$ (A, B). There was a tendency for SIN-1 to attenuate the regulatory effect of aldo, especially in samples where both aldo and SIN-1 were administered simultaneously (A, B). A notable inhibition of the aldo effect by SIN-1 was observed after 24 hours. We verified the effect of SIN-1 using ebselen, which restored the effect of aldo. In contrast, samples lacking MR did not show any regulation in PDK4 expression (C); N=6, n=12, *p < 0.05 vs. control; # p < 0.05 vs. aldo; \$p < 0.05 vs. sin+aldo.

Additionally, in the cells without MR expression, no significant alterations in PDK4 expression were observed in the presence of $600/800 \mu\text{M}$ SIN-1 and 10 nM aldo after 24 hours of incubation. To explore whether the decrease in PDK4 levels was attributable to SIN-1 we utilized ebselen, a specific peroxynitrite scavenger, at a final concentration of $40 \mu\text{M}$. Remarkably, ebselen restored PDK4 protein levels nearly to those observed in the group treated with 10 nM aldo (Figure 29 A, B). In samples treated with both SIN-1 and ebselen concurrently, no changes in PDK4 regulation were observed without aldo. These findings suggested that PDK4 expression in our HEK cells is contingent upon MR activation and expression, highlighting the diverse effects of MR depending on the specific ligand.

4.8.4. Protein Expression of PDK4

We investigated the protein expression of PDK4 in response to SIN-1/MR stimulation. Specifically, we treated cells with 600 μ M and 800 μ M SIN-1 for 24 hours. Control cells were stimulated with DMSO, while cells with 10 nM aldo were our reference for activated MR. The results for PDK4 protein expression mirrored those observed for PDK4 mRNA expression. Cells treated with aldo and SIN-1 exhibited decreased protein expression compared to aldo alone. However, upon treatment with ebselen, a peroxynitrite scavenger, the effect of aldo + Sin-1 was restored to nearly the same levels as aldo (Figure 30 A-D).

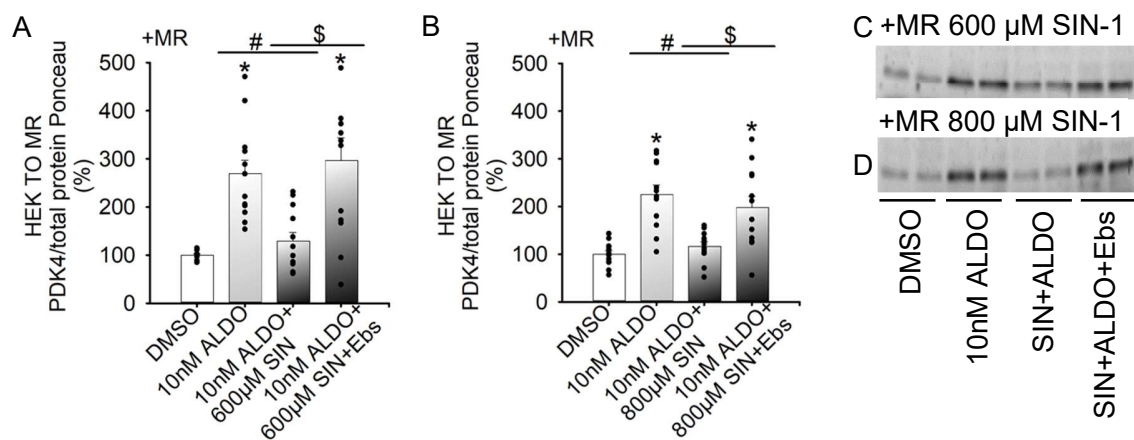


Figure 30. PDK4 protein expression under SIN-1/MR interplay. Samples treated with 10 nM aldo and SIN-1 at concentrations of 600 μ M (A, C) and 800 μ M (B, D) exhibited a reduction in PDK4 protein levels. However, the introduction of 40 μ M ebselen, a peroxynitrite scavenger, effectively reinstated the impact of aldo, bringing it back to levels comparable to aldo treatment alone; N=3 n=12, *p < 0.05 vs. control; #p < 0.05 vs. aldo; \$p < 0.05 vs. sin+aldo.

4.8.5. Influence of the Nitrosative Stress on Aldo/MR Function (Cell Death)

Stimulation with SIN-1 has been found to induce changes in downstream processes, such as apoptosis. Previous observations revealed an increased caspase activity in MR-expressing cells stimulated with 10 nM aldo, indicating that the interaction between 10 nM aldo and MR initiates apoptosis.

In subsequent experiments, tests were conducted at 24 hours, during which cells were additionally stimulated with various concentrations of SIN-1 ranging from 200 μ M to 800 μ M. Results at the 24-hour time showed no significant effect on caspase activity in samples with activated MR when stimulated with SIN-1 alone (Figure 31 A) compared to control DMSO-treated cells. When comparing samples stimulated with 10 nM aldo and SIN-1 to DMSO,

elevated caspase activity was observed after 24 hours for samples stimulated with 200 μM and 400 μM of SIN-1 (Figure 31 B). This increased activity was maintained due to the effect of Aldo. However, for higher concentrations of 600 μM and 800 μM , the observed increase in caspase activity was lost compared to the DMSO control, indicating that the effect of Aldo was suppressed by nitrosative stress at 24 hours. In samples treated with both 10 nM Aldo and SIN-1, caspase activity gradually returned to control levels in a dose-dependent manner compared to Aldo alone. HEK cells without tetracycline addition were used as a negative control to maintain cells without MR expression. No increase in caspase activity was observed after 24 hours in samples treated with 10 nM Aldo and SIN-1 in cells lacking the MR (Figure 31 C, D).

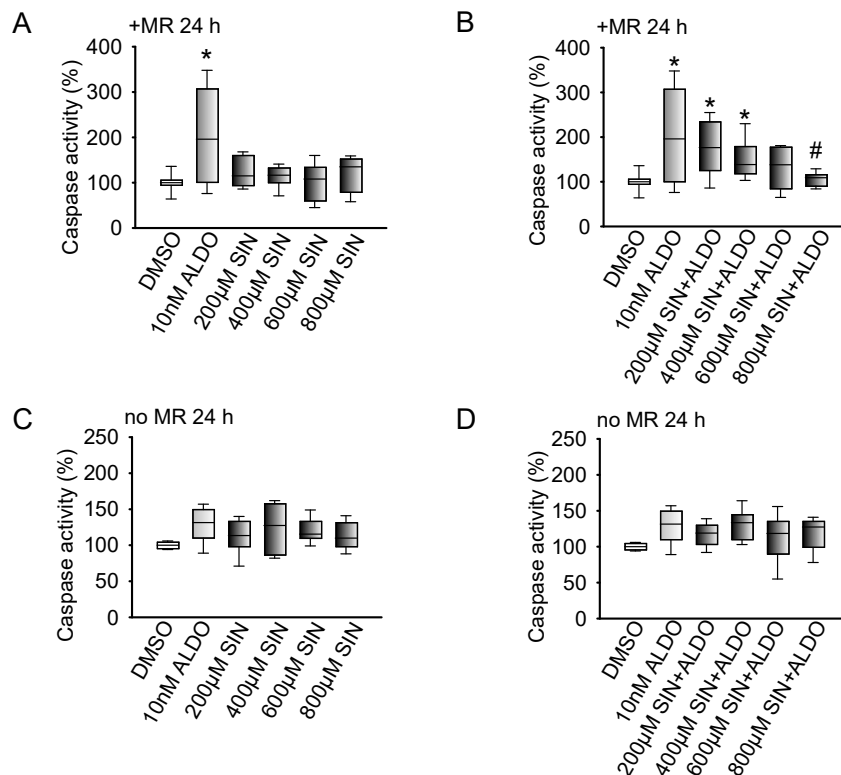


Figure 31. Caspase activity after Aldo, SIN-1 and SIN-1/Aldo stimulation. Caspase activity remained unaltered when cells were exposed to 200 μM , 400 μM , and 600 μM SIN-1 alone for 24 hours (A). 10 nM Aldo led to an increase in caspase-3 activity. However, samples treated with both Aldo and SIN-1 after 24 hours tended to reduce caspase activity compared to the effect of Aldo alone (B). Additionally, samples without MR stimulated with SIN-1 after 24 hours did not exhibit any significant effect (C, D); N=4, n=8, *p < 0.05 vs. control; #p < 0.05 vs. Aldo.

Overall, our results confirm that aldo and MR together trigger apoptosis. However, SIN-1 alone is not capable of increasing caspase activity. Meanwhile, high concentrations of SIN-1 suppress aldo's impact in the presence of MR.

4.8.6. MR Expression Under Nitrosative Stress

We examined the mRNA expression of the MR under nitrosative stress conditions. Following a 6-hour incubation with 200 μ M and 400 μ M SIN-1, no significant changes in MR mRNA expression were observed. However, at higher concentrations of SIN-1, beginning at 600 μ M, a dose-dependent decrease in MR mRNA expression was detected (Figure 32). For our investigation of MR protein expression, we focused on 24-hour stimulation using varying concentrations of SIN-1 (200 μ M, 400 μ M, 600 μ M, 800 μ M). We found that stimulation with 200 μ M and 400 μ M SIN-1 did not affect MR protein expression (Figure 33 A, B, C, D). At higher SIN-1 concentrations (600 μ M and 800 μ M), we observed a decrease in MR protein expression. This trend was consistent for samples stimulated with SIN-1 alone and those co-stimulated with aldo and SIN-1.

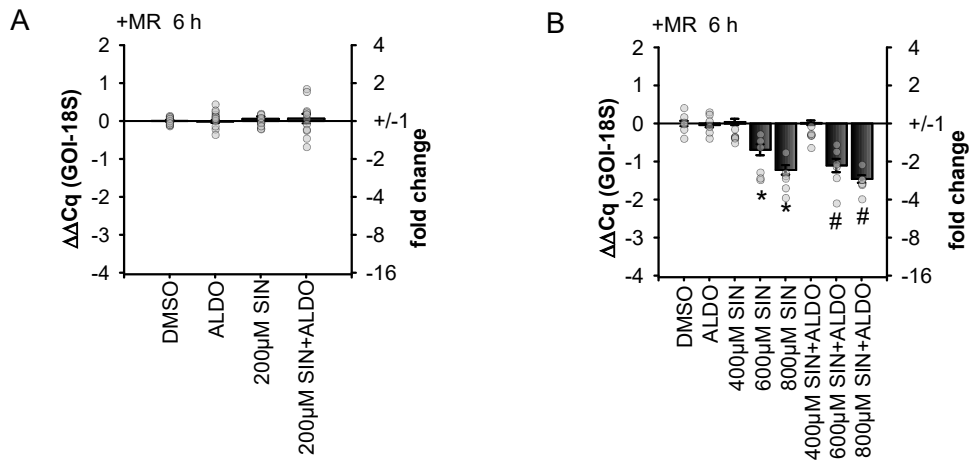


Figure 32. MR mRNA expression under SIN-1. No changes were observed at 200 μ M SIN-1 (A) on MR mRNA expression. Similarly, a concentration of 400 μ M SIN-1 (B) did not affect MR mRNA expression. However, increasing the concentration to 600 μ M and 800 μ M decreased MR mRNA expression after a 6-hour incubation period; N=6, n= 12, *p < 0.05.

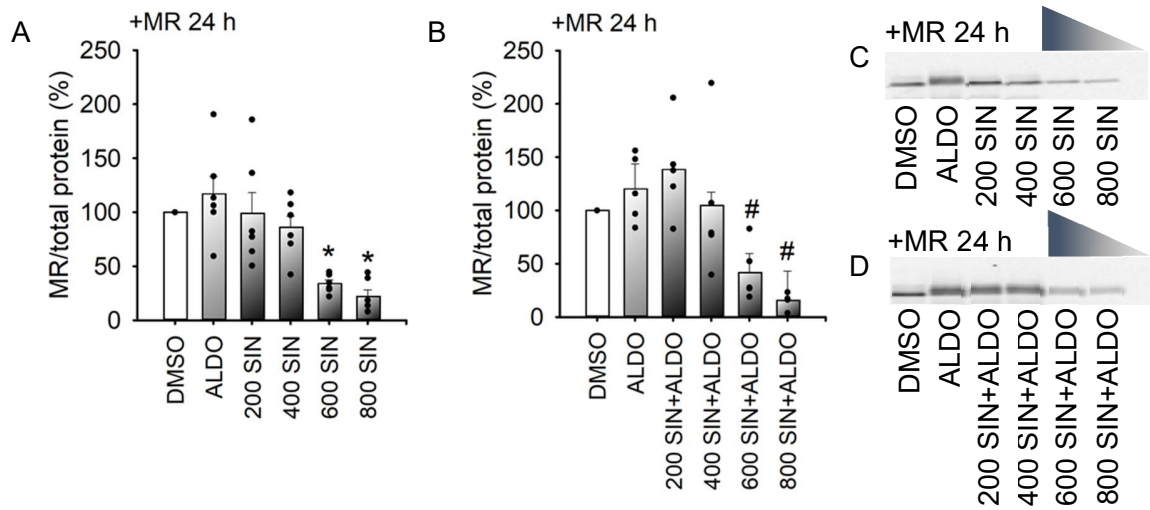


Figure 33. MR protein expression under SIN-1 stimulation for 24 hours. Samples with 600 μM and 800 μM SIN-1 showed a decrease in MR protein levels. In contrast, no significant change was observed for 200 μM and 400 μM SIN-1 treatments (A-D); N=3, n=6, * $p < 0.05$.

4.8.7. Effect of SIN-1 on Protein Expression of Glucocorticoid Receptor

The GR, structurally and functionally similar to MR, was studied to assess nitrosative stress effects. A comprehensive understanding of the distinctions between these two receptors is vital for developing more specific and targeted medications. We found no impact on GR protein expression in samples treated with 200-800 μM SIN-1 alone or in combination with 100 nM dexamethasone (Figure 34 A, B).

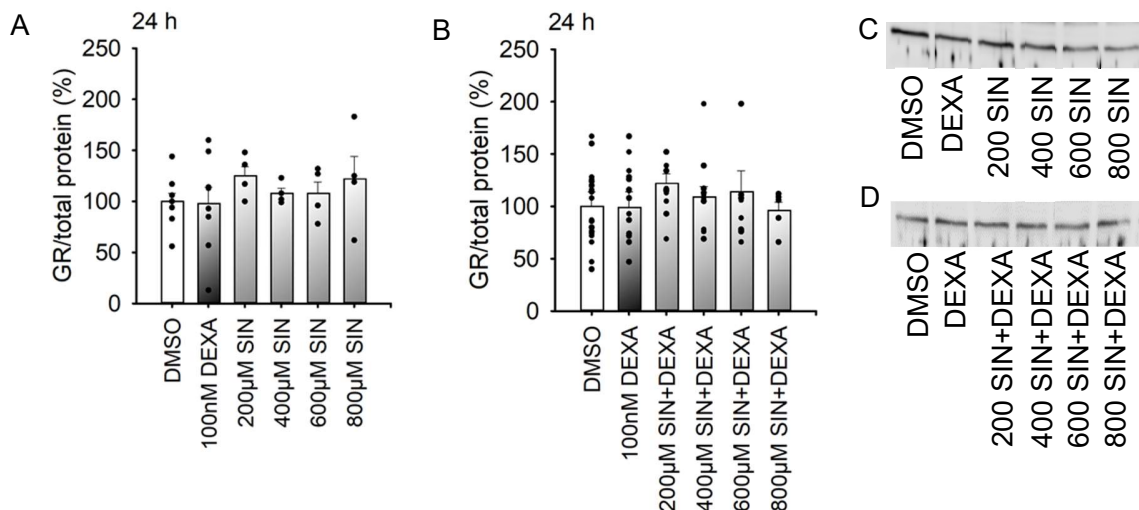


Figure 34. GR protein expression under SIN-1 stimulation 24 hours. At high concentrations (600 μM and 800 μM), GR protein levels remain unchanged after 24 hours of SIN-1 stimulation, both with SIN-1 alone and in combination with 100 nM dexamethasone (A-D); N=3, n=6, * $p < 0.05$.

5. Discussion

This study explores MR's multifaceted roles in cellular homeostasis, particularly in metabolic regulation, ER stress, apoptosis, and autophagy. Traditionally recognized for its involvement in sodium homeostasis within renal epithelial cells, our experiments investigated the impact of MR in broader pathophysiologically relevant cellular processes. Focusing on glucose and energy metabolism, we found alterations in metabolic pathways in MR-overexpressing HEK cells exposed to aldosterone. We hypothesize that genes involved in the regulation of metabolic processes in MR-overexpressing HEK cells may be responsible for observed cellular alterations such as ER stress, apoptosis, and autophagy, each examined in this study. Our objective was to investigate the impact of the MR in the cellular environment, utilizing a tetracycline-inducible overexpression system to facilitate the controlled modulation of MR expression in a switch on and off mode, underlining MR effects (Urlinger et al., 2000).

5.1.1. Energy Metabolism Involves MR Regulation in HEK Cells

The experiments revealed an overlooked role of MR in metabolic regulation. Our study on glucose and energy metabolism showed a consistent increase in glucose consumption in MR-overexpressing HEK cells following aldosterone exposure. Additionally, increased lactate production in these cells suggests a potential effect on glycolytic pathways. In contrast, cells lacking MR expression showed no differences in glucose consumption and lactate production between control and aldosterone-stimulated conditions, highlighting MR's specific influence.

The augmentation of glucose consumption and concurrent lactate production induced by elevated MR activity may represent an adaptive cellular response. This phenomenon could be particularly relevant in scenarios such as aging, where reports indicate increased aldosterone and MR activity and expression levels (Bauersachs et al., 2015; Ibarrola et al., 2023).

Switching to lactate production in MR overexpressing cells can be analyzed using established knowledge. This switch may be attributed to an endeavor to mitigate oxidative stress (Lin et al., 2022). Anaerobic glycolysis plays a crucial role in this process by redirecting glucose away from pathways that engender oxidative stress, a hallmark of aging (Maldonado et al., 2023). Through the production of lactate, instead of proceeding through the tricarboxylic acid (TCA) cycle and oxidative phosphorylation, cells aim to minimize ROS generation (Handy and Loscalzo, 2012; Rashmi et al., 2018). It is widely recognized that

heightened aldo and mineralocorticoid concentrations can elevate reactive oxygen species (ROS) production (Edwards, 2020; Iwashima et al., 2008; Queisser et al., 2011).

To bolster evidence of MR's influence on the glycolytic pathway, we used a Seahorse XF analyzer to systematically measure the ECAR, utilizing various reagents to dissect the contributions of different pathways to proton production. Aldo application to MR-HEK cells increased basal proton efflux rate (PER), basal glycolysis, and compensatory glycolysis. Using Rot/AA, we quantified the PER derived from glycolysis, revealing heightened acidification due to increased proton generation within the glycolytic pathway. These results provided a more precise understanding of the glycolytic contribution to proton efflux. Our results demonstrated an elevated proton efflux rate in cells stimulated with aldo/MR, quantitatively measuring the glycolytic contribution to acidification. Upon suppressing both mitochondrial (Rot/AA inhibition) and glycolytic acidification sources, the introduction of 2-Deoxy-D-glucose showed no significant differences between aldo-treated and DMSO-treated cells regarding other potential acidification sources.

The assessment of oxygen consumption rate (OCR) corroborated our ECAR findings, indicating diminished oxygen utilization in aldo-stimulated cells within the mitochondria. Consequently, compared to control cells, basal respiration was reduced under aldo/MR stimulation. Spare respiratory capacity (SRC) exhibited elevation among mitochondrial respiratory parameters in aldo/MR HEK cells. Non-mitochondrial oxygen consumption decreased in aldo samples with MR presence.

We examined alterations in ATP production pathways to delve deeper into the transition between the glycolytic pathway and oxidative phosphorylation (OXPHOS). Employing a sequential introduction of two inhibitors (oligomycin and Rot/AA) during Seahorse measurements, we observed a shift of ATP production towards the glycolytic pathway, accompanied by a reduction in mitochondrial ATP production. Interestingly, despite the lack of significant changes in overall ATP production, a shift between pathways was observed, particularly towards the glycolytic pathway.

Seahorse experiments clarified our previous observations of elevated lactate production. In these experiments, cells were incubated without CO₂ to ensure sufficient oxygen supply for one hour before measurements. The addition of rotenone and antimycin A (Rot/AA) inhibited mitochondrial CO₂ production, pinpointing glycolysis as the source of increased proton production, aligning with the observed rise in lactate production. The reduction in basal

respiration (OCR) is associated with cardiovascular disorders, where heightened glycolysis compensates for decreased mitochondrial function (Ait-Aissa et al., 2019; Bhullar and Dhalla, 2023). Additionally, we observed a decrease in oxidative phosphorylation (OXPHOS) ATP production due to aldosterone/MR activity, possibly as an effort to mitigate reactive oxygen species (ROS) production. This metabolic switch might also be linked to ER stress, where abnormal calcium release from the ER lumen impairs mitochondrial ATP production via increased inositol trisphosphate receptor (IP3R) activity (Mekahli et al., 2011).

SRC represents the mitochondrial capacity to meet additional energy demands beyond the basal level, mitigating the risk of an ATP crisis during acute cellular stress or a substantial workload (Nicholls, 2009). The heightened spare capacity suggests mitochondrial stress, necessitating an adaptive response, such as modulating ATP production pathways (Marchetti et al., 2020). However, in aldosterone-stimulated cells, elevated SRC, with lower basal respiration, likely reflects a relative increase rather than an absolute enhancement of mitochondrial capacity. When basal respiration decreases, the gap between basal and maximal respiration (spare capacity) can appear more prominent as a percentage or relative value, even though the mitochondria may not have a more functional reserve.

Although mitochondria consume most oxygen in any cell, enzymatic reactions and oxygenases outside mitochondria also somewhat consume oxygen. Non-mitochondrial oxygen consumption, a parameter measured by Seahorse, showed slight changes between aldosterone-treated and control samples, indicating the cells' ability to maintain metabolic demands.

Overall, the observed effects are primarily associated with alterations in glycolysis induced by the aldosterone/MR interplay, leading to a shift to lactate production. Consequently, mitochondrial ATP production was reduced, and glycolytic ATP production increased. This ATP production shift indicated a metabolic adaptation in response to the high concentration of aldosterone stimulation in the presence of the overexpressing MR.

The MR has a diverse impact on glucose metabolism in various tissues. Specifically, in the liver, studies demonstrate MR involvement in regulating genes responsible for hepatic glucose production, notably through the modulation of glucose-6-phosphatase (G6Pase) expression. Antagonizing MR activity or employing shRNA to inhibit MR expression reduces G6Pase expression, whereas aldosterone increases it (Liu et al., 2006). Conversely, in the retina, MR activation may potentially exacerbate diabetic complications (Ohashi et al., 2022). However, in skeletal muscle, MR's impact on glucose metabolism appears neutral (Feraco

et al., 2023). Notably, in cardiomyocytes, elevated glucose levels amplify the hypertrophic effect of aldosterone via MR, suggesting a link between MR activation and glucose-related cellular processes (Sato and Funder, 1996). Moreover, overactivation of MR is implicated in the pathophysiology of metabolic syndrome, including glucose intolerance (Thuzar and Stowasser, 2021). However, studies on low doses of the MR antagonist eplerenone in healthy adult males show no significant alterations in glucose and lipid metabolism (Krug et al., 2013). Other investigations employing MRAs have been linked to decreased progression of diabetic kidney disease and cardiovascular events in diabetic patients, indicating a beneficial impact on metabolic comorbidities associated with glucose metabolism (Dey et al., n.d.). In cardiometabolic diseases, MR antagonists benefit energy and substrate homeostasis (Thuzar and Stowasser, 2021).

While direct evidence regarding ATP production controlled by MR is limited, research implies a link between MR and cellular energetics, with aldosterone/MR potentially influencing cellular metabolism and thus affecting ATP production. Studies investigating aldosterone's impact on glucose metabolism and insulin sensitivity indirectly implicate MR in ATP synthesis due to the critical role of glucose metabolism in ATP production (Kuhn and Lombès, 2013).

Research shows that MR is involved in glucose metabolism, but the mechanisms underlying its regulation remain poorly understood. Investigating alternative metabolic pathways is essential for a comprehensive understanding of energy metabolism under the influence of aldosterone/MR synergy.

5.1.2. MR Serves as an Upstream Regulator of Genes of Energy Metabolism

As a transcription factor, MR may function as an upstream regulator of genes implicated in the observed cellular alterations identified through NGS. The NGS data revealed regulation in the expression of GLUT3, SWEET1 transporters (SLC2A3, SLC50A1), and pyruvate dehydrogenase phosphatase 1 (PDP1).

The increased expression of GLUT3, a glucose transporter, might be correlated with changes in glucose transport within particular tissues and could be related to various diseases or alterations in cellular mechanisms for glucose uptake (Boileau et al., 1995). Overexpression of GLUT3 is frequently observed in cancerous cells, which enhances their demand for and uptake of glucose (Meneses et al., 2008). SWEETs are a newly identified class of sugar transporters involved in glucose transport, particularly in the intestine and mammary glands. In goat mammary gland epithelial cells, SWEET1 was shown to decrease

glucose uptake, while the expression of GLUT1, GLUT4, and GLUT12 increased, potentially due to glucose efflux. In humans, SWEET1 may also contribute to glucose supply for lactose production in the mammary glands. However, the exact transport mechanism of SWEETs remains to be determined. While current evidence supports a role in uniport or facilitated diffusion, more complex transport mechanisms, including cotransport, have not been ruled out (Wang et al., 2019).

Additional evidence of the influence of the aldo/MR system on metabolic flexibility is evident through the downregulation of the PDP1 enzyme. Counteracting the pyruvate dehydrogenase kinases (PDKs), the PDPs dephosphorylate E1 α , thereby restoring pyruvate dehydrogenase (PDHA) activity, allowing pyruvate to enter the tricarboxylic acid cycle (Wang et al., 2021). In humans, two PDP isoforms, PDP1 and PDP2, are identified, each exhibiting distinct yet partially overlapping tissue expression patterns. PDP1 is prominently expressed in the brain, heart, skeletal muscle, and testis, while PDP2 is primarily expressed in the liver and adipose tissue (Gray et al., 2014).

A key finding in our NGS data was the upregulation of the PDK4 enzyme, a central regulator of metabolic flexibility in mammals (Jeon et al., 2021). Although all four known isoforms of PDK were detectable, only PDK4 exhibited differential expression in response to aldo/MR. RNA-Seq results were validated through qRT-PCR and Western blot analyses, with PDK4 activity assessed by analyzing the phosphorylation of the downstream target PDHA1. Additionally, we examined PDK4 expression in EA.hy926 cells, having previously established endogenous MR expression in these cells. Our findings indicated a similar regulatory influence of MR on PDK4 expression at the protein level. This aldo/MR effect was further confirmed by applying a specific MR antagonist in EA.hy926 cells, after which PDK4 expression decreased compared to the samples with aldo.

Moreover, NGS analysis and qPCR revealed the modulation of other genes by aldo/MR, including SGK1, MAP3K6, and PRKAB2, all key players in glucose metabolism regulation (Gomez-Sanchez and Gomez-Sanchez, 2014; Ho et al., 2004; Mueckler and Thorens, 2013). The activation of SGK1 demonstrated the potential to significantly increase glucose uptake in cells detached from the extracellular matrix (ECM). Furthermore, the heightened expression of SGK1 enables ATP synthesis independent of mitochondrial involvement (Cockfield and Schafer, 2021).

PDK4 is a tissue-specific enzyme highly expressed in various organs, including the heart, skeletal muscle, liver, and kidney (Wang et al., 2021). The primary function attributed to PDK4 is the phosphorylation of the pyruvate dehydrogenase (PDHA) complex, leading to its inactivation and thereby preventing the entry of pyruvate into the tricarboxylic acid cycle for oxidative decarboxylation (Jeoung et al., 2006). In conditions such as diabetes and inflammation, elevated expression of PDK4 contributes to the inactivation of the PDHA complex (Kuntz and Harris, 2018). Several factors have been identified as regulators of PDK4 expression, including reduced insulin levels, increased glucocorticoids (GCs), and free fatty acids, as well as the transcription factors PPAR α , FOXO1, and PGC1 α (Huang et al., 2002; Wende et al., 2005). However, limited research has explored the regulation of PDK4 by the MR. We found one study where PDK4 was previously identified as a potential MR target (Ziera et al., 2009).

PDK4 plays a pivotal role as an enzyme in influencing cell metabolism through multiple mechanisms, such as metabolic reprogramming, regulation of autophagy, lipid metabolism, and control of the cell cycle (Araki and Motojima, 2006; Ma et al., 2020; Takubo et al., 2013). These diverse roles underscore the potential of PDK4 as a promising therapeutic target for addressing both metabolic disorders and cancer (Wang et al., 2021).

Our study demonstrated MR-mediated upregulation of PDK4 at the protein level in two distinct cell types expressing MR. Therefore, we propose that activated MR can enhance PDK4 expression, inducing functional consequences such as a metabolic shift to lactate production. The reduced oxidative phosphorylation of glucose could be due to activated PDK4, which may contribute to mitochondrial stress, subsequently inducing ER stress and overall cell death (Kim et al., 2023; Lee et al., 2015; Leem and Lee, 2016). These results suggest that the modulation of PDK4 expression by MR may be one of the causes of metabolic changes that affect cell homeostasis.

Previously, PDK4's role in driving metabolic reprogramming towards a Warburg effect and its involvement in VSMC calcification were highlighted (Ma et al., 2020). Recent research data showed that PDK4 overexpression led to the phosphorylation of non-typical target proteins (IP3R1-GRP75-VDAC1), promoting excessive Ca²⁺ transport into mitochondria through mitochondria-associated endoplasmic reticulum membranes (MAM) (Jeon et al., 2021). Prolonged induction of MAM, however, resulted in mitochondrial dysfunction due to elevated Ca²⁺ levels and increased ROS production (Janikiewicz et al., 2018). Dysregulated MAM function can lead to ER stress (Arruda and Hotamisligil, 2015). Additionally, PDK4

promotes cardiac dysfunction and myocardial apoptosis in immature rats and decreases the ability of antioxidant enzymes (Yin et al., 2021).

5.1.3. ER Stress Signaling Pathways Regulated by MR

Our NGS data identified upregulation of ER-stress markers, particularly ATF6, ERN1 (IRE α), and ITPR1, a protein involved in calcium regulation. Western blot analysis showed a significant increase in IRE α (ERN1) protein expression and phosphorylated form after 24 hours in HEK-TO-MR cells exposed to aldo. Additionally, we observed an elevation in the spliced form of the XBP1 transcription factor at the mRNA level, indicating activation of the IRE α pathway. Control conditions, including HEK cells with DMSO/MR and cells without MR in the presence of aldo, showed no increase in ER stress markers, highlighting that the observed elevation is specific to aldo/MR interaction.

The ER is crucial for protein maturation, managing the translocation and modification of about one-third of cellular proteins, including secretory, luminal, and membrane proteins. In the ER lumen, these proteins are modified by resident enzymes and chaperones to achieve their proper structure, relying on precisely regulated calcium, glucose, and ATP concentrations, as well as an optimal redox environment (Hetz, 2012). Disruption of protein folding results in ER stress, prompting the activation of the unfolded protein response (UPR) (Cybulsky, 2013). The UPR is initiated by three transmembrane proteins: IRE1, PERK, and ATF6. IRE1 α , the most evolutionarily conserved ER membrane protein, functions as a kinase and an endoribonuclease. Upon activation, IRE1 α splices X-box binding protein 1 (XBP1) mRNA, producing a spliced form (XBP1s) that acts as a potent transcription factor, upregulating genes essential for ER-associated degradation (ERAD) and protein folding (Ron and Hubbard, 2008). These processes help cells adapt to ER stress (Blazanin et al., 2017). Additionally, IRE1 α activation can trigger stress kinases such as c-Jun N-terminal kinase (JNK) and p38 MAPK, which are involved in processes like apoptosis, inflammation, and stress responses (Kim et al., 2008). The induction of JNK and p38 MAPK by IRE1 α contributes to the cellular response to ER stress, influencing cell survival or apoptosis depending on the severity and duration of the stress (Maeyashiki et al., 2020).

Likewise, recent evidence underscores the substantial contribution of ER stress to cardiovascular and renal diseases (Mohammed et al., 2010; Yuan et al., 2015). Despite the limited research data on regulating ER stress by aldo/MR, recent studies have shed light on

the role of aldosterone/MR receptor-mediated podocyte injury, highlighting the significance of oxidative stress and ER stress (Yuan et al., 2015).

In our investigations into cellular alterations induced by the aldosterone/MR and its PDK4 regulation, the significance of MAMs must be considered. MAMs serve as a pivotal signaling platform for dynamically modulating metabolic pathways (Gao et al., 2020). PDK4 plays a role in MAM's formation (Thoudam et al., 2019). It is suggested that increased PDK4 expression could potentially worsen MAM integrity (Kim et al., 2023; Thoudam et al., 2023), thereby potentially contributing to the triggering of ER stress due to MAM instability (Arruda and Hotamisligil, 2015). Enhanced interaction between the ER and mitochondria, along with increased calcium transport, has been observed under ER stress conditions, such as treatment with tunicamycin (Arruda et al., 2014). Moreover, additional signaling mechanisms have been elucidated; in addition to heightened ER-mitochondrial connectivity, the expression of the Ca^{2+} channel IP3R and tethering proteins like PACS-2 were notably upregulated in MAMs isolated from liver cells in two distinct obesity models, resulting in augmented oxidative stress and compromised oxidative phosphorylation (Arruda et al., 2014).

These findings emphasize the role of aldosterone/MR in activating downstream signaling pathways, particularly the IRE α pathway, contributing to cellular responses associated with endoplasmic reticulum stress. Emerging data indicates that ER stress may trigger autophagy (Cheng and Yang, 2011). Notably, previous investigation has revealed that IRE1 α can trigger autophagic processes as one of its stress responses to ER stress, thereby fostering the survival of SK-N-SH cells during ER stress (Ogata et al., 2006). Recent research has highlighted the activation of autophagy in hepatic steatosis, triggered by ER stress through the IRE1 α -JNK pathway (Wu et al., 2021).

5.1.4. Autophagy as a Result of Possibly Failed UPR Response

We hypothesized that aldosterone's potential induction of autophagy in conjunction with the MR might be a follow-up cellular response to ER stress and/or changes in MAM protein complexes. Autophagy flux was assessed by employing lysosomal inhibitors (pepstatin and aloxistatin at 10 μ g/ml) to monitor the turnover of LC3B II from LC3B I. Visual and quantitative comparison of bands with inhibitors and without inhibitors enabled the evaluation of LC3B II flux. After 24 hours of stimulation with aldosterone, an elevation in autophagy flux was detected. Conversely, samples without MR did not manifest heightened autophagy,

underscoring the pivotal role of MR in mediating this response. To further assess the involvement of MR, we utilized the MR antagonist eplerenone, presenting an alternative approach to scrutinize the impact of MR on autophagy regulation. The results confirmed the MR's effect in triggering autophagy in HEK cells.

Autophagy constitutes a multi-step cellular self-degradation process where proteins and organelles are enclosed within cytosolic double-membrane vesicles, known as autophagosomes. Subsequently, these autophagosomes are transferred to the lysosome for modification (He and Klionsky, 2009). Autophagosome initiation is mediated by the ULK1 complex, comprising ULK1, ATG13, FIP200, and ATG101, which translocates to autophagy initiation sites to recruit the VPS34 complex. The complex includes UVRAG to form a multiprotein complex with class III phosphatidylinositol 3-kinase (PI3K), which recruits additional ATG proteins (including ATG12) to facilitate vesicle elongation and phagophore nucleation (Vicencio et al., 2009). Cancer research has shown that ULK1 inhibits cancer cell proliferation and colony formation while promoting caspase-dependent apoptosis. Several autophagic proteins, including ULK1, have demonstrated dual roles in autophagy and apoptosis (Mukhopadhyay et al., 2015). For instance, ATG12 has been found to induce mitochondrial apoptosis by inhibiting the anti-apoptotic proteins BCL-2 and MCL-1 through its BH3-like motif (Zachari and Ganley, 2017). Studies have demonstrated that autophagy can selectively target specific cargos (protein aggregates). This selectivity is achieved by linking cargos to LC3 family proteins through ubiquitin-dependent or independent mechanisms. Unlike bulk autophagy, where protein ubiquitination modulates the process, in selective autophagy, ubiquitination marks cargos for recognition and initiates the autophagy process. Ubiquitinated proteins on cargos recruit specific autophagy adaptor proteins, such as p62 or NBR1 (Chen et al., 2019). The stimulation of autophagy is a multifaceted process influenced by various signaling inputs (He and Klionsky, 2009).

One of the possible mechanisms is the involvement of the MAM in the regulation of autophagy (Hamasaki et al., 2013). As previously noted, PDK4, a target MR pathway protein, is closely associated with the MAM complex, specifically the IP3R1-GRP75-VDAC1 complex, suggesting a regulatory role (Jeon et al., 2021). Recent investigations have also implicated IP3R in autophagy control, although data regarding the interplay between Ca^{2+} and IP3R in autophagy remain somewhat conflicting (Parys et al., 2012). One plausible mechanism involves the upregulation of IP3R1 on the ER membrane in conjunction with the VPS34 complex, a key player in autophagic signaling (Vicencio et al., 2009). The regulatory

function of IP3R1 in autophagy is intricate and contingent upon cellular context and stress stimuli. Thapsigargin, a potent inhibitor of endoplasmic reticulum calcium ATPase, has been utilized in several studies to induce elevated cytosolic Ca^{2+} levels and subsequent augmentation of autophagy (Groteimer et al., 2010; Høyer-Hansen et al., 2007). The heightened Ca^{2+} flux, integral to the MAM-resident multiprotein complex IP3R1-GRP75-VDAC1, facilitates calcium transport from the ER to the mitochondria, thereby modulating autophagy regulation (Thoudam et al., 2019). Additionally, in animal cells, the role of IP3R in certain instances of apoptosis is well documented (White et al., 2005).

Some recent investigations have illuminated the pivotal role of autophagy, mediated by aldosterone/MR interplay, in maintaining podocyte homeostasis under both healthy and pathological conditions (Yuan et al., 2015). This process is primarily cytoprotective, exerting beneficial effects in instances of podocyte injury. The MR on myeloid cells regulates macrophage polarization, a factor that influences autophagy (Usher et al., 2010). Our results demonstrated that aldosterone/MR regulates autophagy in MR overexpressing HEK cells. The outcome of autophagy, whether promoting cell survival or cell death, is contingent upon the nature of the cellular stress (Klionsky, 2020). We hypothesized that this regulation becomes relevant as a downstream reaction when the UPR response fails due to prolonged ER stress, resulting in apoptosis.

5.1.5. Cell Death as a Consequence of Altered Cellular Behavior

As previously noted in the literature review, aldosterone-induced apoptosis does not consistently stem from activated MR. In our investigation, we unequivocally established that the effect of activated caspase-3 relied on aldosterone-triggered MR activation. Our negative controls support this assertion, where the absence of aldosterone or MR prevented increased caspase activity.

A significant increase in caspase-3 activity was observed within 24 hours, with a more pronounced effect evident after 48 hours. In further exploration of cellular responses, we scrutinized the marker of necrosis, LDH. There were no alterations in 24 or 48-hour incubation in aldosterone-stimulated cells of LDH activity.

Our findings collectively suggest that aldosterone, combined with MR overexpression, induces caspase-3 activity indicative of apoptosis with a time-dependent effect. The absence of caspase-3 activity in the control groups supports the notion that aldosterone-mediated apoptosis is MR-dependent and occurs without impacting necrotic processes within the observed time frame.

Both GCs and MRs have been implicated in the induction of apoptosis, whereas glucocorticoids have been shown to elevate apoptosis in osteoblastic cells (Lin et al., 2015). Aldo has been observed to initiate apoptosis in human renal proximal tubular (HK2) cells in the presence of MR (Patni et al., 2007). The MR plays a pivotal role in processes such as inflammation, fibrosis, and vascular stiffness, creating an environment conducive to apoptosis (Artunc and Lang, 2014; Hayashi et al., 2008).

Furthermore, PDK4 silencing in myocardial ischemia-reperfusion injury coincided with SMAD protein inactivation (Yin et al., 2021). PDK4 expression and the TGF- β /SMAD pathway were significantly upregulated in atrial fibrillation patients. Knockdown of PDK4 inhibited the TGF- β /SMAD pathway, enhanced cell viability, and reduced apoptosis (Song and Zhang, n.d.). In vascular calcification, PDK4 enhanced the osteogenic differentiation of VSMCs by phosphorylating SMAD1/5/8, leading to mitochondrial dysfunction and apoptosis (Lee et al., 2015). Interestingly, PDK4 can alter the expression of SMAD genes without affecting BMP2 expression, an upstream regulator of SMAD genes. Under calcifying conditions, it was confirmed that PDK4 phosphorylates and activates SMAD1/5/8, resulting in the translocation of phosphorylated SMADs into the nucleus, where they regulate the transcription of target genes, thereby enhancing BMP2 signaling pathway activity (Lee et al., 2015). Various methods were used to show that PDK4 can be transported from the mitochondria into the cytosol in response to calcifying stimuli (Leem and Lee, 2016).

5.2. Activation of MR under Nitrosative Stress

We additionally investigated MR expression, activation, and signaling under nitrosative stress. We exposed MR-overexpressing cells to the peroxynitrite donor SIN-1. This chemical agent generates nitric oxide (NO) and superoxide, commonly used to mimic cellular oxidative stress (Pérez-Torres et al., 2020). We examined MR translocation, expression, apoptosis, and PDK4 expression under nitrosative stress. Alternative mechanisms may activate MR, shifting its function towards pathophysiological effects. Our hypothesis considers the potential involvement of nitrosative stress and the interplay between MR and reactive oxygen and nitrogen species.

5.2.1. MR Translocates and Activates Genes Under the Nitrosative Stress

We observed partial translocation of MR when stimulated with 200 μ M of SIN-1 for 1 hour. Under SIN-1 stimulation, a portion of MR moved from the cytoplasm to the nucleus. The nucleus fraction was significantly smaller in the vehicle control group, where MR

predominantly remained in the cytoplasm. When stimulated only with SIN-1, the nucleus exhibited substantially lower MR levels than aldosterone, where all cytosolic MR translocated to the nucleus. This effect could be attributed to the relatively low concentration of SIN-1 and the 1-hour exposure time. Nevertheless, the transition of MR under SIN-1 stimulation from the cytosol indicates the initiation of translocation similar to that observed with typical aldosterone stimulation.

Typically, MR exists in cytoplasmic heterocomplexes with the HSP90 chaperone system, stabilizing the inactive receptor and preventing hormone binding and transcriptional activity. Upon ligand binding, the receptor undergoes conformational changes, dimerizes, translocates to the nucleus, and binds to hormone-responsive elements to initiate gene transcription. Distinct gene expression patterns specific to MR or aldosterone may result from variations in the assembly of MR-associated cofactors despite a common HRE shared with GR (Obradović et al., 2004). Previous research has shown that the peroxynitrite donor SIN-1 induces nuclear translocation of the MR, whereas the GR remains unaffected. The nuclear MR translocation stimulated by peroxynitrite (ONOO⁻) and its transactivation activity were effectively blocked by geldanamycin, a potent HSP90 inhibitor. Geldanamycin completely prevented MR nuclear translocation under ONOO⁻ stimulation, highlighting the critical role of HSP90 in facilitating MR activation and transcriptional activity under oxidative stress induced by ONOO⁻ (Galigniana et al., 1998).

These findings suggest that SIN-1 acts as a partial MR agonist, inducing MR nuclear localization and transactivation activity without affecting GR localization or activity (Ruhs et al., 2012). ROS species can hinder MR nuclear translocation in intact kidney cells (Fiebeler and Luft, 2005).

Upon activation by aldosterone, MR typically translocates to the nucleus and binds to the promoters of target genes. We anticipated gene regulation under SIN-1/MR stimulation, given SIN-1's ability to partially initiate MR translocation. However, the number of activated genes observed in the SIN-1/MR sample from our NGS data was relatively small. Despite this, some activated genes caught our attention, as they are associated with the onset of CVDs. Interestingly, these genes were regulated by both aldosterone and SIN-1 in our validation experiments.

The selected genes, including FOSL2, MMP15, and SKIDA1, exhibited responsiveness to SIN-1 in the presence of the MR in 6 hours post-treatment. These genes might also be

classified as MR-target genes, as evidenced by their regulation under aldosterone/MR. Conversely, cells lacking MR induction, serving as the negative control, did not display these gene expressions. Our results suggested an activation of MR under 200 μ M SIN-1 6-hour stimulation.

Studies have shown the enhancement of MR transcriptional activity under oxidative stress in cultured rat cardiomyocytes (H9c2). In these experiments, oxidative stress induced by BSO (buthionine sulfoximine) triggers the activation of Rac1. This activation subsequently led to MR activation, as demonstrated by an increase in MR-driven transcriptional activity and the nuclear accumulation of MR. These findings suggest a direct link between oxidative stress-induced Rac1 activation and MR-mediated transcriptional responses in cardiomyocytes (Nagase et al., 2012). Furthermore, aldosterone has been demonstrated to elevate superoxide anion formation in macrophages and the aorta of mice, promoting the development of atherosclerotic lesions (Keidar et al., 2004). Moreover, MR contributes to oxidative stress by upregulating NADPH oxidase subunits NOX2 and NOX4 in vascular cells and cultured neonatal atrial myocytes, thereby modulating its microenvironment (Lu et al., 2019).

Another interpretation of our results concerning translocation and gene activation could be that MR overexpression may lead to potential autoactivation of the receptor. This intriguing possibility, while not typical under normal physiological circumstances, opens up a new avenue of understanding. The receptor's primary mode of action is ligand-dependent, and abnormal activation often leads to pathological outcomes such as hypertension or kidney disorders. It was demonstrated for the orphan nuclear receptor OR1 that autoactivation can also result from overexpression. When OR1 heterodimerizes with retinoid X receptor alpha (RXR α), it undergoes a conformational change that activates its transcriptional potential, primarily through its AF-2 domain (Wiebel and Gustafsson, 1997). Another example of context-driven plasticity of nuclear receptor activation comes from GR through its specific alterations in conformation. In this sense, the activities of GR reflect its molecular conformations, which emerge owing to the context-specific microenvironment. In contrast, the functions of GR are integrated regulatory outcomes of co-regulatory enzyme actions associated with those various conformations (Weikum et al., 2017).

This data reinforces our hypothesis that microenvironment changes, such as increased oxidative stress during aging, can activate MR independently of aldosterone, potentially leading to a shift from the physiological to the pathophysiological role of MR.

5.2.2. MR Effects and Expression under Nitrosative Stress

To assess the biological effect of MR under SIN-1 stimulation, we examined PDK4 expression following treatment with 200 μM SIN-1/MR. The addition of SIN-1 did not change PDK4 expression in samples treated with SIN-1 alone and in those treated with Aldo/SIN-1. Consequently, we increased the SIN-1 concentration to 600 μM and 800 μM and time to 24 hours. Quantitative PCR analysis showed that at 600 μM and 800 μM and in the presence of Aldo, PDK4 mRNA expression was inhibited, a finding corroborated by corresponding decreases in PDK4 protein levels. We introduced ebselen, a known peroxynitrite scavenger, to investigate whether peroxynitrite was responsible for this downregulation (Daiber et al., 2000). Ebselen restored PDK4 expression at both the mRNA and protein levels, nearly reaching Aldo levels. Additionally, we investigated caspase activity under SIN-1/MR stimulation. In the case of Aldo/SIN-1 stimulation with MR, we found inhibited caspase activity under higher SIN-1 concentrations. We included a 400 μM SIN-1 concentration to bridge the gap between 200 μM and 600 μM . SIN-1 alone did not affect caspase-3 activity, but in combination with Aldo, a dose-dependent decrease in caspase-3 activity was observed, suggesting that SIN-1 suppressed Aldo's effect. We hypothesized that this suppression may depend on altered MR activity or expression, as caspase activity was not altered in cells lacking MR.

Our findings revealed that MR expression decreased significantly at higher SIN-1 concentrations (600 μM and 800 μM) at the mRNA and protein levels. Similarly, the expression in samples combined with SIN-1 and Aldo reduced MR expression. In contrast, GR protein expression was unaffected by SIN-1 treatment after 24 hours, suggesting it to be an MR-specific effect.

Our study observed an inhibited Aldo/MR response, as indicated by reduced PDK4 expression and diminished caspase activity. We hypothesize that this inhibition is associated with decreased MR mRNA expression, potentially resulting from nitrosative stress (SIN-1 stimulation).

Nitrosative stress is believed to influence various mechanisms at the mRNA level of the MR. This mechanism includes the regulation of transcription factors binding to the promoter regions of the MR gene, with their activity modulated by oxidative stress. For example, oxidative stress can activate transcription factors such as NF- κ B and AP-1, which can either

upregulate or downregulate MR gene expression depending on specific conditions (Kolla and Litwack, 2000; Korkmaz et al., 2009; Lingappan, 2018). ROS/RNS can induce epigenetic changes, including DNA methylation, histone modifications, and chromatin remodeling (Campos et al., 2007; Khan et al., 2016). These alterations can affect the accessibility of the MR gene to the transcriptional machinery. Elevated oxidative stress, for instance, can lead to hypermethylation of the MR gene promoter, thereby reducing its expression. Oxidative stress also activates intracellular signaling pathways, such as MAPK, JNK, and PI3K/Akt (Liu et al., 2022). These pathways can converge on transcriptional regulators and other proteins involved in gene expression, thereby influencing MR mRNA synthesis. For example, activating the JNK pathway can increase the phosphorylation of transcription factors that regulate MR gene transcription (Weston and Davis, 2007).

Oxidation of MR can decrease its biological response by reducing its ability to bind aldosterone and DNA. This effect can be reversed by reducing agents. Kidney MR is highly sensitive to oxidation, mainly due to reactive cysteine residues that respond to sulfhydryl-reducing agents and metal ions, which can exacerbate H₂O₂-induced inhibition of aldosterone and DNA binding (Galigniana, 1996; Piwien-Pilipuk et al., 2002). One inhibitory mechanism involves MR oxidation, likely through essential cysteine groups, supported by evidence of reduced reactive thiols after *in vivo* glutathione depletion. Prolonged glutathione depletion can also affect the protein translation system, leading to high carbonylation levels of MR (Piwien-Pilipuk et al., 2002). Nitrosative stress during aging also impacts MR signaling (Ruhs et al., 2012). NO can form S-nitrosothiols with sulfhydryl groups, inhibiting GR ligand binding without affecting MR-HSP90 interaction and reducing MR and GR transactivation activity upon corticosteroid treatment (Galigniana et al., 1998). It has also been shown that peroxynitrite can induce ligand-independent MR transactivation through nuclear translocation while genomic GR activity remains unaffected (Ruhs et al., 2012).

5.3. Conclusion and Suggestions

In conclusion, the intricate interplay between the aldosterone/MR and its impact on cell metabolism, particularly in MR-overexpressing HEK cells, is discussed. The observed augmentation of glucose consumption and lactate production in response to elevated aldosterone/MR activity suggests an adaptive cellular response, which may hold significance in conditions such as aging, where increased aldosterone and MR activity have been reported.

Furthermore, our investigation into the metabolic shift towards lactate production under aldosterone/MR stimulation aligns with existing knowledge, indicating a potential mechanism to mitigate oxidative stress. This metabolic adaptation, characterized by heightened glycolysis and reduced mitochondrial ATP production, may contribute to cellular alterations such as ER stress and apoptosis.

Moreover, our study elucidates the regulatory role of the MR in the expression of PDK4, offering insights into its potential involvement in metabolic reprogramming and cellular homeostasis. The upregulation of PDK4 by activated MR suggests a link between aldosterone/MR signaling and metabolic changes, highlighting PDK4 as a potential therapeutic target in metabolic disorders.

Our investigation into ER stress, autophagy, and apoptosis pathways also elucidates the cellular responses induced by aldosterone/MR activation. The specificity of aldosterone/MR interplay in inducing ER stress and activating downstream signaling pathways, particularly the IRE1 α pathway, uncovers a part of the complex molecular mechanisms involved in cellular adaptation to stress.

We observed a phenomenon where the MR partially translocated from the cytosol to the nucleus in response to alterations in the microenvironment. This partial translocation implies the involvement of a non-classical ligand activation pathway for MR. We hypothesize that this nuclear translocation may lead to the activation of MR-target genes, potentially contributing to pathophysiological processes due to changed microenvironment, such as those involved in CVDs. We detected the following genes: SKIDA1, FOSL2, and MMP15 regulated by 200 μ M SIN-1/MR.

Interestingly, co-stimulation of higher SIN-1 concentrations (600 μ M and 800 μ M) with aldosterone resulted in a downregulatory effect on PDK4. Subsequently, we observed a dose-dependent decrease in caspase-3 activity in cells co-stimulated with SIN-1 and aldosterone. MR protein and mRNA expression was also found to be reduced. These results suggest that nitrosative stress generated by SIN-1 may inhibit the MR mRNA synthesis or influence the tetracycline-inducible system responsible for MR gene expression in our cells. Furthermore, the observed decrease in MR expression highlights the intricate response of MR to nitrosative stress.

Our discoveries enhance comprehension of the molecular mechanisms governing aldosterone/MR signaling and its impact on cellular metabolism and homeostasis. Further exploration in this

field is crucial to elucidate the potential pathways influenced by aldo/MR amid numerous others. Likewise, our study sheds light on the multifaceted role of MR in cellular responses to nitrosative stress, paving the way for future discoveries in this emerging field.

5.4. Limitations

MR signaling is complex, involving various pathways and interactions with other receptors. Understanding these interactions is vital for determining the specific roles of MRs in different cell types, but this is challenging.

Our study utilized 10 nM aldo to activate all expressed MRs. This aldo concentration is higher than physiological levels but is in the range of pathophysiological expected concentrations. MR-overexpressing HEK cells were employed to simulate the increased MR activity and expression observed during aging. We aimed to validate these findings in a more differentiated or primary cell line. However, we encountered significant challenges, particularly with MR degradation and low expression in our tested cells. Transfection proved especially problematic and did not provide a robust cell model. Of the tested lines, only Ea.hy926 cells exhibited some responsiveness, but transfection attempts were unsuccessful.

PDK4 regulation is complex and influenced by hormones, nutrients, and energy status, making it difficult to determine its exact role. Alternative pathways involving glutamate and fatty acids need exploration. Identifying a suitable PDK4 inhibitor proved challenging, as dichloroacetate (DCA) is known to affect both autophagy and apoptosis. For instance, this made it difficult to use DCA in experiments to assess the specific link between PDK4 and autophagy. Effective antibodies for PDK4 detection were identified, but detecting PDK4 protein levels was complicated by multiple bands.

The Seahorse assay measures the oxygen consumption rate (OCR) and extracellular acidification rate (ECAR) across a cell population, but cellular heterogeneity can complicate result interpretation. Comparing results with other cell types expressing MR is essential for clarity. Evaluating oxidative stress levels and their origins in cells stimulated by aldo/MR activation provides insights into metabolic adaptations. It is crucial to determine if increased glucose consumption is a response to oxidative stress, which can be tested by administering antioxidants and monitoring glucose consumption and lactate production. Exploring alternative nutritional substrates for aldo/MR-exposed cells is also necessary.

Assessing autophagy's role under aldo/MR conditions is crucial; inhibiting autophagy and observing ROS levels or apoptosis changes can offer insights. The influence of the T-REX system used alongside SIN-1 stimulation in cell models must be evaluated for potential cellular toxicity due to high-level transactivator expression. It is essential to investigate the interplay between SIN-1 and tetracycline. Previous reports suggest a possible impact of RNS on tetracycline (Colicchia et al., 2022), where tetracycline undergoes chemical alterations when exposed to RNS. RNS can modify tetracycline through nitration or nitrosation processes. Nitrosation, for instance, can add a nitroso group (NO) to amines (Wichitnithad et al., 2023), while nitration can introduce a nitro group (NO₂) to aromatic rings, potentially altering the antibiotic's structure and function (Fukuto et al., 2012). Peroxynitrite, a potent oxidant, can cause oxidative modifications to a broad range of biological molecules, including nucleic acids, proteins, lipids, and small molecules like tetracycline. This oxidation can lead to structural changes that might affect tetracycline's antibiotic properties (Fukuto et al., 2012; Markley and Wencewicz, 2018). Consequently, these modifications could prevent tetracycline from binding to the Tet repressor, thereby influencing the expression of target genes in the tetracycline-inducible system.

Exploring different experimental conditions, such as time points and SIN-1 concentrations, is necessary to understand their impact on MR expression and translocation. Using eplerenone, an MR antagonist, against SIN-1 could reveal shared mechanisms with aldo. Developing a more physiologically relevant system for MR expression under oxidative stress, particularly with elevated peroxynitrite levels, would be beneficial. Understanding how SIN-1 impacts cell phenotype compared to aldo activation of MR will provide insights into the interactions between oxidative stress, MR signaling, and cellular responses. Controlling SIN-1-induced peroxynitrite generation with a fluorescent probe could aid in this effort.

6. Reference

- Agarwal, M.K., Mirshahi, M., 1999. General overview of mineralocorticoid hormone action. *Pharmacology & Therapeutics* 84, 273–326. [https://doi.org/10.1016/S0163-7258\(99\)00038-8](https://doi.org/10.1016/S0163-7258(99)00038-8)
- Ait-Aissa, K., Blaszkak, S.C., Beutner, G., Tsaih, S.-W., Morgan, G., Santos, J.H., Flister, M.J., Joyce, D.L., Camara, A.K.S., Gutterman, D.D., Donato, A.J., Porter, G.A., Beyer, A.M., 2019. Mitochondrial Oxidative Phosphorylation defect in the Heart of Subjects with Coronary Artery Disease. *Sci Rep* 9, 7623. <https://doi.org/10.1038/s41598-019-43761-y>
- Alvarez Quintero, G.S., Lima, A., Roig, P., Meyer, M., De Kloet, E.R., De Nicola, A.F., Garay, L.I., 2024. Effects of the mineralocorticoid receptor antagonist eplerenone in experimental autoimmune encephalomyelitis. *The Journal of Steroid Biochemistry and Molecular Biology* 238, 106461. <https://doi.org/10.1016/j.jsbmb.2024.106461>
- Araki, M., Motojima, K., 2006. Identification of ERRalpha as a specific partner of PGC-1alpha for the activation of PDK4 gene expression in muscle. *FEBS J* 273, 1669–1680. <https://doi.org/10.1111/j.1742-4658.2006.05183.x>
- Armstrong, C., Editor, A.S.A., n.d. JNC 8 Guidelines for the Management of Hypertension in Adults.
- Arriza, J.L., Weinberger, C., Cerelli, G., Glaser, T.M., Handelin, B.L., Housman, D.E., Evans, R.M., 1987. Cloning of human mineralocorticoid receptor complementary DNA: structural and functional kinship with the glucocorticoid receptor. *Science* 237, 268–275. <https://doi.org/10.1126/science.3037703>
- Arruda, A.P., Hotamisligil, G.S., 2015. Calcium Homeostasis and Organelle Function in the Pathogenesis of Obesity and Diabetes. *Cell Metab* 22, 381–397. <https://doi.org/10.1016/j.cmet.2015.06.010>
- Arruda, A.P., Pers, B.M., Parlakgöl, G., Güney, E., Inouye, K., Hotamisligil, G.S., 2014. Chronic enrichment of hepatic ER-mitochondria contact sites leads to calcium dependent mitochondrial dysfunction in obesity. *Nat Med* 20, 1427–1435. <https://doi.org/10.1038/nm.3735>
- Artunc, F., Lang, F., 2014. Mineralocorticoid and SGK1-Sensitive Inflammation and Tissue Fibrosis. *Nephron Physiology* 128, 35–39. <https://doi.org/10.1159/000368267>
- Bakris, G.L., Agarwal, R., Anker, S.D., Pitt, B., Ruilope, L.M., Rossing, P., Kolkhof, P., Nowack, C., Schloemer, P., Joseph, A., Filippatos, G., 2020. Effect of Finerenone on Chronic Kidney Disease Outcomes in Type 2 Diabetes. *N Engl J Med* 383, 2219–2229. <https://doi.org/10.1056/NEJMoa2025845>
- Barrera-Chimal, J., Girerd, S., Jaisser, F., 2019. Mineralocorticoid receptor antagonists and kidney diseases: pathophysiological basis. *Kidney International* 96, 302–319. <https://doi.org/10.1016/j.kint.2019.02.030>
- Bauersachs, J., Jaisser, F., Toto, R., 2015. Mineralocorticoid Receptor Activation and Mineralocorticoid Receptor Antagonist Treatment in Cardiac and Renal Diseases. *Hypertension* 65, 257–263. <https://doi.org/10.1161/HYPERTENSIONAHA.114.04488>
- Benetos, A., Gardner, J.P., Kimura, M., Labat, C., Nzietchueng, R., Dousset, B., Zannad, F., Lacolley, P., Aviv, A., 2005. Aldosterone and Telomere Length in White Blood Cells. *The Journals of Gerontology Series A: Biological Sciences and Medical Sciences* 60, 1593–1596. <https://doi.org/10.1093/gerona/60.12.1593>
- Bergmeyer, H.-U., 2012. *Methods of Enzymatic Analysis*. Elsevier.
- Bhullar, S.K., Dhalla, N.S., 2023. Status of Mitochondrial Oxidative Phosphorylation during the Development of Heart Failure. *Antioxidants* 12, 1941. <https://doi.org/10.3390/antiox12111941>
- Binart, N., Lombès, M., Baulieu, E.E., 1995. Distinct functions of the 90 kDa heat-shock protein (hsp90) in oestrogen and mineralocorticosteroid receptor activity: effects of hsp90 deletion mutants. *Biochem J* 311 (Pt 3), 797–804. <https://doi.org/10.1042/bj3110797>
- Blazanin, N., Son, J., Craig-Lucas, A.B., John, C.L., Breech, K.J., Podolsky, M.A., Glick, A.B., 2017. ER stress and distinct outputs of the IRE1α RNase control proliferation and senescence in response to oncogenic Ras. *Proceedings of the National Academy of Sciences* 114, 9900–9905. <https://doi.org/10.1073/pnas.1701757114>
- Boileau, P., Mrejen, C., Girard, J., Mouzon, S.H., 1995. Overexpression of GLUT3 placental glucose transporter in diabetic rats. *J Clin Invest* 96, 309–317. <https://doi.org/10.1172/JCI118036>

- Buonafine, M., Bonnard, B., Jaisser, F., 2018. Mineralocorticoid Receptor and Cardiovascular Disease. *Am J Hypertens* 31, 1165–1174. <https://doi.org/10.1093/ajh/hpy120>
- Caamano, C.A., Morano, M.I., Patel, P.D., Watson, S.J., Akil, H., 1993. A bacterially expressed mineralocorticoid receptor is associated in vitro with the 90-kilodalton heat shock protein and shows typical hormone- and DNA-binding characteristics. *Biochemistry* 32, 8589–8595. <https://doi.org/10.1021/bi00084a028>
- Campos, A.C.E., Molognoni, F., Melo, F.H.M., Galdieri, L.C., Carneiro, C.R.W., D'Almeida, V., Correa, M., Jasiulionis, M.G., 2007. Oxidative Stress Modulates DNA Methylation during Melanocyte Anchorage Blockade Associated with Malignant Transformation. *Neoplasia* 9, 1111–1121. <https://doi.org/10.1593/neo.07712>
- Cezar, M.D.M., Damatto, R.L., Pagan, L.U., Lima, A.R.R., Martinez, P.F., Bonomo, C., Rosa, C.M., Campos, D.H.S., Cicogna, A.C., Gomes, M.J., Oliveira-Jr, S.A., Blotta, D.A., Okoshi, M.P., Okoshi, K., 2015. Early Spironolactone Treatment Attenuates Heart Failure Development by Improving Myocardial Function and Reducing Fibrosis in Spontaneously Hypertensive Rats. *Cellular Physiology and Biochemistry* 36, 1453–1466. <https://doi.org/10.1159/000430310>
- Chapman, K., Holmes, M., Seckl, J., 2013. 11 β -Hydroxysteroid Dehydrogenases: Intracellular Gatekeepers of Tissue Glucocorticoid Action. *Physiol Rev* 93, 1139–1206. <https://doi.org/10.1152/physrev.00020.2012>
- Chen, L., Ding, M.-L., Wu, F., He, W., Li, J., Zhang, X.-Y., Xie, W.-L., Duan, S.-Z., Xia, W.-H., Tao, J., 2016. Impaired Endothelial Repair Capacity of Early Endothelial Progenitor Cells in Hypertensive Patients With Primary Hyperaldosteronemia: Role of 5,6,7,8-Tetrahydrobiopterin Oxidation and Endothelial Nitric Oxide Synthase Uncoupling. *Hypertension* 67, 430–439. <https://doi.org/10.1161/HYPERTENSIONAHA.115.06597>
- Chen, R.-H., Chen, Y.-H., Huang, T.-Y., 2019. Ubiquitin-mediated regulation of autophagy. *J Biomed Sci* 26, 80. <https://doi.org/10.1186/s12929-019-0569-y>
- Cheng, Y., Yang, J.-M., 2011. Survival and death of endoplasmic-reticulum-stressed cells: Role of autophagy. *World J Biol Chem* 2, 226–231. <https://doi.org/10.4331/wjbc.v2.i10.226>
- Cockfield, J.A., Schafer, Z.T., 2021. SGK1-regulated metabolism: key for the survival of cells detached from the extracellular matrix. *Molecular & Cellular Oncology* 8, 1976583. <https://doi.org/10.1080/23723556.2021.1976583>
- Colicchia, V., Häggblad, M., Sirozh, O., Porebski, B., Balan, M., Li, X., Lidemalm, L., Carreras-Puigvert, J., Hühn, D., Fernandez-Capetillo, O., 2022. New regulators of the tetracycline-inducible gene expression system identified by chemical and genetic screens. *FEBS Open Bio* 12, 1896–1908. <https://doi.org/10.1002/2211-5463.13482>
- Cybulsky, A.V., 2013. The intersecting roles of endoplasmic reticulum stress, ubiquitin-proteasome system, and autophagy in the pathogenesis of proteinuric kidney disease. *Kidney Int* 84, 25–33. <https://doi.org/10.1038/ki.2012.390>
- Daiber, A., Zou, M.-H., Bachschmid, M., Ullrich, V., 2000. Ebselen as a peroxynitrite scavenger in vitro and ex vivo. *Biochemical Pharmacology* 59, 153–160. [https://doi.org/10.1016/S0006-2952\(99\)00309-3](https://doi.org/10.1016/S0006-2952(99)00309-3)
- Dey, S., Garg, J., Wang, A., Holzner, E., Frishman, W.H., Aronow, W.S., n.d. Finerenone: Efficacy of a New Nonsteroidal Mineralocorticoid Receptor Antagonist in Treatment of Patients With Chronic Kidney Disease and Type 2 Diabetes. *Cardiology in Review* 10.1097/CRD.0000000000000548. <https://doi.org/10.1097/CRD.0000000000000548>
- Dickson, L.M., Buchmann, E.J., Janse Van Rensburg, C., Norris, S.A., 2019. The impact of differences in plasma glucose between glucose oxidase and hexokinase methods on estimated gestational diabetes mellitus prevalence. *Sci Rep* 9, 7238. <https://doi.org/10.1038/s41598-019-43665-x>
- DuPont, J.J., McCurley, A., Davel, A.P., McCarthy, J., Bender, S.B., Hong, K., Yang, Y., Yoo, J.-K., Aronovitz, M., Baur, W.E., Christou, D.D., Hill, M.A., Jaffe, I.Z., 2016. Vascular mineralocorticoid receptor regulates microRNA-155 to promote vasoconstriction and rising blood pressure with aging [WWW Document]. <https://doi.org/10.1172/jci.insight.88942>
- Edwards, C., 2020. New Horizons: Does Mineralocorticoid Receptor Activation by Cortisol Cause ATP Release and COVID-19 Complications? *J Clin Endocrinol Metab* 106, 622–635. <https://doi.org/10.1210/clinem/dgaa874>

- Edwards, C.R., Stewart, P.M., Burt, D., Brett, L., McIntyre, M.A., Sutanto, W.S., de Kloet, E.R., Monder, C., 1988. Localisation of 11 beta-hydroxysteroid dehydrogenase--tissue specific protector of the mineralocorticoid receptor. *Lancet* 2, 986–989. [https://doi.org/10.1016/s0140-6736\(88\)90742-8](https://doi.org/10.1016/s0140-6736(88)90742-8)
- Fejes-Tóth, G., Pearce, D., Náray-Fejes-Tóth, A., 1998. Subcellular localization of mineralocorticoid receptors in living cells: Effects of receptor agonists and antagonists. *Proc. Natl. Acad. Sci. U.S.A.* 95, 2973–2978. <https://doi.org/10.1073/pnas.95.6.2973>
- Feraco, A., Gorini, S., Mammi, C., Lombardo, M., Armani, A., Caprio, M., 2023. Neutral Effect of Skeletal Muscle Mineralocorticoid Receptor on Glucose Metabolism in Mice. *IJMS* 24, 7412. <https://doi.org/10.3390/ijms24087412>
- Feraco, A., Marzolla, V., Scuteri, A., Armani, A., Caprio, M., 2020. Mineralocorticoid Receptors in Metabolic Syndrome: From Physiology to Disease. *Trends in Endocrinology & Metabolism* 31, 205–217. <https://doi.org/10.1016/j.tem.2019.11.006>
- Fiebeler, A., Haller, H., 2003. Participation of the mineralocorticoid receptor in cardiac and vascular remodeling. *Nephron Physiol* 94, p47-50. <https://doi.org/10.1159/000072029>
- Fiebeler, A., Luft, F.C., 2005. The Mineralocorticoid Receptor and Oxidative Stress. *Heart Fail Rev* 10, 47–52. <https://doi.org/10.1007/s10741-005-2348-y>
- Fiebeler, A., Schmidt, F., Müller, D.N., Park, J.-K., Dechend, R., Bieringer, M., Shagdarsuren, E., Breu, V., Haller, H., Luft, F.C., 2001. Mineralocorticoid Receptor Affects AP-1 and Nuclear Factor- κ B Activation in Angiotensin II-Induced Cardiac Injury. *Hypertension* 37, 787–793. <https://doi.org/10.1161/01.HYP.37.2.787>
- Filippatos, G., Anker, S.D., Böhm, M., Gheorghide, M., Køber, L., Krum, H., Maggioni, A.P., Ponikowski, P., Voors, A.A., Zannad, F., Kim, S.-Y., Nowack, C., Palombo, G., Kolkhof, P., Kimmeskamp-Kirschbaum, N., Pieper, A., Pitt, B., 2016. A randomized controlled study of finerenone vs. eplerenone in patients with worsening chronic heart failure and diabetes mellitus and/or chronic kidney disease. *Eur Heart J* 37, 2105–2114. <https://doi.org/10.1093/eurheartj/ehw132>
- Fischer, K., Kelly, S.M., Watt, K., Price, N.C., McEwan, I.J., 2010. Conformation of the Mineralocorticoid Receptor N-terminal Domain: Evidence for Induced and Stable Structure. *Molecular Endocrinology* 24, 1935–1948. <https://doi.org/10.1210/me.2010-0005>
- Förstermann, U., Münzel, T., 2006. Endothelial Nitric Oxide Synthase in Vascular Disease: From Marvel to Menace. *Circulation* 113, 1708–1714. <https://doi.org/10.1161/CIRCULATIONAHA.105.602532>
- Fukuto, J.M., Carrington, S.J., Tantillo, D.J., Harrison, J.G., Ignarro, L.J., Freeman, B.A., Chen, A., Wink, D.A., 2012. Small Molecule Signaling Agents: The Integrated Chemistry and Biochemistry of Nitrogen Oxides, Oxides of Carbon, Dioxide, Hydrogen Sulfide, and Their Derived Species. *Chem. Res. Toxicol.* 25, 769–793. <https://doi.org/10.1021/tx2005234>
- Fuller, P.J., Yang, J., Young, M.J., 2017. 30 YEARS OF THE MINERALOCORTICOID RECEPTOR: Coregulators as mediators of mineralocorticoid receptor signalling diversity. *Journal of Endocrinology* 234, T23–T34. <https://doi.org/10.1530/JOE-17-0060>
- Fuller, P.J., Yao, Y.-Z., Yang, J., Young, M.J., 2021. Structural determinants of activation of the mineralocorticoid receptor: an evolutionary perspective. *J Hum Hypertens* 35, 110–116. <https://doi.org/10.1038/s41371-020-0360-2>
- Funder, J.W., 2005a. Mineralocorticoid Receptors: Distribution and Activation. *Heart Fail Rev* 10, 15–22. <https://doi.org/10.1007/s10741-005-2344-2>
- Funder, J.W., 2005b. RALES, EPHESUS and redox. *The Journal of Steroid Biochemistry and Molecular Biology, Proceedings of the 16th International Symposium of The Journal of Steroid Biochemistry and Molecular Biology* 93, 121–125. <https://doi.org/10.1016/j.jsbmb.2004.12.010>
- Funder, J.W., 1993. Mineralocorticoids, glucocorticoids, receptors and response elements. *Science* 259, 1132–1133. <https://doi.org/10.1126/science.8382375>
- Galigniana, M.D., 1996. Stability study on renal type I mineralocorticoid receptor. *Life Sciences* 59, 511–521. [https://doi.org/10.1016/0024-3205\(96\)00331-1](https://doi.org/10.1016/0024-3205(96)00331-1)
- Galigniana, M.D., Erlejman, A.G., Monte, M., Gomez-Sanchez, C., Piwien-Pilipuk, G., 2010. The hsp90-FKBP52 Complex Links the Mineralocorticoid Receptor to Motor Proteins and Persists

- Bound to the Receptor in Early Nuclear Events. *Mol Cell Biol* 30, 1285–1298. <https://doi.org/10.1128/MCB.01190-09>
- Galigniana, M.D., Scruggs, J.L., Herrington, J., Welsh, M.J., Carter-Su, C., Housley, P.R., Pratt, W.B., 1998. Heat shock protein 90-dependent (geldanamycin-inhibited) movement of the glucocorticoid receptor through the cytoplasm to the nucleus requires intact cytoskeleton. *Mol Endocrinol* 12, 1903–1913. <https://doi.org/10.1210/mend.12.12.0204>
- Gao, P., Yan, Z., Zhu, Z., 2020. Mitochondria-Associated Endoplasmic Reticulum Membranes in Cardiovascular Diseases. *Front. Cell Dev. Biol.* 8, 604240. <https://doi.org/10.3389/fcell.2020.604240>
- Gomez-Sanchez, E., Gomez-Sanchez, C.E., 2014. The Multifaceted Mineralocorticoid Receptor. *Compr Physiol* 4, 965–994. <https://doi.org/10.1002/cphy.c130044>
- Gray, L.R., Tompkins, S.C., Taylor, E.B., 2014. Regulation of pyruvate metabolism and human disease. *Cell. Mol. Life Sci.* 71, 2577–2604. <https://doi.org/10.1007/s00018-013-1539-2>
- Green, S., Chambon, P., 1987. Oestradiol induction of a glucocorticoid-responsive gene by a chimaeric receptor. *Nature* 325, 75–78. <https://doi.org/10.1038/325075a0>
- Griesler, B., Schuelke, C., Uhlig, C., Gadasheva, Y., Grossmann, C., 2022. Importance of Micromilieu for Pathophysiologic Mineralocorticoid Receptor Activity—When the Mineralocorticoid Receptor Resides in the Wrong Neighborhood. *IJMS* 23, 12592. <https://doi.org/10.3390/ijms232012592>
- Grossmann, C., Ruhs, S., Langenbruch, L., Mildenerger, S., Strätz, N., Schumann, K., Gekle, M., 2012. Nuclear Shuttling Precedes Dimerization in Mineralocorticoid Receptor Signaling. *Chemistry & Biology* 19, 742–751. <https://doi.org/10.1016/j.chembiol.2012.04.014>
- Grotmeier, A., Alers, S., Pfisterer, S.G., Paasch, F., Daubrawa, M., Dieterle, A., Viollet, B., Wesselborg, S., Proikas-Cezanne, T., Stork, B., 2010. AMPK-independent induction of autophagy by cytosolic Ca²⁺ increase. *Cell Signal* 22, 914–925. <https://doi.org/10.1016/j.cellsig.2010.01.015>
- Hamasaki, M., Furuta, N., Matsuda, A., Nezu, A., Yamamoto, A., Fujita, N., Oomori, H., Noda, T., Haraguchi, T., Hiraoka, Y., Amano, A., Yoshimori, T., 2013. Autophagosomes form at ER-mitochondria contact sites. *Nature* 495, 389–393. <https://doi.org/10.1038/nature11910>
- Handy, D.E., Loscalzo, J., 2012. Redox Regulation of Mitochondrial Function. *Antioxidants & Redox Signaling* 16, 1323–1367. <https://doi.org/10.1089/ars.2011.4123>
- Hayashi, H., Kobara, M., Abe, M., Tanaka, N., Gouda, E., Toba, H., Yamada, H., Tatsumi, T., Nakata, T., Matsubara, H., 2008. Aldosterone Nongenomically Produces NADPH Oxidase-Dependent Reactive Oxygen Species and Induces Myocyte Apoptosis. *Hypertens Res* 31, 363–375. <https://doi.org/10.1291/hypres.31.363>
- He, C., Klionsky, D.J., 2009. Regulation Mechanisms and Signaling Pathways of Autophagy. *Annu Rev Genet* 43, 67–93. <https://doi.org/10.1146/annurev-genet-102808-114910>
- Hernández-Díaz, I., Giraldez, T., Arnau, M.R., Smits, V.A.J., Jaisser, F., Farman, N., Alvarez De La Rosa, D., 2010. The Mineralocorticoid Receptor Is a Constitutive Nuclear Factor in Cardiomyocytes due to Hyperactive Nuclear Localization Signals. *Endocrinology* 151, 3888–3899. <https://doi.org/10.1210/en.2010-0099>
- Hetz, C., 2012. The unfolded protein response: controlling cell fate decisions under ER stress and beyond. *Nat Rev Mol Cell Biol* 13, 89–102. <https://doi.org/10.1038/nrm3270>
- Hirono, Y., Yoshimoto, T., Suzuki, N., Sugiyama, T., Sakurada, M., Takai, S., Kobayashi, N., Shichiri, M., Hirata, Y., 2007. Angiotensin II Receptor Type 1-Mediated Vascular Oxidative Stress and Proinflammatory Gene Expression in Aldosterone-Induced Hypertension: The Possible Role of Local Renin-Angiotensin System. *Endocrinology* 148, 1688–1696. <https://doi.org/10.1210/en.2006-1157>
- Ho, R.C., Alcazar, O., Fujii, N., Hirshman, M.F., Goodyear, L.J., 2004. p38gamma MAPK regulation of glucose transporter expression and glucose uptake in L6 myotubes and mouse skeletal muscle. *Am J Physiol Regul Integr Comp Physiol* 286, R342-349. <https://doi.org/10.1152/ajpregu.00563.2003>
- Høyer-Hansen, M., Bastholm, L., Szyniarowski, P., Campanella, M., Szabadkai, G., Farkas, T., Bianchi, K., Fehrenbacher, N., Elling, F., Rizzuto, R., Mathiasen, I.S., Jäättelä, M., 2007. Control of macroautophagy by calcium, calmodulin-dependent kinase kinase-beta, and Bcl-2. *Mol Cell* 25, 193–205. <https://doi.org/10.1016/j.molcel.2006.12.009>

- Hu, D., Dong, R., Zhang, Y., Yang, Y., Chen, Z., Tang, Y., Fu, M., Xu, X., Tu, L., 2020. Age-related changes in mineralocorticoid receptors in rat hearts. *Mol Med Rep* 22, 1859–1867. <https://doi.org/10.3892/mmr.2020.11260>
- Huang, B., Wu, P., Bowker-Kinley, M.M., Harris, R.A., 2002. Regulation of pyruvate dehydrogenase kinase expression by peroxisome proliferator-activated receptor-alpha ligands, glucocorticoids, and insulin. *Diabetes* 51, 276–283. <https://doi.org/10.2337/diabetes.51.2.276>
- Hudson, W.H., Youn, C., Ortlund, E.A., 2014. Crystal Structure of the Mineralocorticoid Receptor DNA Binding Domain in Complex with DNA. *PLoS ONE* 9, e107000. <https://doi.org/10.1371/journal.pone.0107000>
- Ibarrola, J., Lu, Q., Zennaro, M.-C., Jaffe, I.Z., 2023. Mechanism by Which Inflammation and Oxidative Stress Induce Mineralocorticoid Receptor Gene Expression in Aging Vascular Smooth Muscle Cells. *Hypertension* 80, 111–124. <https://doi.org/10.1161/HYPERTENSIONAHA.122.19213>
- Ibrahim, H.N., Rosenberg, M.E., Hostetter, T.H., 1997. Role of the renin-angiotensin-aldosterone system in the progression of renal disease: a critical review. *Semin Nephrol* 17, 431–440.
- Igbekele, A.E., Jia, George, Hill, M.A., Sowers, J., Jia, Guanghong, 2022. Mineralocorticoid Receptor Activation in Vascular Insulin Resistance and Dysfunction. *International Journal of Molecular Sciences* 23. <https://doi.org/10.3390/ijms23168954>
- Iwashima, F., Yoshimoto, T., Minami, I., Sakurada, M., Hirono, Y., Hirata, Y., 2008. Aldosterone Induces Superoxide Generation via Rac1 Activation in Endothelial Cells. *Endocrinology* 149, 1009–1014. <https://doi.org/10.1210/en.2007-0864>
- Janikiewicz, J., Szymański, J., Malinska, D., Patalas-Krawczyk, P., Michalska, B., Duszyński, J., Giorgi, C., Bonora, M., Dobrzyn, A., Wieckowski, M.R., 2018. Mitochondria-associated membranes in aging and senescence: structure, function, and dynamics. *Cell Death Dis* 9, 332. <https://doi.org/10.1038/s41419-017-0105-5>
- Jausonslofreda, N., Chabret, C., Pons, M., 1994. Role of the A/B Region of the Human Mineralocorticoid Receptor in Aldosterone Response Selectivity. *Biochemical and Biophysical Research Communications* 205, 1610–1616. <https://doi.org/10.1006/bbrc.1994.2851>
- Jeon, J.-H., Thoudam, T., Choi, E.J., Kim, M.-J., Harris, R.A., Lee, I.-K., 2021. Loss of metabolic flexibility as a result of overexpression of pyruvate dehydrogenase kinases in muscle, liver and the immune system: Therapeutic targets in metabolic diseases. *Journal of Diabetes Investigation* 12, 21–31. <https://doi.org/10.1111/jdi.13345>
- Jeoung, N.H., Wu, P., Joshi, M.A., Jaskiewicz, J., Bock, C.B., Depaoli-Roach, A.A., Harris, R.A., 2006. Role of pyruvate dehydrogenase kinase isoenzyme 4 (PDHK4) in glucose homeostasis during starvation. *Biochem J* 397, 417–425. <https://doi.org/10.1042/BJ20060125>
- Jia, G., Lockette, W., Sowers, J.R., 2021. Mineralocorticoid receptors in the pathogenesis of insulin resistance and related disorders: from basic studies to clinical disease. *American Journal of Physiology-Regulatory, Integrative and Comparative Physiology* 320, R276–R286. <https://doi.org/10.1152/ajpregu.00280.2020>
- Johar, S., Cave, A.C., Narayanapanicker, A., Grieve, D.J., Shah, A.M., 2006. Aldosterone mediates angiotensin II-induced interstitial cardiac fibrosis via a Nox2-containing NADPH oxidase. *FASEB J* 20, 1546–1548. <https://doi.org/10.1096/fj.05-4642fje>
- Keidar, S., Kaplan, M., Pavlotzky, E., Coleman, R., Hayek, T., Hamoud, S., Aviram, M., 2004. Aldosterone Administration to Mice Stimulates Macrophage NADPH Oxidase and Increases Atherosclerosis Development: A Possible Role for Angiotensin-Converting Enzyme and the Receptors for Angiotensin II and Aldosterone. *Circulation* 109, 2213–2220. <https://doi.org/10.1161/01.CIR.0000127949.05756.9D>
- Kellner, M., Wiedemann, K., 2008. Mineralocorticoid receptors in brain, in health and disease: Possibilities for new pharmacotherapy. *European Journal of Pharmacology* 583, 372–378. <https://doi.org/10.1016/j.ejphar.2007.07.072>
- Khan, M.A., Alam, K., Dixit, K., Rizvi, M.M.A., 2016. Role of peroxynitrite induced structural changes on H2B histone by physicochemical method. *International Journal of Biological Macromolecules* 82, 31–38. <https://doi.org/10.1016/j.ijbiomac.2015.10.085>

- Kiellerich, P., Triqueneaux, G., Christensen, N.M., Trayer, V., Terrien, X., Lombès, M., Prunet, P., 2015. Interaction between the trout mineralocorticoid and glucocorticoid receptors in vitro. *Journal of Molecular Endocrinology* 55, 55–68. <https://doi.org/10.1530/JME-15-0002>
- Kim, I., Xu, W., Reed, J.C., 2008. Cell death and endoplasmic reticulum stress: disease relevance and therapeutic opportunities. *Nat Rev Drug Discov* 7, 1013–1030. <https://doi.org/10.1038/nrd2755>
- Kim, M.-J., Sinam, I.S., Siddique, Z., Jeon, J.-H., Lee, I.-K., 2023. The Link between Mitochondrial Dysfunction and Sarcopenia: An Update Focusing on the Role of Pyruvate Dehydrogenase Kinase 4. *Diabetes Metab J* 47, 153–163. <https://doi.org/10.4093/dmj.2022.0305>
- Kim, S.K., McCurley, A.T., DuPont, J.J., Aronovitz, M., Moss, M.E., Stillman, I.E., Karumanchi, S.A., Christou, D.D., Jaffe, I.Z., 2018. SMOOTH MUSCLE CELL MINERALOCORTICOID RECEPTOR AS A MEDIATOR OF CARDIOVASCULAR STIFFNESS WITH AGING. *Hypertension* 71, 609–621. <https://doi.org/10.1161/HYPERTENSIONAHA.117.10437>
- Klionsky, D.J., 2020. Autophagy participates in, well, just about everything. *Cell Death Differ* 27, 831–832. <https://doi.org/10.1038/s41418-020-0511-6>
- Kolla, V., Litwack, G., 2000. Inhibition of Mineralocorticoid-Mediated Transcription by NF-κB. *Archives of Biochemistry and Biophysics* 383, 38–45. <https://doi.org/10.1006/abbi.2000.2045>
- Korkmaz, A., Oter, S., Seyrek, M., Topal, T., 2009. Molecular, genetic and epigenetic pathways of peroxynitrite-induced cellular toxicity. *Interdiscip Toxicol* 2, 219–228. <https://doi.org/10.2478/v10102-009-0020-4>
- Krug, A.W., Allenhöfer, L., Monticone, R., Spinetti, G., Gekle, M., Wang, M., Lakatta, E.G., 2010. Elevated Mineralocorticoid Receptor Activity in Aged Rat Vascular Smooth Muscle Cells Promotes a Proinflammatory Phenotype via Extracellular Signal-Regulated Kinase 1/2 Mitogen-Activated Protein Kinase and Epidermal Growth Factor Receptor-Dependent Pathways. *Hypertension* 55, 1476–1483. <https://doi.org/10.1161/HYPERTENSIONAHA.109.148783>
- Krug, A.W., Stelzner, L., Rao, A.D., Lichtman, A.H., Williams, G.H., Adler, G.K., 2013. Effect of Low Dose Mineralocorticoid Receptor Antagonist Eplerenone on Glucose and Lipid Metabolism in Healthy Adult Males. *Metabolism* 62, 386–391. <https://doi.org/10.1016/j.metabol.2012.08.011>
- Kuhn, E., Lamribet, K., Viengchareun, S., Le Menuet, D., Fève, B., Lombès, M., 2019. UCP1 transrepression in Brown Fat in vivo and mineralocorticoid receptor anti-thermogenic effects. *Annales d'Endocrinologie* 80, 1–9. <https://doi.org/10.1016/j.ando.2018.04.018>
- Kuhn, E., Lombès, M., 2013. The mineralocorticoid receptor: a new player controlling energy homeostasis. *Hormone Molecular Biology and Clinical Investigation* 15, 59–69. <https://doi.org/10.1515/hmbci-2013-0033>
- Kuntz, M.J., Harris, R.A., 2018. Pyruvate Dehydrogenase Kinase, in: Choi, S. (Ed.), *Encyclopedia of Signaling Molecules*. Springer New York, New York, NY, pp. 1–9. https://doi.org/10.1007/978-1-4614-6438-9_101636-1
- Lee, S.J., Jeong, J.Y., Oh, C.J., Park, S., Kim, J.-Y., Kim, H.-J., Doo Kim, N., Choi, Y.-K., Do, J.-Y., Go, Y., Ha, C.-M., Choi, J.-Y., Huh, S., Ho Jeoung, N., Lee, K.-U., Choi, H.-S., Wang, Y., Park, K.-G., Harris, R.A., Lee, I.-K., 2015. Pyruvate Dehydrogenase Kinase 4 Promotes Vascular Calcification via SMAD1/5/8 Phosphorylation. *Sci Rep* 5, 16577. <https://doi.org/10.1038/srep16577>
- Leem, J., Lee, I.-K., 2016. Mechanisms of Vascular Calcification: The Pivotal Role of Pyruvate Dehydrogenase Kinase 4. *Endocrinol Metab (Seoul)* 31, 52–61. <https://doi.org/10.3803/EnM.2016.31.1.52>
- Lefranc, C., Friederich-Persson, M., Foufelle, F., Nguyen Dinh Cat, A., Jaisser, F., 2021. Adipocyte-Mineralocorticoid Receptor Alters Mitochondrial Quality Control Leading to Mitochondrial Dysfunction and Senescence of Visceral Adipose Tissue. *IJMS* 22, 2881. <https://doi.org/10.3390/ijms22062881>
- Leopold, J.A., Dam, A., Maron, B.A., Scribner, A.W., Liao, R., Handy, D.E., Stanton, R.C., Pitt, B., Loscalzo, J., 2007. Aldosterone impairs vascular reactivity by decreasing glucose-6-phosphate dehydrogenase activity. *Nat Med* 13, 189–197. <https://doi.org/10.1038/nm1545>
- Lin, H., Gao, X., Chen, G., Sun, J., Chu, J., Jing, K., Li, P., Zeng, R., Wei, B., 2015. Indole-3-carbinol as inhibitors of glucocorticoid-induced apoptosis in osteoblastic cells through blocking ROS-

- mediated Nrf2 pathway. *Biochem Biophys Res Commun* 460, 422–427. <https://doi.org/10.1016/j.bbrc.2015.03.049>
- Lin, Y., Wang, Y., Li, P., 2022. Mutual regulation of lactate dehydrogenase and redox robustness. *Frontiers in Physiology* 13.
- Lingappan, K., 2018. NF- κ B in Oxidative Stress. *Curr Opin Toxicol* 7, 81–86. <https://doi.org/10.1016/j.cotox.2017.11.002>
- Liu, G., Grifman, M., Keily, B., Chatterton, J.E., Staal, F.-W., Li, Q.-X., 2006. Mineralocorticoid receptor is involved in the regulation of genes responsible for hepatic glucose production. *Biochemical and Biophysical Research Communications* 342, 1291–1296. <https://doi.org/10.1016/j.bbrc.2006.02.065>
- Liu, R., Bian, Y., Liu, Lin, Liu, Lianchang, Liu, X., Ma, S., 2022. Molecular pathways associated with oxidative stress and their potential applications in radiotherapy (Review). *Int J Mol Med* 49, 65. <https://doi.org/10.3892/ijmm.2022.5121>
- Lombès, M., Binart, N., Delahaye, F., Baulieu, E.E., Rafestin-Oblin, M.E., 1994. Differential intracellular localization of human mineralocorticosteroid receptor on binding of agonists and antagonists. *Biochemical Journal* 302, 191–197. <https://doi.org/10.1042/bj3020191>
- Lombès, M., Oblin, M.E., Gasc, J.M., Baulieu, E.E., Farman, N., Bonvalet, J.P., 1992. Immunohistochemical and biochemical evidence for a cardiovascular mineralocorticoid receptor. *Circulation Research* 71, 503–510. <https://doi.org/10.1161/01.RES.71.3.503>
- Lothar, A., Fürst, D., Bergemann, S., Gilsbach, R., Grahammer, F., Huber, T.B., Hilgendorf, I., Bode, C., Moser, M., Hein, L., 2016. Deoxycorticosterone Acetate/Salt-Induced Cardiac But Not Renal Injury Is Mediated By Endothelial Mineralocorticoid Receptors Independently From Blood Pressure. *Hypertension* 67, 130–138. <https://doi.org/10.1161/HYPERTENSIONAHA.115.06530>
- Lu, G., Li, J., Zhai, Y., Li, Q., Xie, D., Zhang, J., Xiao, Y., Gao, X., 2019. Spironolactone suppresses aldosterone-induced Kv1.5 expression by attenuating mineralocorticoid receptor-Nox1/2/4-mediated ROS generation in neonatal rat atrial myocytes. *Biochemical and Biophysical Research Communications* 520, 379–384. <https://doi.org/10.1016/j.bbrc.2019.10.039>
- Luisi, B.F., Xu, W.X., Otwinowski, Z., Freedman, L.P., Yamamoto, K.R., Sigler, P.B., 1991. Crystallographic analysis of the interaction of the glucocorticoid receptor with DNA. *Nature* 352, 497–505. <https://doi.org/10.1038/352497a0>
- Ma, W.-Q., Sun, X.-J., Zhu, Y., Liu, N.-F., 2020. PDK4 promotes vascular calcification by interfering with autophagic activity and metabolic reprogramming. *Cell Death Dis* 11, 1–23. <https://doi.org/10.1038/s41419-020-03162-w>
- Maeyashiki, C., Melhem, H., Hering, L., Baebler, K., Cosin-Roger, J., Schefer, F., Weder, B., Hausmann, M., Scharl, M., Rogler, G., de Vallière, C., Ruiz, P.A., 2020. Activation of pH-Sensing Receptor OGR1 (GPR68) Induces ER Stress Via the IRE1 α /JNK Pathway in an Intestinal Epithelial Cell Model. *Sci Rep* 10, 1438. <https://doi.org/10.1038/s41598-020-57657-9>
- Maldonado, E., Morales-Pison, S., Urbina, F., Solari, A., 2023. Aging Hallmarks and the Role of Oxidative Stress. *Antioxidants (Basel)* 12, 651. <https://doi.org/10.3390/antiox12030651>
- Marchetti, P., Fovez, Q., Germain, N., Khamari, R., Kluza, J., 2020. Mitochondrial spare respiratory capacity: Mechanisms, regulation, and significance in non-transformed and cancer cells. *The FASEB Journal* 34, 13106–13124. <https://doi.org/10.1096/fj.202000767R>
- Markley, J.L., Wenczewicz, T.A., 2018. Tetracycline-Inactivating Enzymes. *Front Microbiol* 9, 1058. <https://doi.org/10.3389/fmicb.2018.01058>
- Marzolla, V., Armani, A., Mammi, C., Moss, M.E., Pagliarini, V., Pontecorvo, L., Antelmi, A., Fabbri, A., Rosano, G., Jaffe, I.Z., Caprio, M., 2017. Essential role of ICAM-1 in aldosterone-induced atherosclerosis. *Int J Cardiol* 232, 233–242. <https://doi.org/10.1016/j.ijcard.2017.01.013>
- Mekahli, D., Bultynck, G., Parys, J.B., Smedt, H.D., Missiaen, L., 2011. Endoplasmic-Reticulum Calcium Depletion and Disease. *Cold Spring Harb Perspect Biol* 3, a004317. <https://doi.org/10.1101/cshperspect.a004317>
- Meneses, A.M., Medina, R.A., Kato, S., Pinto, M., Jaque, M.P., Lizama, I., García, M. de los Á., Nualart, F., Owen, G.I., 2008. Regulation of GLUT3 and glucose uptake by the cAMP signalling pathway in the breast cancer cell line ZR-75. *Journal of Cellular Physiology* 214, 110–116. <https://doi.org/10.1002/jcp.21166>

- Messaoudi, S., Gravez, B., Tarjus, A., Pelloux, V., Ouvrard-Pascaud, A., Delcayre, C., Samuel, J., Launay, J.-M., Sierra-Ramos, C., De La Rosa, D.A., Clément, K., Farman, N., Jaisser, F., 2013. Aldosterone-Specific Activation of Cardiomyocyte Mineralocorticoid Receptor In Vivo. *Hypertension* 61, 361–367. <https://doi.org/10.1161/HYPERTENSIONAHA.112.198986>
- Mohammed, S.F., Ohtani, T., Korinek, J., Lam, C.S.P., Larsen, K., Simari, R.D., Valencik, M.L., Burnett, J.C., Redfield, M.M., 2010. Mineralocorticoid Accelerates Transition to Heart Failure With Preserved Ejection Fraction Via “Nongenomic Effects.” *Circulation* 122, 370–378. <https://doi.org/10.1161/CIRCULATIONAHA.109.915215>
- Morrison, N., Harrap, S.B., Arriza, J.L., Boyd, E., Connor, J.M., 1990. Regional chromosomal assignment of the human mineralocorticoid receptor gene to 4q31.1. *Hum Genet* 85, 130–132. <https://doi.org/10.1007/BF00276340>
- Mueckler, M., Thorens, B., 2013. The SLC2 (GLUT) Family of Membrane Transporters. *Mol Aspects Med* 34, 121–138. <https://doi.org/10.1016/j.mam.2012.07.001>
- Mukhopadhyay, S., Das, D.N., Panda, P.K., Sinha, N., Naik, P.P., Bissoyi, A., Pramanik, K., Bhutia, S.K., 2015. Autophagy protein Ulk1 promotes mitochondrial apoptosis through reactive oxygen species. *Free Radical Biology and Medicine* 89, 311–321. <https://doi.org/10.1016/j.freeradbiomed.2015.07.159>
- Nagase, M., Ayuzawa, N., Kawarazaki, W., Ishizawa, K., Ueda, K., Yoshida, S., Fujita, T., 2012. Oxidative Stress Causes Mineralocorticoid Receptor Activation in Rat Cardiomyocytes: Role of Small GTPase Rac1. *Hypertension* 59, 500–506. <https://doi.org/10.1161/HYPERTENSIONAHA.111.185520>
- Nagata, D., Takahashi, M., Sawai, K., Tagami, T., Usui, T., Shimatsu, A., Hirata, Y., Naruse, M., 2006. Molecular Mechanism of the Inhibitory Effect of Aldosterone on Endothelial NO Synthase Activity. *Hypertension* 48, 165–171. <https://doi.org/10.1161/01.HYP.0000226054.53527.bb>
- Nicholls, D.G., 2009. Spare respiratory capacity, oxidative stress and excitotoxicity. *Biochem Soc Trans* 37, 1385–1388. <https://doi.org/10.1042/BST0371385>
- Obradović, D., Tirard, M., Némethy, Z., Hirsch, O., Gronemeyer, H., Almeida, O.F.X., 2004. DAXX, FLASH, and FAF-1 Modulate Mineralocorticoid and Glucocorticoid Receptor-Mediated Transcription in Hippocampal Cells—Toward a Basis for the Opposite Actions Elicited by Two Nuclear Receptors? *Mol Pharmacol* 65, 761–769. <https://doi.org/10.1124/mol.65.3.761>
- Ogata, M., Hino, S., Saito, A., Morikawa, K., Kondo, S., Kanemoto, S., Murakami, T., Taniguchi, M., Tanii, I., Yoshinaga, K., Shiosaka, S., Hammarback, J.A., Urano, F., Imaizumi, K., 2006. Autophagy is activated for cell survival after endoplasmic reticulum stress. *Mol Cell Biol* 26, 9220–9231. <https://doi.org/10.1128/MCB.01453-06>
- Ohashi, K., Hayashi, T., Utsunomiya, K., Nishimura, R., 2022. The mineralocorticoid receptor signal could be a new molecular target for the treatment of diabetic retinal complication. *Expert Opinion on Therapeutic Targets* 26, 479–486. <https://doi.org/10.1080/14728222.2022.2072730>
- Parasiliti-Caprino, M., Bollati, M., Merlo, F.D., Ghigo, E., Maccario, M., Bo, S., 2022. Adipose Tissue Dysfunction in Obesity: Role of Mineralocorticoid Receptor. *Nutrients* 14, 4735. <https://doi.org/10.3390/nu14224735>
- Parfianowicz, D., Shah, S., Nguyen, C., Maitz, T.N., Hajra, A., Goel, A., Sreenivasan, J., Aronow, W.S., Vyas, A., Gupta, R., 2022. Finerenone: A New Era for Mineralocorticoid Receptor Antagonism and Cardiorenal Protection. *Curr Probl Cardiol* 47, 101386. <https://doi.org/10.1016/j.cpcardiol.2022.101386>
- Parys, J.B., Decuypere, J.-P., Bultynck, G., 2012. Role of the inositol 1,4,5-trisphosphate receptor/Ca²⁺-release channel in autophagy. *Cell Commun Signal* 10, 17. <https://doi.org/10.1186/1478-811X-10-17>
- Pascual-Le Tallec, L., Lombès, M., 2005. The Mineralocorticoid Receptor: A Journey Exploring Its Diversity and Specificity of Action. *Molecular Endocrinology* 19, 2211–2221. <https://doi.org/10.1210/me.2005-0089>
- Patni, H., Mathew, J.T., Luan, L., Franki, N., Chander, P.N., Singhal, P.C., 2007. Aldosterone promotes proximal tubular cell apoptosis: role of oxidative stress. *Am J Physiol Renal Physiol* 293, F1065-1071. <https://doi.org/10.1152/ajprenal.00147.2007>

- Pérez-Torres, I., Manzano-Pech, L., Rubio-Ruíz, M.E., Soto, M.E., Guarner-Lans, V., 2020. Nitrosative Stress and Its Association with Cardiometabolic Disorders. *Molecules* 25, 2555. <https://doi.org/10.3390/molecules25112555>
- Pitt, B., 2012. The role of mineralocorticoid receptor antagonists (MRAs) in very old patients with heart failure. *Heart Fail Rev* 17, 573–579. <https://doi.org/10.1007/s10741-011-9286-7>
- Pitt, B., Pfeffer, M.A., Assmann, S.F., Boineau, R., Anand, I.S., Claggett, B., Clausell, N., Desai, A.S., Diaz, R., Fleg, J.L., Gordeev, I., Harty, B., Heitner, J.F., Kenwood, C.T., Lewis, E.F., O'Meara, E., Probstfield, J.L., Shaburishvili, T., Shah, S.J., Solomon, S.D., Sweitzer, N.K., Yang, S., McKinlay, S.M., 2014. Spironolactone for Heart Failure with Preserved Ejection Fraction. *N Engl J Med* 370, 1383–1392. <https://doi.org/10.1056/NEJMoa1313731>
- Pitt, B., Reichek, N., Willenbrock, R., Zannad, F., Phillips, R.A., Roniker, B., Kleiman, J., Krause, S., Burns, D., Williams, G.H., 2003. Effects of Eplerenone, Enalapril, and Eplerenone/Enalapril in Patients With Essential Hypertension and Left Ventricular Hypertrophy. *Circulation* 108, 1831–1838. <https://doi.org/10.1161/01.CIR.0000091405.00772.6E>
- Pitt, B., Zannad, F., Remme, W.J., Cody, R., Castaigne, A., Perez, A., Palensky, J., Wittes, J., 1999. The effect of spironolactone on morbidity and mortality in patients with severe heart failure. Randomized Aldactone Evaluation Study Investigators. *N Engl J Med* 341, 709–717. <https://doi.org/10.1056/NEJM199909023411001>
- Piwien-Pilipuk, G., Ayala, A., Machado, A., Galigniana, M.D., 2002. Impairment of Mineralocorticoid Receptor (MR)-dependent Biological Response by Oxidative Stress and Aging: CORRELATION WITH POST-TRANSLATIONAL MODIFICATION OF MR AND DECREASED ADP-RIBOSYLATABLE LEVEL OF ELONGATION FACTOR 2 IN KIDNEY CELLS *. *Journal of Biological Chemistry* 277, 11896–11903. <https://doi.org/10.1074/jbc.M109530200>
- Prager, E.M., Brielmaier, J., Bergstrom, H.C., McGuire, J., Johnson, L.R., 2010. Localization of Mineralocorticoid Receptors at Mammalian Synapses. *PLOS ONE* 5, e14344. <https://doi.org/10.1371/journal.pone.0014344>
- Queisser, N., Oteiza, P.I., Stopper, H., Oli, R.G., Schupp, N., 2011. Aldosterone induces oxidative stress, oxidative DNA damage and NF-κB-activation in kidney tubule cells. *Molecular Carcinogenesis* 50, 123–135. <https://doi.org/10.1002/mc.20710>
- Rashmi, R., Huang, X., Floberg, J.M., Elhammali, A.E., McCormick, M.L., Patti, G.J., Spitz, D.R., Schwarz, J.K., 2018. Radioresistant Cervical Cancers Are Sensitive to Inhibition of Glycolysis and Redox Metabolism. *Cancer Research* 78, 1392–1403. <https://doi.org/10.1158/0008-5472.CAN-17-2367>
- Rogerson, F.M., Brennan, F.E., Fuller, P.J., 2004. Mineralocorticoid receptor binding, structure and function. *Molecular and Cellular Endocrinology* 217, 203–212. <https://doi.org/10.1016/j.mce.2003.10.021>
- Rossier, M.F., Python, M., Maturana, A.D., 2010. Contribution of mineralocorticoid and glucocorticoid receptors to the chronotropic and hypertrophic actions of aldosterone in neonatal rat ventricular myocytes. *Endocrinology* 151, 2777–2787. <https://doi.org/10.1210/en.2009-1375>
- Ruhs, S., Strätz, N., Schlör, K., Meinel, S., Mildenerger, S., Rabe, S., Gekle, M., Grossmann, C., 2012. Modulation of transcriptional mineralocorticoid receptor activity by nitrosative stress. *Free Radical Biology and Medicine* 53, 1088–1100. <https://doi.org/10.1016/j.freeradbiomed.2012.06.028>
- Sakurabayashi-Kitade, S., Aoka, Y., Nagashima, H., Kasanuki, H., Hagiwara, N., Kawana, M., 2009. Aldosterone blockade by Spironolactone improves the hypertensive vascular hypertrophy and remodeling in angiotensin II overproducing transgenic mice. *Atherosclerosis* 206, 54–60. <https://doi.org/10.1016/j.atherosclerosis.2009.01.039>
- Sato, A., Funder, J.W., 1996. High glucose stimulates aldosterone-induced hypertrophy via type I mineralocorticoid receptors in neonatal rat cardiomyocytes. *Endocrinology* 137, 4145–4153. <https://doi.org/10.1210/endo.137.10.8828470>
- Savory, J.G.A., Préfontaine, G.G., Lamprecht, C., Liao, M., Walther, R.F., Lefebvre, Y.A., Haché, R.J.G., 2001. Glucocorticoid Receptor Homodimers and Glucocorticoid-Mineralocorticoid Receptor Heterodimers Form in the Cytoplasm through Alternative Dimerization Interfaces. *Molecular and Cellular Biology* 21, 781–793. <https://doi.org/10.1128/MCB.21.3.781-793.2001>

- Schwerdt, G., Holzinger, H., Sauvant, C., Königs, M., Humpf, H.-U., Gekle, M., 2007. Long-term effects of ochratoxin A on fibrosis and cell death in human proximal tubule or fibroblast cells in primary culture. *Toxicology* 232, 57–67. <https://doi.org/10.1016/j.tox.2006.12.008>
- Shibata, S., 2017. 30 YEARS OF THE MINERALOCORTICOID RECEPTOR: Mineralocorticoid receptor and NaCl transport mechanisms in the renal distal nephron. *Journal of Endocrinology* 234, T35–T47. <https://doi.org/10.1530/JOE-16-0669>
- Smith, P.K., Krohn, R.I., Hermanson, G.T., Mallia, A.K., Gartner, F.H., Provenzano, M.D., Fujimoto, E.K., Goeke, N.M., Olson, B.J., Klenk, D.C., 1985. Measurement of protein using bicinchoninic acid. *Anal Biochem* 150, 76–85. [https://doi.org/10.1016/0003-2697\(85\)90442-7](https://doi.org/10.1016/0003-2697(85)90442-7)
- Smutok, O., Karkovska, M., Smutok, H., Gonchar, M., 2013. Flavocytochrome b2-Based Enzymatic Method of L-Lactate Assay in Food Products. *ScientificWorldJournal* 2013, 461284. <https://doi.org/10.1155/2013/461284>
- Song, L., Zhang, Z., n.d. PDK4 regulates human cardiomyocyte viability.
- Stavreva, D.A., Müller, W.G., Hager, G.L., Smith, C.L., McNally, J.G., 2004. Rapid glucocorticoid receptor exchange at a promoter is coupled to transcription and regulated by chaperones and proteasomes. *Mol Cell Biol* 24, 2682–2697. <https://doi.org/10.1128/MCB.24.7.2682-2697.2004>
- Sturm, A., Bury, N., Dengreville, L., Fagart, J., Flouriot, G., Rafestin-Oblin, M.E., Prunet, P., 2005. 11-Deoxycorticosterone Is a Potent Agonist of the Rainbow Trout (*Oncorhynchus mykiss*) Mineralocorticoid Receptor. *Endocrinology* 146, 47–55. <https://doi.org/10.1210/en.2004-0128>
- Takubo, K., Nagamatsu, G., Kobayashi, C.I., Nakamura-Ishizu, A., Kobayashi, H., Ikeda, E., Goda, N., Rahimi, Y., Johnson, R.S., Soga, T., Hirao, A., Suematsu, M., Suda, T., 2013. Regulation of Glycolysis by Pdk Functions as a Metabolic Checkpoint for Cell Cycle Quiescence in Hematopoietic Stem Cells. *Cell Stem Cell* 12, 49–61. <https://doi.org/10.1016/j.stem.2012.10.011>
- Tanaka, M., Nishi, M., Morimoto, M., Sugimoto, T., Kawata, M., 2005. Imaging analysis of mineralocorticoid receptor and importins in single living cells by using GFP color variants. *Cell Tissue Res* 320, 447–453. <https://doi.org/10.1007/s00441-004-0984-5>
- Taylor, T.A., Pollock, J.S., Pollock, D.M., 2003. Down-regulation of soluble guanylyl cyclase in the inner medulla of DOCA-salt hypertensive rats. *Vascular Pharmacology* 40, 155–160. [https://doi.org/10.1016/S1537-1891\(03\)00048-X](https://doi.org/10.1016/S1537-1891(03)00048-X)
- Thoudam, T., Chanda, D., Lee, J.Y., Jung, M.-K., Sinam, I.S., Kim, B.-G., Park, B.-Y., Kwon, W.H., Kim, H.-J., Kim, M., Lim, C.W., Lee, H., Huh, Y.H., Miller, C.A., Saxena, R., Skill, N.J., Huda, N., Kusumanchi, P., Ma, J., Yang, Z., Kim, M.-J., Mun, J.Y., Harris, R.A., Jeon, J.-H., Liangpunsakul, S., Lee, I.-K., 2023. Enhanced Ca²⁺-channeling complex formation at the ER-mitochondria interface underlies the pathogenesis of alcohol-associated liver disease. *Nat Commun* 14, 1703. <https://doi.org/10.1038/s41467-023-37214-4>
- Thoudam, T., Ha, C.-M., Leem, J., Chanda, D., Park, J.-S., Kim, H.-J., Jeon, J.-H., Choi, Y.-K., Liangpunsakul, S., Huh, Y.H., Kwon, T.-H., Park, K.-G., Harris, R.A., Park, K.-S., Rhee, H.-W., Lee, I.-K., 2019. PDK4 Augments ER–Mitochondria Contact to Dampen Skeletal Muscle Insulin Signaling During Obesity. *Diabetes* 68, 571–586. <https://doi.org/10.2337/db18-0363>
- Thuzar, M., Stowasser, M., 2021. The mineralocorticoid receptor-an emerging player in metabolic syndrome? *J Hum Hypertens* 35, 117–123. <https://doi.org/10.1038/s41371-020-00467-3>
- Trapp, T., Rupprecht, R., Castrén, M., Reul, J.M., Holsboer, F., 1994. Heterodimerization between mineralocorticoid and glucocorticoid receptor: a new principle of glucocorticoid action in the CNS. *Neuron* 13, 1457–1462. [https://doi.org/10.1016/0896-6273\(94\)90431-6](https://doi.org/10.1016/0896-6273(94)90431-6)
- Tsai, C.-T., Chiang, F.-T., Tseng, C.-D., Hwang, J.-J., Kuo, K.-T., Wu, C.-K., Yu, C.-C., Wang, Y.-C., Lai, L.-P., Lin, J.-L., 2010. Increased expression of mineralocorticoid receptor in human atrial fibrillation and a cellular model of atrial fibrillation. *J Am Coll Cardiol* 55, 758–770. <https://doi.org/10.1016/j.jacc.2009.09.045>
- Tsai, M.-J., O'Malley, B.W., 1994. Molecular Mechanisms of Action of Steroid/Thyroid Receptor Superfamily Members. *Annual Review of Biochemistry* 63, 451–486. <https://doi.org/10.1146/annurev.bi.63.070194.002315>

- Urlinger, S., Baron, U., Thellmann, M., Hasan, M.T., Bujard, H., Hillen, W., 2000. Exploring the sequence space for tetracycline-dependent transcriptional activators: novel mutations yield expanded range and sensitivity. *Proc Natl Acad Sci U S A* 97, 7963–7968. <https://doi.org/10.1073/pnas.130192197>
- Usher, M.G., Duan, S.Z., Ivaschenko, C.Y., Frieler, R.A., Berger, S., Schütz, G., Lumeng, C.N., Mortensen, R.M., 2010. Myeloid mineralocorticoid receptor controls macrophage polarization and cardiovascular hypertrophy and remodeling in mice. *J Clin Invest* 120, 3350–3364. <https://doi.org/10.1172/JCI41080>
- Vicencio, J.M., Ortiz, C., Criollo, A., Jones, A.W.E., Kepp, O., Galluzzi, L., Joza, N., Vitale, I., Morselli, E., Tailler, M., Castedo, M., Maiuri, M.C., Molgó, J., Szabadkai, G., Lavandro, S., Kroemer, G., 2009. The inositol 1,4,5-trisphosphate receptor regulates autophagy through its interaction with Beclin 1. *Cell Death Differ* 16, 1006–1017. <https://doi.org/10.1038/cdd.2009.34>
- Viengchareun, S., Le Menuet, D., Martinerie, L., Munier, M., Pascual-Le Tallec, L., Lombès, M., 2007. The mineralocorticoid receptor: insights into its molecular and (patho)physiological biology. *Nucl Recept Signal* 5, e012. <https://doi.org/10.1621/nrs.05012>
- Viridis, A., Neves, M.F., Amiri, F., Viel, E., Touyz, R.M., Schiffrin, E.L., 2002. Spironolactone Improves Angiotensin-Induced Vascular Changes and Oxidative Stress. *Hypertension* 40, 504–510. <https://doi.org/10.1161/01.HYP.0000034738.79310.06>
- Vlassi, M., Brauns, K., Andrade-Navarro, M.A., 2013. Short tandem repeats in the inhibitory domain of the mineralocorticoid receptor: prediction of a β -solenoid structure. *BMC Struct Biol* 13, 17. <https://doi.org/10.1186/1472-6807-13-17>
- Wang, D., Liu, Y.-H., Yang, X.-P., Rhaleb, N.-E., Xu, J., Peterson, E., Rudolph, A.E., Carretero, O.A., 2004. Role of a selective aldosterone blocker in mice with chronic heart failure. *Journal of Cardiac Failure* 10, 67–73. [https://doi.org/10.1016/S1071-9164\(03\)00578-5](https://doi.org/10.1016/S1071-9164(03)00578-5)
- Wang, X., Shen, X., Yan, Y., Li, H., 2021. Pyruvate dehydrogenase kinases (PDKs): an overview toward clinical applications. *Bioscience Reports* 41, BSR20204402. <https://doi.org/10.1042/BSR20204402>
- Wang, Y., Shu, Y., Gu, C., Fan, Y., 2019. The novel sugar transporter SLC50A1 as a potential serum-based diagnostic and prognostic biomarker for breast cancer. *Cancer Manag Res* 11, 865–876. <https://doi.org/10.2147/CMAR.S190591>
- Watson, L.C., Kuchenbecker, K.M., Schiller, B.J., Gross, J.D., Pufall, M.A., Yamamoto, K.R., 2013. The glucocorticoid receptor dimer interface allosterically transmits sequence-specific DNA signals. *Nat Struct Mol Biol* 20, 876–883. <https://doi.org/10.1038/nsmb.2595>
- Wei, D., Liu, X., Jiang, J., Tu, R., Qiao, D., Li, R., Wang, Y., Fan, M., Yang, X., Zhang, J., Hou, J., Huo, W., Yu, S., Li, L., Wang, C., Mao, Z., 2020. Mineralocorticoids, glucose homeostasis and type 2 diabetes mellitus: The Henan Rural Cohort study. *Journal of Diabetes and its Complications* 34, 107558. <https://doi.org/10.1016/j.jdiacomp.2020.107558>
- Weikum, E.R., Knuesel, M.T., Ortlund, E.A., Yamamoto, K.R., 2017. Glucocorticoid receptor control of transcription: precision and plasticity via allostery. *Nat Rev Mol Cell Biol* 18, 159–174. <https://doi.org/10.1038/nrm.2016.152>
- Wende, A.R., Huss, J.M., Schaeffer, P.J., Giguère, V., Kelly, D.P., 2005. PGC-1 α coactivates PDK4 gene expression via the orphan nuclear receptor ERR α : a mechanism for transcriptional control of muscle glucose metabolism. *Mol Cell Biol* 25, 10684–10694. <https://doi.org/10.1128/MCB.25.24.10684-10694.2005>
- Weston, C.R., Davis, R.J., 2007. The JNK signal transduction pathway. *Current Opinion in Cell Biology, Cell regulation* 19, 142–149. <https://doi.org/10.1016/j.ceb.2007.02.001>
- White, C., Li, C., Yang, J., Petrenko, N.B., Madesh, M., Thompson, C.B., Foskett, J.K., 2005. The endoplasmic reticulum gateway to apoptosis by Bcl-XL modulation of the InsP3R. *Nat Cell Biol* 7, 1021–1028. <https://doi.org/10.1038/ncb1302>
- Wichitnithad, W., Nantaphol, S., Noppakhunsomboon, K., Rojsitthisak, P., 2023. An update on the current status and prospects of nitrosation pathways and possible root causes of nitrosamine formation in various pharmaceuticals. *Saudi Pharm J* 31, 295–311. <https://doi.org/10.1016/j.jsps.2022.12.010>

- Wiebel, F.F., Gustafsson, J.-Å., 1997. Heterodimeric Interaction between Retinoid X Receptor and Orphan Nuclear Receptor OR1 Reveals Dimerization-Induced Activation as a Novel Mechanism of Nuclear Receptor Activation. *MOL. CELL. BIOL.* 17.
- Wu, P., Tian, T., Zhao, J., Song, Q., Wu, X., Guo, Y., Yu, Y., Tan, S., Xia, H., 2021. IRE1 α -JNK pathway-mediated autophagy promotes cell survival in response to endoplasmic reticulum stress during the initial phase of hepatic steatosis. *Life Sciences* 264, 118668. <https://doi.org/10.1016/j.lfs.2020.118668>
- Xue, S., Yanghong, D., Jiabin, G., Wenxiu, L., Yue, L., 2023. Research Progress in Finerenone in Cardiovascular Diseases. *CVIA* 8. <https://doi.org/10.15212/CVIA.2023.0060>
- Yang, J., Chen, Y., Li, X., Xu, D., 2022. New insights into the roles of glucocorticoid signaling dysregulation in pathological cardiac hypertrophy. *Heart Fail Rev* 27, 1431–1441. <https://doi.org/10.1007/s10741-021-10158-x>
- Yin, Q., Wang, P., Wu, X., 2021. MicroRNA -148 alleviates cardiac dysfunction, immune disorders, and myocardial apoptosis in myocardial ischemia-reperfusion (MI/R) injury by targeting pyruvate dehydrogenase kinase (PDK4). *Bioengineered* 12, 5552–5565. <https://doi.org/10.1080/21655979.2021.1965812>
- Yuan, Y., Xu, X., Zhao, C., Zhao, M., Wang, H., Zhang, B., Wang, N., Mao, H., Zhang, A., Xing, C., 2015. The roles of oxidative stress, endoplasmic reticulum stress, and autophagy in aldosterone/mineralocorticoid receptor-induced podocyte injury. *Laboratory Investigation* 95, 1374–1386. <https://doi.org/10.1038/labinvest.2015.118>
- Zachari, M., Ganley, I.G., 2017. The mammalian ULK1 complex and autophagy initiation. *Essays in Biochemistry* 61, 585–596. <https://doi.org/10.1042/EBC20170021>
- Zannad, F., Gattis Stough, W., Rossignol, P., Bauersachs, J., McMurray, J.J.V., Swedberg, K., Struthers, A.D., Voors, A.A., Ruilope, L.M., Bakris, G.L., O'Connor, C.M., Gheorghiade, M., Mentz, R.J., Cohen-Solal, A., Maggioni, A.P., Beygui, F., Filippatos, G.S., Massy, Z.A., Pathak, A., Piña, I.L., Sabbah, H.N., Sica, D.A., Tavazzi, L., Pitt, B., 2012. Mineralocorticoid receptor antagonists for heart failure with reduced ejection fraction: integrating evidence into clinical practice. *Eur Heart J* 33, 2782–2795. <https://doi.org/10.1093/eurheartj/ehs257>
- Zannad, F., McMurray, J.J.V., Krum, H., van Veldhuisen, D.J., Swedberg, K., Shi, H., Vincent, J., Pocock, S.J., Pitt, B., 2011. Eplerenone in Patients with Systolic Heart Failure and Mild Symptoms. *New England Journal of Medicine* 364, 11–21. <https://doi.org/10.1056/NEJMoa1009492>
- Zendaoui, A., Lachance, D., Roussel, E., Couet, J., Arsenault, M., 2012. Effects of spironolactone treatment on an experimental model of chronic aortic valve regurgitation. *J Heart Valve Dis* 21, 478–486.
- Zennaro, M.-C., 1997. Tissue-Specific Expression of and Messenger Ribonucleic Acid Isoforms of the Human Mineralocorticoid Receptor in Normal and Pathological States. *Journal of Clinical Endocrinology & Metabolism* 82, 1345–1352. <https://doi.org/10.1210/jc.82.5.1345>
- Ziera, T., Irlbacher, H., Fromm, A., Latouche, C., Krug, S.M., Fromm, M., Jaisser, F., Borden, S.A., 2009. Cnksr3 is a direct mineralocorticoid receptor target gene and plays a key role in the regulation of the epithelial sodium channel. *FASEB j.* 23, 3936–3946. <https://doi.org/10.1096/fj.09-134759>

7. Theses

1. Activation of the mineralocorticoid receptor by aldosterone leads to an augmentation in glucose consumption and an elevation in lactate production.
2. Upon stimulation by aldosterone and mineralocorticoid receptors, mitochondrial ATP production diminishes while glycolytic ATP production increases in MR-overexpressing HEK cells.
3. Interaction between aldosterone and the mineralocorticoid receptor triggers endoplasmic reticulum stress via the IRE α pathway, resulting in altered autophagy and apoptosis.
4. Analysis of the genetic profile of MR-overexpressing HEK cells stimulated with aldosterone revealed upregulation of metabolic regulatory genes such as PDK4, alongside others including SGK1, MAP3K6, and PRKAB2.
5. Furthermore, aldosterone stimulation of MR-overexpressing HEK cells led to increased expression of genes associated with glucose uptake, such as GLUT 3 and SWEET1, and decreased expression of PDP1, consequently shifting metabolism from the tricarboxylic acid cycle towards lactate production.
6. Stimulation of the mineralocorticoid receptor using peroxynitrite demonstrated MR activation through translocation, regulating genes such as FOSL2, SKIDA1, and MMP15.
7. Conversely, elevated levels of nitrosative stress inhibited the biological response to aldosterone, suggesting potential deactivation of the mineralocorticoid receptor on the mRNA level.

8. Supplement material

List of manufacturers and distributors

Abcam - Cambridge, UK
Agilent Technologies - Santa Clara, USA
Applichem – Darmstadt, Germany
Applied Biosystems via Life Technologies - Darmstadt, Germany
Berthold Technologies - Bad Wildbad, Germany
BioRad - Munich, Germany
Biometra – Jena, Germany
Biomol – Hamburg, Germany
Biosan – Riga, Latvia
Biotrend – Köln, Germany
Boster Bio – California, USA
Capricorn Scientific - Ebsdorfergrund, Germany
Carl Roth – Karlsruhe, Germany
Carl Zeiss - Oberkochen, Germany
Cell Signaling Technology - Danvers, USA
Dunn - Asbach, Germany
Fisher Scientific – Schwerte, Germany
GE Healthcare - Berlin, Germany
Hielscher - Teltow, Germany
Honeywell Fluka - Charlotte, North Carolina, USA
Invitrogen via Life Technologies - Darmstadt, Germany
Keyence - Osaka, Japan
LI-COR - Lincoln, Nebraska, USA
Life Technologies - Darmstadt, Germany
Merck - Billerica, Massachusetts, USA
Microsoft - Redmond, Washington, USA
Microsynth Seqlab – Göttingen, Germany
New England Biolabs - Frankfurt, Germany
OMNI Life Science – Bremen, Germany
Roche – Mannheim, Germany
Sigma Aldrich - Munich, Germany
Serva – Heidelberg, Heidelberg
Selleckchem – München, Germany
Tecan - Männedorf, Schweiz
Thermo Fisher Scientific - Waltham, Massachusetts, USA

The supplementary material includes a list of reagents used in the experiments and their respective manufacturer reference numbers.

Supplementary table 1. Reagents for cell culture and cell stimulation.

Reagent name	Distributor
Dulbecco's modified Eagle's (DMEM) medium	Sigma-Aldrich D5523
D – Glucose	Sigma-Aldrich G7528
Blastatidin	Life technologies R210-01
Zeocin	Invitrogen R25001
Instant Foetal Bovine Serum	Sigma-Aldrich F0685-3G
EDTA solution	Merck 1,084,180,100
Trypsin from porcine pancreas	Sigma-Aldrich T0303
Poly-L-lysine	Sigma-Aldrich P-0899
Dimethyl Sulfoxide (DMSO)	Riedel-de Haën 472301
Aldosterone	Sigma-Aldrich A9477-100MG
Tetracycline	Invitrogen 550205
Eplerenone	Sigma-Aldrich E6657
Pepstatin A	Sigma-Aldrich P-4265
Aloxistatin	Selleckchem S7393
SIN-1 (Morpholinonydronimine, hydrochloride)	Merck/Millipore 567028
Ebselen	Calbiochem 324483
Nuclear-free water	Sigma-Aldrich W4502

Supplementary table 2. Reagents for protein isolation and measurement.

Reagents name	Distributor
Phosphatase Inhibitor Cocktail 1	Sigma-Aldrich P8340
Phosphatase Inhibitor Cocktail 3	Sigma-Aldrich P0044
Bensonaze	Merck 71205-3
BCA Protein Assay Reagent A	Thermo Fisher Scientific 23222
BCA Protein Assay Reagent B	Thermo Fisher Scientific 23224
Bovine Serum Albumin Standard	Thermo Fisher Scientific 23208

Supplementary table 3. Western blot reagents for gel casting and incubations.

Reagents name	Distributor
APS 10%	Roth 9592.2
SDS 10%	Roth CN30.3
TEMED	Sigma-Aldrich T9281
Tween 20	Sigma-Aldrich P1379
BSA	Capricorn BSA-FAF-1U
Non-fat dried milk powder	Hartenstein CM35
Acrylamide (40%) Solutions	Thermo Fisher Scientific J62480.K2
Ponceau S	Sigma-Aldrich P3504
Trans-Blot-Turbo 5× Transfer buffer	BioRad 10026938
ECL	BioRad 170-5061

Supplementary table 4. RNA isolation reagents.

Reagents name	Distributor
Bluezol	Serva 003980801
Chloroform	Sigma-Aldrich C-2432
Isopropanol	Sigma-Aldrich 33539
95% Ethanol	Merck 24105
Glycogen	Thermo Fisher Scientific R0551
Na-Acetate	Sigma-Aldrich S-2889
RNA 6000 Nano Kit	Agilent Technology 5067-1511
RNA 6000 Nano Chips	Agilent Technology 5067-1512
RNA 6000 Ladder	Agilent Technology 5067-1529
1000UTurbo DNA-free Kit	Invitrogen AM2238

Supplementary table 5. Reagents for DNase digestion and reverse transcription.

Reagents name	Distributor
Reverse Transcriptase, Random Primer, RnaseOut, DTT, 5x first strand buffer	Thermo Fisher Scientific 18080051
Dnase I (2000 U/ml) und 10× Dnase-Buffer	NEB M0570S
dNTPs	Peqlab 732-3155, 732-3161, 732-3160, 732-3171
Water – Dnase RNase free	Sigma-Aldrich

Supplementary table 6. Reagents used for qPCR.

Reagents name	Distributor
Universal SYBR Green Supermix	BioRad 1725274
Reference dye ROX	Thermo Fisher Scientific 12223012

Supplementary table 7. Glucose measurement reagents.

Reagents name	Distributor
MgSO ₄	Merk 5886
Triethanolamine hydrochloride	Sigma-Aldrich T1502
NAOH	Sigma-Aldrich 930-65
ATP	Sigma-Aldrich A2383
NADP	Sigma-Aldrich N0505
Hexokinase+ Glukose-6-phosphat-Dehydrogenase	Sigma-Aldrich H8629

Supplementary table 8. Lactate measurements reagents.

Reagents name	Distributors
The sodium salt of lactic acid	Sigma-Aldrich 71720
Lactate dehydrogenase	Roche 10127876001
NAD	Roche 10127973001
Hydrazine	Sigma-Aldrich 225819
Glycine	Serva 23390.03

Supplementary table 9. Caspase activity measurements reagents.

Reagents name	Distributor
1 M DTT	Sigma-Aldrich D-9779
Caspase-3-Substrat	Biotrend BP0012
PIPES	Sigma-Aldrich P7643
CHAPS	Sigma-Aldrich C-3023
80 µM AFC	Biomol ABD-13401

Supplementary table 10. LDH measurement.

Reagents name	Distibutors
NADH	Sigma-Aldrich N8129
Pyruvate	Sigma-Aldrich P-3637

Supplementary table 11. Agilent Technologies reagents.

Reagents name	Distributor
Seahorse XF Mito Stress test	Agilent 103015-100
XFp FluxPak (cartridges, mini plates, and calibrant)	Agilent 103022-100
Seahorse Glycolytic Rate assay	Agilent 103344-100
Hoechst 20 mM	Thermo Fisher Scientific 33342
Seahorse XF DMEM medium	Agilent 103575-100
Seahorse XF Calibrant	Agilent 100840-000
Seahorse XF 1M glucose solution 50 mL	Agilent 103577-100

Supplementary table 12. ATP reagents.

Reagents name	Distributor
ATP Bioluminescence Assay Kit HS II	Roche 11699709001
Agilent RNA 6000 Nano Kit NGS	Agilent 5067-1511

Supplementary table 13. Other Chemicals

Reagents name	Distributors
Tris	Applichem A1086,1000
NaCl	Roth 3957.2
Triton X-100	Serva 37240
NP-40	Pierce 20148G
Na-deoxycholate	Sigma D6750
Na-Orthovanadate	Sigma S6508
Bromophenol Blue	Serva 15375
Mercaptoethanol	Sigma M3148
KCl	Serva 26868.02
MgCl ₂	Sigma M-9272
CaCl	Merk 1.02382.1000
NaH ₂ PO ₄	Fluka 71645
KH ₂ PO ₄	Sigma P-5379
HEPES	Sigma H3034
Tris-HCl	Merk1.08219.1000
NaHCO ₃	Sigma S8875
Casytone	OMNI Life Science GmbH 5651808

Declarations:

1. I declare that I have not commenced or pursued a doctoral procedure at any other academic institution.
2. Declaration concerning the truth of information given: I declare that all information provided is truthful and comprehensive. This thesis has not been previously utilized to attain any academic degree at this university or elsewhere.
3. Declaration under Oath: I declare that this thesis is entirely my work and has been produced without assistance from any other individuals. I have adhered to all regulations of good scientific practice and have exclusively utilized the sources referenced, ensuring proper citation of both content and wording.

Yekaterina Gadasheva
Leipzig, October 2024

Acknowledgements

I want to express my deepest gratitude to all those who contributed their time, effort, and expertise to this work, offering invaluable advice and constructive feedback. Special thanks to my thesis committee members, Prof. Dr. Claudia Grossmann, Prof. Dr. Regine Heller, and Prof. Dr. Rüdiger Horstkorte, for their continuous guidance throughout the project.

This dissertation would not have been possible without the dedicated contributions and insights from the team at the Julius-Bernstein Institute for Physiology. I am incredibly grateful to Prof. Dr. med. Michael Gekle, Prof. Dr. med. Oliver Thews, Dr. rer. nat. Alexander Nolze, PD Dr. rer. nat. Anne Riemann, Dr. rer. nat. Virginie Dubourg, Dr. rer. nat. Stefanie Ruhs, and PD Dr. rer. nat. Gerald Schwerdt. I would also like to extend my heartfelt thanks to the laboratory technicians—Nicole Strätz, Sarah Reime, Sindy Rabe, Sigrid Mildenberger, Michael Kopf, and Katja Quarch—who provided unwavering support throughout my PhD journey and from whom I have learned so much.

A special acknowledgment goes to the ProMoAge scientific cohort, which not only educated me in modern approaches to aging research but also helped me build a robust scientific network. I am deeply grateful to our spokesperson, Prof. Dr. Andreas Simm, and Deputy Spokesperson, Prof. Dr. Regine Heller. Thanks to Dr. Nancy Zimmermann and Ramona Balmelli, whose organizational skills and dedication greatly supported the PhD students.

I am also thankful to my collaborators from the Center for Basic Medical Research at University Clinic Halle (ZMG), especially Dr. rer. nat. Samiya Al-Robaiy's expertise in Seahorse assays was instrumental to my research.

The Summer School of Molecular Medicine in Jena played a pivotal role in shaping my path, and I extend my sincere thanks to Prof. Heller for steering me toward this PhD field and offering me the opportunity to demonstrate my motivation and passion for research.

I am immensely grateful to Prof. Dr. Claudia Grossmann, whose daily support—whether in the form of theoretical guidance, practical advice, or hands-on troubleshooting—was invaluable to the success of this project.

Finally, I would not be where I am today without the unwavering support of my family. To my partner Ulisses, my sister Diana, and her partner Zaur: your intelligence, drive, and professionalism have always been my greatest inspirations. Thank you for always believing in me and supporting my aspirations.